

NASA Contractor Report 4325

Suspension Systems for Ground Testing Large Space Structures

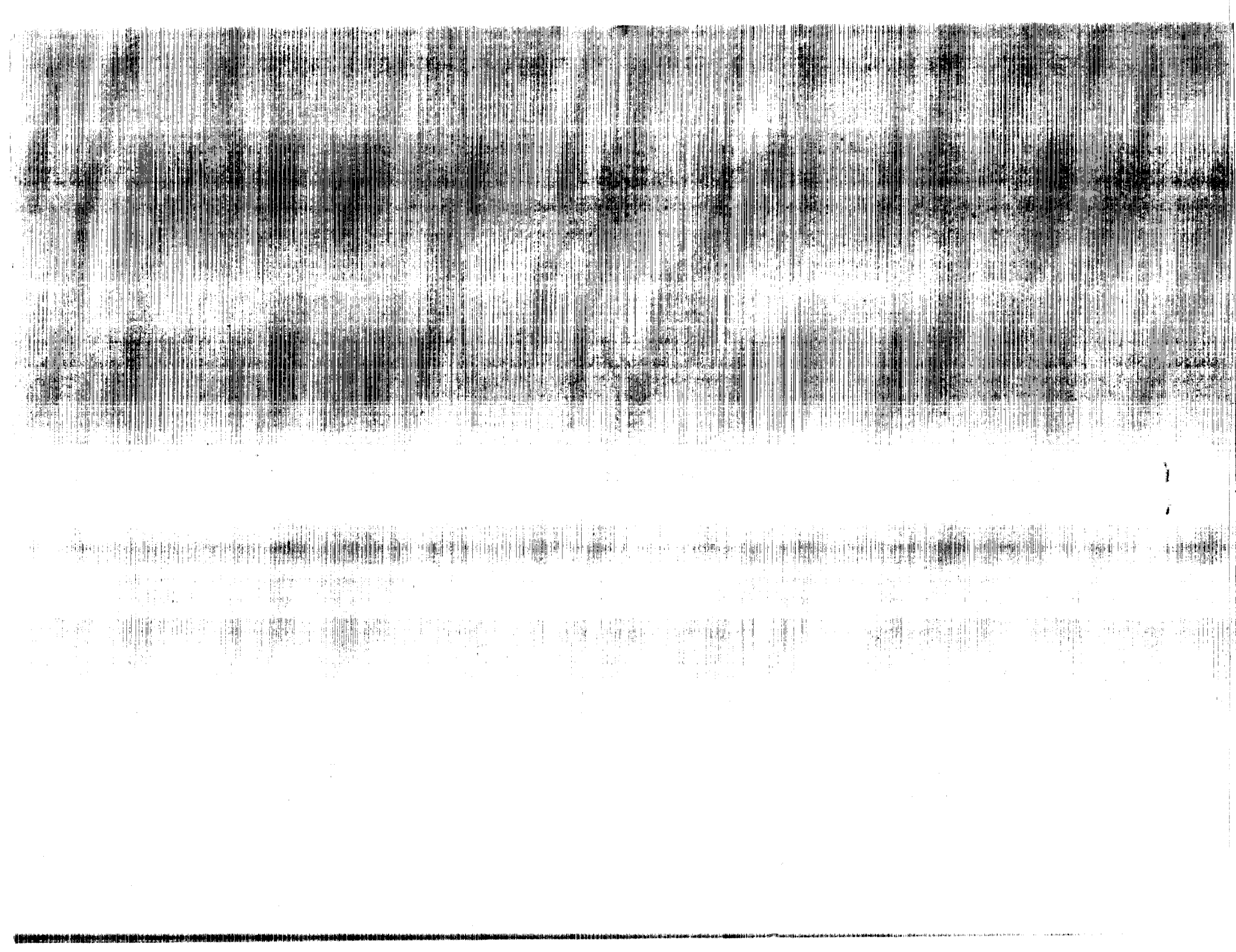
Ronald R. Gold, Inger P. Friedman,
Wilmer H. Reed III, and W. L. Hallauer

CONTRACT NAS1-18798
OCTOBER 1990

(NASA CONTRACTOR REPORT) SUSPENSION SYSTEMS FOR
GROUND TESTING LARGE SPACE STRUCTURES Final
Report (Dynamic Engineering) 112 DCSCU 220

NO-27474

Unclas
H1/L8 0304006



NASA Contractor Report 4325

Suspension Systems for Ground Testing Large Space Structures

Ronald R. Gold, Inger P. Friedman,
and Wilmer H. Reed III
Dynamic Engineering, Inc.
Newport News, Virginia

W. L. Hallauer
Virginia Polytechnic Institute and State University
Aerospace and Ocean Engineering Department
Blacksburg, Virginia

Prepared for
Langley Research Center
under Contract NAS1-18798



National Aeronautics and
Space Administration
Office of Management
Scientific and Technical
Information Division

1990

TABLE OF CONTENTS

TABLE OF CONTENTS	iii
LIST OF FIGURES	vi
SUMMARY	ix
1.0 INTRODUCTION	1
2.0 TEST APPARATUS	3
3.0 VERTICAL SUSPENSION SYSTEM	4
3.1 Description	4
3.2 Analytical Development	5
3.3 Experimental Test Set-Up	8
3.4 Performance Characteristics/Test Results	10
4.0 LATERAL SUSPENSION	13
4.1 Moving Cart Analogy	14
4.2 Damping Effects	15
5.0 TORSION SUSPENSION	18
5.1 Description of Concept	18
5.2 Test Results	19
5.3 Application to Evolutionary Model	20

TABLE OF CONTENTS, CON'T

6.0	PASSIVE LATERAL/TORSION ANALYTICAL MODEL	22
6.1	Equations of Motion	22
6.2	Undamped Vibration Modes	27
6.2.1	Cart Fixed (2-DOF Model)	27
6.2.2	Cart Free (3-DOF Model)	28
6.3	Damped Vibration Modes	28
7.0	ACTIVE CONTROL OF LATERAL/TORSION SUSPENSION	30
7.1	General Design Considerations	30
7.2	Proportional Control	33
7.3	Proportional-Integral-Derivative Control	35
7.4	Experimental Results	38
8.0	CONCLUDING REMARKS	40
9.0	REFERENCES	42
	APPENDIX A, SUSPENSION SYSTEM ASSEMBLY PROCEDURE	43
	APPENDIX B, PC-MATLAB DATA FILES	48
	B.1, 2-DOF Model of Full System in 1-g with Cart Fixed	48
	B.2, 2-DOF Model of Test Structure in 0-g	52
	B.3, 3-DOF Model of Undamped Full System in 1-g	54

TABLE OF CONTENTS, CON'T

B.4, Damping Constant Representing Linear Bearing Friction .	57
B.5, Proportional Control	58
B.6, Rigid Body Modes	60
B.7, PID Control	62
APPENDIX C, DIGITAL CONTROLLER PROGRAM	64

LIST OF FIGURES

Figure 1. Vertical Suspension Test Apparatus	68
Figure 2. Lateral/Torsion Suspension Test Apparatus	69
Figure 3. Zero Spring Rate Mechanism (ZSRM)	70
Figure 4. ZSRM Stiffness Characteristics	71
Figure 5. Effect of Side Spring Preload on System Frequency	72
Figure 6. 3-DOF Suspension Test Apparatus	73
Figure 7. Stiffness and Frequency Comparisons, Main Spring vs. ZSRM	74
Figure 8a. Vertical Suspension Test Results, 145 lb Load	75
Figure 8b. Vertical Suspension Test Results, 80 lb Load	76
Figure 8c. Vertical Suspension Test Results, 42.5 lb Load	77
Figure 9a. Comparison of Analytical and Experimental Results, 145 lb Load	78
Figure 9b. Comparison of Analytical and Experimental Results, 80 lb Load	79
Figure 10. Change in Frequency with Side Spring Vertical Location	80
Figure 11. Change in ζ with Frequency	81
Figure 12. Moving Cart Analogy	82
Figure 13. Lateral Suspension Model	83
Figure 14. Effect of Cart Damping on Lateral-Mode Root	84

LIST OF FIGURES, CONT'D

Figure 15. Equivalent Viscous Damping of Cart on Linear Bearing	85
Figure 16. Linear-Bearing Breakout Force Coefficient	86
Figure 17. Low-Frequency Torsional Suspension System	87
Figure 18. Effect of h on Frequency Spectra of Torsion Suspension System	88
Figure 19. Phase Zero Evolutionary Model with Torsion Suspension . . .	89
Figure 20. Phase Zero Evolutionary Model with Torsion Suspension - 1st Torsion Mode	90
Figure 21. Test Article Geometry and DOFs	91
Figure 22. Natural Frequencies of the Lateral/Torsion System with Cart Fixed	92
Figure 23. Natural Frequencies of the Lateral/Torsional System with Cart Free	93
Figure 24. Transient Response of Damped 1-g 3-DOF Model, $x_c(t)$ is solid, $x_o(t)$ is dot dash	94
Figure 25. Effect of Active Control on Lateral-Mode Root Control Force $F_c = C_p(x_2 - x_1)$	97
Figure 26. Zero Stiffness Open-Loop Loci of Roots as c_v Varies from 0 thru 0.4 ($m_g = 100$ lb, $m_w g = 5.65$ lb, $h = 17.5$ in, $L = 62.12$ in)	98
Figure 27. Zero-Stiffness Proportional-Control Loci of Roots $d/b = 1$	99

LIST OF FIGURES, CONT'D

Figure 28. Loci of Roots for P, PD, and PI Types of Control for
 $h = 0"$, $d/b = 1.084$, $c_v = 0.5$ lb/ips, $\tau = 0.025$ sec 101

SUMMARY

This report documents a research program for the development of improved suspension techniques for ground vibration testing of large, flexible space structures. The suspension system must support the weight of the structure and simultaneously allow simulation of unconstrained rigid-body movement as in the space environment. Exploratory analytical and experimental studies were conducted for suspension systems designed to provide minimum vertical, horizontal, and rotational degrees of freedom. The effects of active feedback control added to the passive system were also investigated.

An experimental suspension apparatus was designed, fabricated and tested. This test apparatus included a zero spring rate mechanism (ZSRM) designed to support a range of weights from 50 to 300 lbs and provide vertical suspension mode frequencies less than 0.1 Hertz (Hz).

The lateral suspension consisted of a pendulum suspended from a moving cart (linear bearing) which served to increase the effective length of the pendulum. The torsion suspension concept involved dual pendulum cables attached from above to a pivoting support (bicycle wheel). A simple test structure having variable weight and stiffness characteristics was used to simulate the vibration characteristics of a large space structure.

The suspension hardware for the individual degrees of freedom was analyzed and tested separately and then combined to achieve a 3 Degree-of-Freedom (DOF) suspension system. Results from the exploratory studies should provide useful guidelines for the

development of future suspension systems for ground vibration testing of large space structures.

This research program was conducted under NASA Langley Research Center Contract NAS1-18798 funded by the Controls-Structures Interaction Guest Investigator Program.

1.0 INTRODUCTION

The proposed use of large space structures has created unique and challenging requirements. The extremely large size and light weight of the structures coupled with the near zero gravity, vacuum environment of space causes difficulty with the control and movement of such structures. To understand and document these difficulties a significant number of ground-based tests on sample or model large space structures will be required. Ground Vibration Tests (GVT's) are necessary to characterize a structure's behavior under dynamic conditions such as slewing a large space antenna or performing a docking maneuver with a space station. Ground Vibration Tests provide the engineer with data specifying the structure's natural modes, frequencies, damping, and mode shapes. These data are critical in determining methods of moving and controlling large, lightweight space structures.

One of the major difficulties with ground vibration testing of large space structures is suspending the structure to allow freedom of motion similar to that found in space. It is, of course, impossible to match the near zero gravity environment of space in ground-based facilities, therefore, suspension systems must support the structure and must do so in a manner that does not overly constrain its motion. The structural members themselves are not designed to take significant loads such as the weight loading which occurs in a ground test environment. Therefore, the suspension system must, while allowing freedom of motion, adequately distribute the weight loading throughout the frail structural members. Freedom of motion requires that the suspension system allow the structure rigid-body movement, that is, minimal coupling with the flexible or vibrational modes of the structure. This freedom is required to adequately simulate movement of the structure in space.

The extremely large size and relative frailty of the structures themselves, or even scaled models of the structures, create unique problems associated with suspension systems. These large structures typically have extremely low natural frequencies. The fundamental frequencies will often be below 0.5 Hz. The addition of a suspension system creates non-zero rigid body modes of the large space structure. The frequency of the rigid body modes is dependent on the suspension stiffness. To adequately uncouple the rigid body modes of the structure from the fundamental flexible modes, the rigid body modes should have frequencies substantially lower than the first fundamental mode. Attempts are often made to suspend structures with long cables, pendulum fashion, from a high ceiling. However, at the extremely low frequencies involved, the required cable lengths become prohibitively long.

Pendulum cable supports limit structural testing to one plane of motion at a time. This support technique ignores the coupling of structural modes in more than one plane and does not address the distortion of torsion modes of beam-like structures nor the distortion of bending modes in the vertical plane. Improved suspension systems using both active and passive technologies have been proposed for support of large space structures. It is felt that initial improvements using simple passive techniques should be examined as a starting point and supplemented with active systems as necessary. As such, this report will document studies, both passive and active, which provide improved suspension in three degrees-of-freedom. Techniques will be described which "effectively" lengthen fixed pendulum cables and which offer soft suspension in both the vertical and torsional degrees of freedom.

2.0 TEST APPARATUS

An illustration of the apparatus used to provide a soft vertical suspension is shown in Figure 1. The main springs bear the weight of the large space structure (represented by laboratory weights in the figure), but the dynamic stiffness of the system is decreased by the addition of the side spring forces. The system tested was designed to support a range of payloads from 50 to 300 lbs and to provide a minimum suspended frequency of less than 0.1 Hz. The suspension system is designed to allow a vertical travel of ± 3 inches. A complete description of the mechanism and its performance is included in Section 3.0 of this report.

The coupled lateral/torsion suspension system is shown conceptually in Figure 2. The soft lateral suspension is provided by a linear bearing which serves to effectively lengthen the support cables. The torsion suspension is shown as a simple wheel concept. In the laboratory tests a good quality bicycle wheel was used for the torsion suspension because it best met the overall requirements of minimum weight, high load capacity, minimum bearing friction, and low cost. The choice of a bicycle wheel is not surprising since the basic design of such wheels has been optimized over many years. For more heavy duty (high payload) requirements a simple three-bar linkage may be substituted. Complete descriptions of the lateral and torsion suspension devices are included in Sections 4.0 and 5.0, respectively.

While originally analyzed and tested independently, the vertical suspension and the lateral/torsion suspension were coupled as a three degree-of-freedom (DOF) suspension in later tests. The lateral and torsion suspension are heavily coupled and have been analyzed and tested together. Coupling the vertical suspension to the lateral/torsion was

not significant in that they are basically uncoupled. However, the addition of the vertical suspension did complicate the active control system as described in Section 7.0.

In order to test the suspension systems, a simple test structure was fabricated which simulated the characteristics of a large space structure. Also shown in Figure 2, the simulated structure is a rigid frame loaded with laboratory weights and restrained elastically by three long rods. The structure is designed to have three basic low frequency modes of interest, horizontal (lateral) and vertical translation and rotation (torsion) in the plane normal to the rods. The lateral and vertical mode natural frequencies are between 0.2 and 0.3 Hz, and the torsion mode frequency is designed to be between 1.0 and 2.0 Hz. The structural weight can be varied from 20 to 200 lbs. This range of payload and low natural frequencies provide an excellent test bed and allow a rigorous evaluation of the suspension devices.

3.0 VERTICAL SUSPENSION SYSTEM

3.1 Description

The primary objective of a vertical suspension system is to provide a near zero vertical stiffness and yet be strong and stiff enough to support a heavy load with a limited amount of initial deflection. The Dynamic Engineering Incorporated (DEI) vertical suspension system is based on the concept of a Zero Spring Rate Mechanism (ZSRM) which has been discussed by others including Kienholz et al in Reference 1. This type of system can be designed to have very low vertical stiffness characteristics and at the same time support large loads with moderate initial deflections. The components of the ZSRM configuration incorporated into the DEI vertical suspension system are shown in Figure 3a. The weight of the structure is supported by the main vertical spring, which

has a spring constant K_m . In order to limit the initial deflection of the spring under load, a relatively stiff spring is used. The ZSRM configuration consists of four linkages, two vertical and two horizontal. The horizontal members are joined together at one end and are connected to the vertical members on the opposite ends. The vertical members are supported at the upper end by a fixed support through a hinge joint. All the connections between the members are also hinge joints. A horizontal spring, with stiffness K_s stretches between the outward ends of the horizontal members, applying a compressive force to them.

When the system is in equilibrium, the horizontal members are exactly horizontal and the vertical members are perpendicular to them. The structural weight is balanced by the restoring force of the main spring, and the compressive force has no component in the vertical direction. As the system is deflected away from the neutral point, the compressive load in the horizontal members develops a vertical component. This vertical force acts in a direction opposite to the restoring force of the main spring, effectively reducing the stiffness of the main spring. With the proper combination of springs and compressive load, the system will exhibit near zero stiffness and will require very little force to deflect it from the neutral point. The structural weight will behave as if it is floating.

3.2 Analytical Development

The vertical suspension system was analyzed to determine the best configuration by examining the effect of each of the design parameters on the behavior of the system. By summing the vertical forces acting at the center point (see Figure 3b), the restoring force, F_R , can be determined from the following equation:

$$F_R + W - F_{km} + 2F_C \sin(\alpha) = 0 \quad (1)$$

where: W is the structural weight

F_{km} is the restoring force of the main spring

F_C is the compressive force in the horizontal members

α is the rotation angle of the horizontal member

The compressive force in the horizontal members, F_C , is a function of the side spring force, F_S .

$$F_C = \frac{F_S}{(\cos(\alpha) - \sin(\alpha)\tan(\theta))} \quad (2)$$

$$F_S = P_C - 2K_S r (1 - \cos(\alpha)) \quad (3)$$

where: P_C is the pretension in the side spring and

r is the length of each horizontal member

θ is the rotation angle of the vertical member

K_S is the stiffness of the side (horizontal) springs

The main spring force F_{km} is:

$$F_{km} = K_m Z + K_m Z_0 \quad (4)$$

where: Z is the vertical deflection of the main spring

Z_0 is the initial deflection of the main spring

K_m is the main spring stiffness

For static balance $W = K_m * Z_0$, and therefore the restoring force of the system is :

$$F_R = K_m Z - \frac{2F_s \sin(\alpha)}{\cos(\alpha) - \sin(\alpha) \tan(\theta)} \quad (5)$$

For small values of Z , angle θ is very small and the equation for F_R can be reduced to the following:

$$F_R = K_m Z - 2F_s \tan(\alpha) \quad (6)$$

The system is designed so that F_R is zero when $Z=0$. The effective vertical stiffness of the system, K_{eff} is $\partial F_R / \partial Z$, which for small values of α is:

$$K_{eff} = K_m - \frac{2P_c}{r} \quad (7)$$

The effective stiffness of the system is therefore a function of the main spring stiffness, the pretension in the side springs and the length, r , of the horizontal members. The system will exhibit linear behavior with this constant stiffness for small values of Z . As Z increases, the nonlinearity of the system also increases. The behavior of the ZSRM as compared to a linear spring with the same stiffness at small deflections is illustrated in the force vs. displacement plot in Figure 4. The ZSRM exhibits linear behavior within a ± 1 inch range of Z , beyond which the nonlinearity of the system is evident. The difference between the linear and nonlinear responses of the system is also plotted as a function of Z in Figure 4. This nonlinear offset can be defined as a third order curve which could be used as a gain function for active feedback. The system stiffness could be linearized by applying the required feedback compensation as a function of vertical displacement, Z .

The nonlinearity of the system is a function of several parameters, including K_m , K_s , r and L , where L is the length of the vertical members. In general, for a given structural weight, decreasing the stiffness of the springs (while maintaining the correct K_m/K_s ratio) will reduce the nonlinearity of the system. However, a reduction in K_m is limited by strength requirements and limits on the static deflection of the spring. The stiffness of the system is not symmetric with respect to the Z direction, due to the motion of the vertical member. As L increases, θ decreases to the point where there is no motion of the vertical members within the vertical travel limit of the system. If θ is zero the stiffness will be symmetric with respect to the Z direction. Physical limitations on the length of the vertical members must be considered, however, when designing the system.

The equation for K_{eff} indicates that the stiffness will decrease as the preload in the side springs increases. For a fixed structural weight, this decrease in stiffness corresponds to a decrease in frequency. The effect of the preload on frequency is illustrated in Figure 5. Without any preload, the system frequency is solely a function of the main spring stiffness and the weight. If the preload is increased the frequency will decrease. The limiting load is called the buckling load, P_{crit} , which gives the system a zero stiffness and will cause the system to buckle.

3.3 Experimental Test Set-up

The ZSRM concept was incorporated into a vertical suspension system which was fabricated and tested at the DEI facility. A drawing of the 3 DOF suspension test apparatus which combines the vertical, lateral, and torsion suspensions is shown in Figure 6. The outer dimensions of the system were sized to allow for testing in the DEI facility. The rigid members are made of 1 inch square aluminum tubing. Steel flexures made out of 0.020 inch blue spring steel are used as hinge joints. They are held

between aluminum blocks which fit into the ends of the tubing. These low damping flexures provide rotational freedom without adding significant friction to the system. The side springs are connected to bar fixtures which can be positioned at any location along the vertical members. By changing the vertical position of the side springs, the compressive loading in the lower horizontal members can be adjusted without adjusting the preload in the side springs. In this configuration, the initial compressive loading in the horizontal members is less than the spring preload, determined as follows:

$$F_{C_0} = \frac{K_S d_0 a}{L} \quad (8)$$

where: L is the vertical distance between the upper and lower joints
 a is the distance from the upper joint to the side spring location
 d_0 is the prestretch of the side spring

Both the main and side springs are connected to eye bolts which can be adjusted to set the correct prestretch or preload in the springs. A force gauge is used to monitor the static preload in the side springs. A strain gauge was mounted on the bottom right flexure and calibrated to the vertical travel at the center point. The vertical frequencies of the system were verified by examining the frequency spectrum of the response from a Kaman non-contact probe placed underneath the structural weight as it is displaced from equilibrium.

A very soft vertical spring, stretched between one of the lower horizontal members and a motor gear belt is used to fine tune the stiffness of the main spring. The tension in the soft spring is adjusted to center the system at its equilibrium point. A simple switch is used to drive the motor in either direction.

This experimental vertical suspension was designed to support a maximum load of 300 lbs. The range of vertical travel is ± 3 inches. Protective stops have been installed on the system to prevent any further travel which could damage the flexures. Two different spring combinations were tested on this system, the first with a load capacity of 150 lbs and the second with a load capacity of 50 lbs. Complete instructions for the assembly, installation and tuning of the vertical system are included in Appendix A.

This type of vertical suspension system can be customized to a large range of weight loadings by installing the appropriate combination of main and side springs. The weight range for a particular spring combination is dependent on the adjustment features available for large changes in initial deflection of the main spring. The vertical stroke is limited primarily by flexure deflection limits. The stroke can be increased by lengthening the horizontal members, which will increase the ratio between the vertical travel and the deflection of the flexures.

3.4 Performance Characteristics/Test Results

In order to support a load of 145 lbs and constrain the initial deflection within the physical limits of the system, a combination of springs giving a main spring stiffness of 7.65 lbs/in was chosen. The side spring stiffness selected was 3.6 lbs/in. The selection of spring combinations was based on stiffness requirements, deflection limits within the physical system and availability through stock spring sources. The reduction in stiffness and frequency which can be achieved with the ZSRM system is illustrated in Figure 7. The force vs. displacement curves for both the main spring alone and the ZSRM are plotted. When the 145 lb is supported solely by the main spring, with a stiffness of 7.65 lbs/in, the system frequency is 0.78 Hz. By implementing the ZSRM concept with the proper compressive load setting, the effective stiffness is reduced to .148 lbs/in, which

corresponds to a frequency of 0.1 Hz. As mentioned previously, the stiffness of the ZSRM becomes nonlinear as Z increases. This nonlinearity can be observed in the force vs. displacement curve for magnitudes of Z greater than one inch.

For a constant supported weight, the frequency of the vertical system can be adjusted to any value less than the frequency of the main spring by applying the correct compressive loading to the lower horizontal members. For a given mass, M, and a desired frequency, ω , the required effective stiffness of the system, K_{eff} is $\omega^2 \cdot M$. The equation for K_{eff} derived in the analysis section, can be used to solve for the preload in the side springs as follows:

$$P_c = (K_m - K_{eff}) \frac{rL}{2a} \quad (9)$$

The force gauge is used to set the correct preload determined from this equation. The spring deflection is changed by adjusting the location of the eye bolts or the spring attachment bar. Fine tuning adjustments may be necessary to match the desired frequency.

Initial attempts at matching frequencies indicated that the vertical stiffness of the system was higher than expected due to the stiffness of the flexures. In calculating the proper preload, K_m must include the main spring and flexure stiffnesses.

The desired frequency chosen for the experimental test apparatus was 0.1 Hz. The frequency of the system was verified using a Kaman non-contact probe, placed underneath the supported weight. The system was displaced from its neutral point about two inches and allowed to oscillate freely. The frequency spectrum from the

probe response was used to determine the frequency. A free response time history and corresponding frequency spectrum for the vertical system supporting a 145 lb load are presented in Figure 8a. The frequency of the vertical mode is 0.105 Hz. The vertical system was tested with various weight loadings to verify that the desired frequencies could be achieved for a range of weights. The minimum weight tested on the 145 lb spring system was 80 lbs. The 0.1 Hz frequency of this configuration was verified by the frequency spectrum of the free response, shown in Figure 8b. A second set of springs was installed for a maximum load of 50 lbs. The frequency spectrum from the free response of this configuration with a 42 lb load is shown in Figure 8c.

Force deflection tests were performed on the various configurations to determine the restoring force of the system in the ± 3 inch vertical range. Weight was added to the system in small increments and deflection measurements were taken for each incremental weight. The force vs. deflection curve obtained from these measurements along with the analytical curve are presented in Figure 9a for the 145 lb case. The experimental curve demonstrates slightly more nonlinearity for values of Z beyond two inches, but the differences are relatively small. The force vs. displacement curve shown in Figure 9b for the vertical system with an 80 lb load demonstrates similar behavior.

As mentioned previously, the vertical location of the side spring mounting brackets can be adjusted to provide a means of changing the compressive load in the lower horizontal members without changing the preload in the side springs. The sensitivity of this adjustment with respect to compressive loading and frequency is illustrated in Figure 10. The frequency can be reduced from .185 Hz to .068 Hz by lowering the position of the springs 1.75 inches which corresponds to a 2 lb change in compressive loading. This high degree of sensitivity not only allows the system to be tuned for very low

frequencies (near zero), but also makes the system more sensitive to changes in temperature and air disturbances.

Damping measurements were obtained from the free decay response of the system to an initial deflection. The percent critical damping, ζ , was calculated using the logarithmic decrement method. Damping was examined for a range of system frequency settings corresponding to various levels of compressive loading. The damping measurements taken from the experimental data are presented in Figure 11. As expected, ζ increases as frequency decreases. Since there are no moving parts in the system, the source of the damping must be structural damping in the flexures. At such low frequencies, air damping could also be a contributing factor.

4.0 LATERAL SUSPENSION

The suspension of large space structures from long pendulum cables provides a convenient means for allowing the test article to move laterally as a rigid body. To minimize dynamic coupling of the pendulum and elastic modes of the suspended structure, excessively long pendulum cables may be required. For the test article suspended as a simple pendulum with cables fixed at the upper ends, the lowest suspension mode frequency is

$$\omega_p = \sqrt{g/L} \text{ , rad/sec} \quad (10)$$

where: g is the gravitational constant and
 L the support cable length

The techniques described below provide a means for increasing the effective length of pendulum cables. Some of these ideas were originally introduced in Reference 2.

4.1 Moving Cart Analogy

The moving-cart analogy depicted in Figure 12 provides a useful means of studying the application of extended pendulum techniques such as the inverted pendulum, tensioned-cable suspension and other techniques for reducing the natural frequency of a simple pendulum. The primary goal of all of these methods is to reduce the system's fundamental frequency. This frequency is dependent upon the stiffness of a spring between the cart and ground. If the spring is infinitely stiff, the suspension system

frequency is $\sqrt{g/L}$, the simple pendulum frequency. As the spring stiffness, K_x , approaches zero, the suspension frequency, ω_p , likewise approaches zero.

The tensioned cable may also be replaced with a fixed rail or beam on which a pulley rides. This system has the advantage that large tensions and long lengths are not required to lower the restoring force. The restoring spring K_x is controlled by the shape of the rail, specifically, the depth, d , of the rail. The value of K_x shown in Figure 12 is for a circular arc shape and yields a linear spring for small motions on the rail. This system offers very low values of K_x , in fact, the rail can be flat ($d = 0$), allowing the restoring force to approach zero.

The system also has a higher-frequency cart mode. For $K_x = 0$ the ratio of the cart-mode frequency, ω_c , to the simple pendulum frequency is

$$\frac{\omega_c}{\sqrt{g/L}} = \sqrt{\frac{W}{w}} \quad (11)$$

where W and w are the weights of the suspended structure and the cart respectively. It is interesting to note that in all cases, the effective spring stiffness K_x , and consequently the suspension system frequency, is strongly dependent on the suspended weight. This feature differs from the simple pendulum whose frequency is independent of pendulum weight.

4.2 Damping Effects

In the preceding discussion of lateral suspension systems, the effects of damping or friction forces were neglected. The effect of such forces acting on the moving cart is considered next. For ease of analysis, it is assumed throughout that the damping mechanism can be modeled as an equivalent linear viscous damper. To investigate damping effects, the lateral suspension model shown in Figure 13 is analyzed. The definition of parameters and the specific example cases to be considered are also given in Figure 13. Note that the suspended mass is connected to the ground by a spring

of stiffness k . Thus, $\sqrt{k/M}$ represents the undamped lateral mode frequency of the "test article" in a zero-gravity (0-g) environment. The equations of motion for the model shown in Figure 13 are as follows:

$$\begin{aligned}
M\ddot{x}_1 + c_v\dot{x}_1 + \frac{Mg}{L}x_1 - \frac{Mg}{L}x_2 &= F_c \\
M\ddot{x}_2 + \left(\frac{Mg}{L} + k\right)x_2 - \frac{Mg}{L}x_1 &= 0
\end{aligned}
\tag{12}$$

The term F_c is a feedback-control force acting on the cart which will be discussed later in consideration of active control of suspension system modes.

Figure 14 shows the loci of lateral-mode eigenvalues of the above equations of motion as the damping coefficient, c_v , is varied from 0 to 10 lb/ips. This display of eigenvalues is not the usual plot of imaginary part versus real part, but rather a more physically meaningful plot of damped frequency (in Hz) versus damping ratio (relative to critical damping). Significant features of this plot are the frequencies of the lateral mode as the cart damping coefficient approaches limiting maximum and minimum values. For $c_v = 0$ lb/ips the frequency is that of the unsuspended (zero-g) test article (0.27 Hz); for large damping ($c_v > 10$ lb/ips) the system frequency approaches 0.426 Hz, the frequency for simple-pendulum suspension at one g.

Because of the sensitivity of the lateral-mode suspension frequency to damping in the moving cart mechanism, efforts were made to quantify the damping and breakout friction of the linear bearing system, which becomes the "moving cart" used in the experimental laboratory suspension system (see Figure 6).

First, the equivalent viscous damping of the linear bearing on a circular-rod track was determined experimentally by the method illustrated in Figure 15. Weights were suspended from a cable of length L attached to the bearing. The weights were restrained laterally by attachment of horizontal cables at the weight's center of gravity.

The linear bearing was displaced from its equilibrium position on the track and then released. The equivalent viscous damping coefficient, c_v , was determined experimentally from the logarithmic decrement of the resultant lateral transient motion of the bearing on its track by means of the approximate equation

$$c_v = \frac{0.11 T \left(\frac{W}{L} \right)}{\pi N_{1/2}} \quad (13)$$

where: T = period of oscillation
 W = suspended weight
 L = pendulum length
 $N_{1/2}$ = number of oscillations for vibration amplitude to reach one-half of the initial displacement.

Figure 15 indicates that the derived damping value of $c_v \approx 0.04$ lb/ips is essentially independent of load over the weight range tested (50 lb to 200 lb).

The breakout force required to overcome friction of the linear bearing was experimentally determined by measuring the lateral deflection of the pendulum weight at the instant of breakout. In Figure 16, the friction coefficient, i.e., the breakout force relative to the applied normal load in percent, is plotted versus load. Here it is seen that the friction coefficient falls off with increasing load. For the maximum test load of 190 lbs the measured friction coefficient $F/W = 0.2$ percent; for the minimum test load of 2.0 lb, $F/W = 0.4$ percent.

5.0 TORSION SUSPENSION

In previous sections of the paper, various means of achieving low-frequency suspension modes in the vertical and lateral directions have been considered. To alleviate coupling between the suspension system and the structure's torsion modes, there is equal need for consideration of low-frequency suspension to allow undistorted torsional vibration modes.

5.1 Description of Concept

Figure 17 shows the proposed low-frequency torsional suspension system. This system uses a dual cable approach and a rotating support pivot to lower the frequency of the suspension system's torsion or rotation mode. The body is suspended by two cables of equal length L from a pivoting support structure. The cables are configured as a parallelogram such that at rest, the center of gravity of the body hangs directly below the pivot axis.

The system has two uncoupled natural pendulum modes. One is the "simple" pendulum mode whose frequency is described by:

$$\omega_s = \sqrt{g/L}, \quad \text{rad/sec} \quad (14)$$

where: g is the gravitational constant
 L is the pendulum cable length

The second mode is the torsion or "compound pendulum" mode involving rotation of the body about its own center of gravity. The frequency of the compound pendulum mode can be determined by noting that the cable length L has no effect on this uncoupled mode. Thus, letting $L = 0$ in the figure, the rotational frequency of the suspended body can be found by considering the body as being suspended from a rotation axis located a distance, h , above the center of gravity. Note in the figure that $h = h_1 - h_2$. The resulting equation for the frequency of the compound pendulum is:

$$\omega_c = \sqrt{\frac{(g/L)(h/L)}{(h/L)^2 + (\kappa/L)^2}} \quad (15)$$

where κ is the radius of gyration of the suspended body about its center of gravity. As h/L is reduced, the ratio of the compound to simple pendulum frequency tends to zero as shown in Figure 17.

5.2 Test Results

Figure 18 shows the results of tests of the torsion mode suspension for several values of the offset parameter h . In the tests, h is varied by moving the lower attachment point of the cables relative to the center-of-gravity of the 100 lb supported mass. Three curves are plotted in the figure corresponding to different values of h . For each curve there are two peaks shown. The lower frequency peaks represent the pendulum mode and remain constant in frequency as h is varied. The higher frequency peaks represent the torsion mode for the three values of h . It is apparent from the plot that the frequency of the torsion mode decreases considerably as h decreases. The parameter h is seen to be quite effective in reducing the system torsion frequency while having virtually no effect on the pendulum mode frequency. However, the increasing width of

the pendulum mode peaks for decreasing values of h indicates an increase in damping of this mode.

5.3 Application to Evolutionary Model

The Evolutionary Model is a structure currently being tested at the NASA Langley Research Center. It is intended to serve as a test-bed structure for evaluating control-structure interaction phenomena. A preliminary analytical model of the Evolutionary Model was used to evaluate how the torsion suspension concept introduced here might be incorporated in the test structure.

A NASTRAN model of the Phase-0 Evolutionary Model was analyzed both as a free-free structure and with two support stations. The NASTRAN model was modified to include an analytical representation of the two suspension devices. Figure 19 shows the model suspended at two stations with a torsion suspension wheel at the top of each set of support cables. The cable attachment points on the structure were chosen to be as near to the first bending mode node points as possible, but the large dish antenna prohibits one cable support from attaching exactly at the node point.

The model was analyzed using a differential stiffness solution. The parameter h was not varied extensively in the analysis, but it was adjusted as necessary to provide a stable configuration. The Evolutionary Model is unique in that a large offset mass causes the center-of-gravity (c.g.) of the model to lie above the cable attachment points at the top of the truss. This characteristic requires the torsion wheel or linkage to be configured as shown in the detail view in Figure 19. The pivot point in this application lies above the cable attachment points thus creating a positive h value and stabilizing the entire truss/suspension system.

Figure 20 shows the 1st torsion mode of the supported structure. Motion of the cables and the suspension linkage are also apparent. A summary of the analytically derived modes is contained in the table below:

COMPARISON OF MODAL FREQUENCIES PHASE ZERO EVOLUTIONARY MODEL		
	Frequency (Hz)	
Mode Description	Free-Free	Suspended
Rigid Yaw - Pendulum		0.092
Rigid Y - Pendulum		0.099
Rigid X - Pendulum		0.102
Rigid Roll		0.581
1st Vertical Bending	1.85	1.84
1st Lateral Bending	1.86	1.86
Cable Modes (8)		2.20- 2.39
Cable Stretch (Rigid Plunge)		3.07
1st Torsion	3.14	3.18

The table indicates the effect of the added suspension devices. In particular, the rigid body modes now have non-zero frequencies, and the cable supports add 8 additional modes between 2.2 and 2.4 Hz. Higher order cable modes occur at integer multiples of these frequencies. The important results indicated in the table are that the frequencies for the vertical and lateral bending and, more importantly here, the 1st torsion mode are not changed significantly from the free-free analysis. The lack of distortion of the bending modes can be attributed to the placement of the suspension supports near the node points for each bending mode. The lack of distortion of the torsion mode must be attributed to the use of the torsion suspension devices.

6.0 PASSIVE LATERAL/TORSION ANALYTICAL MODEL

This section of the paper concerns the development of the analytical model for a passive suspension system with combined lateral and torsional degrees of freedom. In later sections, active feedback control will be added to the passive system for the purpose of improving the simulation of a zero-g test environment.

6.1 Equations of Motion

The equations of motion (EOM) for the combined lateral/torsion suspension system, which is depicted in Figure 21, are derived from Lagrange's equations. Characters under bars are matrices, and a prime (') denotes matrix transposition. The EOMs in matrix form for three DOFs are:

$$\overline{M}_a \overline{\ddot{q}}_a + \overline{C}_a \overline{\dot{q}}_a + \overline{K}_a \overline{q}_a = [f_c \ 0 \ 0]'$$
(16)

$$\text{where } \overline{q}_a = [x_c \ \phi \ \theta]'$$

$$\overline{M}_a = \begin{bmatrix} (m + m_w) & m\ell & -mh \\ m\ell & m\ell^2 & -m\ell h \\ -mh & -m\ell h & (I_T + mh^2) \end{bmatrix} \quad \overline{C}_a = \begin{bmatrix} c_v & 0 & 0 \\ 0 & 0 & 0 \\ 0 & 0 & 0 \end{bmatrix}$$

$$\overline{K}_a = \begin{bmatrix} k_x & k_x \ell & -k_x(h + b) \\ k_x \ell & (k_x \ell^2 + mg\ell) & -k_x \ell(h + b) \\ -k_x(h + b) & -k_x \ell(h + b) & [k_\theta + mgh + k_x(h + b)^2] \end{bmatrix}$$

The definitions of the notations in Eq. 16 are:

$g = 386.4 \text{ in/s}^2$, acceleration due to gravity

$mg = 99.48 \text{ lb}$, weight of the test structure

$m_w = 2/g \text{ lb-s}^2/\text{in}$, mass of the wheel (3-bar linkage) and cart

$I = 1,777/g \text{ lb-s}^2\text{-in}$, c.g. moment of inertia of the test structure

$I_w = 338/g \text{ lb-s}^2\text{-in}$, moment of inertia of the wheel (3-bar linkage) about its c.g.

$I_T = I + I_w$

$\ell = 88.625 \text{ in}$, cable length

$b = 3.00 \text{ in}$, distance above the spring elastic center of the test structure's c.g.

$k_x = 0.756 \text{ lbs/in}$, horizontal-translation spring constant

$k_\theta = 194.5 \text{ lb-in/rad}$, rotational spring constant

$c_v =$ viscous damping constant representing friction of the linear bearing

$h = h_1 - h_2$ (see Fig. 21), a variable parameter

$f_c =$ feedback-control force

$x_c =$ cart translation DOF

$\phi =$ rotation angle of the cables

$\theta =$ rotation angle of the test structure

Note that the values listed match those of the experimental test apparatus described in section 2.0. A viscous damping matrix with one non-zero damping constant c_v has been added to approximate the friction of the linear bearing. Estimation of c_v based on measured response of the system is described in Section 4.4.

In later considerations of closed-loop control of horizontal motion, translations of the wheel-cart and the test structure are the measured quantities used as input to the control system. It is appropriate, therefore, to replace the rotations in Eq. 16 with translations, and two reasonable quantities to use are x_o , translation of the test structure

c.g., and x_θ , translation of the elastic center of the external spring system, as illustrated on Figure 21. Hence, we define a new set of DOFs, $\bar{q}_b = [x_c \ x_o \ x_\theta]'$. The

transformation between the two sets of DOFs is

$$\bar{q}_a = \bar{T} \bar{q}_b \quad (17)$$

$$\bar{T} = \begin{bmatrix} 1 & 0 & 0 \\ -\frac{1}{l} & \frac{h+b}{lb} & -\frac{h}{lb} \\ 0 & \frac{1}{b} & -\frac{1}{b} \end{bmatrix}$$

Hence, we transform the original mass, damping and stiffness matrices with the matrix

product $\bar{M}_b = \bar{T}' \bar{M}_a \bar{T}$, etc. Then the EOMs in the second set of DOFs are

$$\bar{M}_b \ddot{\bar{q}}_b + \bar{C}_b \dot{\bar{q}}_b + \bar{K}_b \bar{q}_b = [f_c \ 0 \ 0]'$$
(18)

$$\bar{M}_b = \begin{bmatrix} m_w & 0 & 0 \\ 0 & (m + \frac{l_T}{b^2}) & -\frac{l_T}{b^2} \\ 0 & -\frac{l_T}{b^2} & \frac{l_T}{b^2} \end{bmatrix} \quad \bar{C}_b = \bar{C}_a$$

$$\overline{K}_b = \begin{bmatrix} \frac{mg}{\ell} & -\frac{mg h + b}{\ell b} & \frac{mg h}{\ell b} \\ -\frac{mg h + b}{\ell b} \left[\frac{k_\theta}{b^2} + \frac{mg}{\ell} \left(\frac{h+b}{b} \right)^2 + \frac{\ell h}{b b} \right] & -\left[\frac{k_\theta}{b^2} + \frac{mg h}{\ell b} \left(\frac{h+b}{b} + \frac{\ell}{b} \right) \right] \\ \frac{mg h}{\ell b} & -\left[\frac{k_\theta}{b^2} + \frac{mg h}{\ell b} \left(\frac{h+b}{b} + \frac{\ell}{b} \right) \right] & \left[k_x + \frac{k_\theta}{b^2} + \frac{mg h}{\ell b} \left(\frac{\ell}{b} + \frac{h}{b} \right) \right] \end{bmatrix}$$

Setting $g = 0$ in Eq. 18 gives a set of three EOMs in which translation x_c of the wheel and cart is completely decoupled from the other two translation DOFs. Hence, we have

the following equation in DOFs $\overline{q}_{b2} = [x_o \ x_e]'$ governing the motion of the test

structure:

$$\overline{M}_{b2} \overline{\ddot{q}}_{b2} + \overline{K}_{b2} \overline{q}_{b2} = 0 \quad (19)$$

$$\overline{M}_{b2} = \begin{bmatrix} \left(m + \frac{I_T}{b^2}\right) & -\frac{I_T}{b^2} \\ -\frac{I_T}{b^2} & \frac{I_T}{b^2} \end{bmatrix} \quad \overline{K}_{b2} = \begin{bmatrix} \frac{k_\theta}{b^2} & -\frac{k_\theta}{b^2} \\ -\frac{k_\theta}{b^2} & \left(k_x + \frac{k_\theta}{b^2}\right) \end{bmatrix}$$

If we were to turn off gravity and cut the cables connecting the wheel and the test structure, then the EOM for the test structure by itself would be the same as Eq. 19, except that the total inertia $I_T = I + I_w$ in Eq. 19 would simply be I . With the type of horizontal-motion control to be applied, we cannot change the effect of wheel moment

of inertia I_w . Hence, the modes of Eq. 19 should be considered the target modes for the controlled system, even though I_w is not present in the 0-g EOMs of the test structure by itself. (It is interesting to note that, in principle, I_w could be canceled if it were possible to implement a rotational acceleration feedback control on the wheel.)

With x_c restrained to be zero by friction of the linear bearing, Eq. 16 for the motion of the remainder of the system in DOFs, $\overline{q_{a2}} = [\phi \ \theta]'$, becomes:

$$\overline{M_{a2}} \overline{\ddot{q}_{a2}} + \overline{K_{a2}} \overline{q_{a2}} = 0 \quad (20)$$

$$\overline{M_{a2}} = \begin{bmatrix} m\ell^2 & -m\ell h \\ -m\ell h & (I_T + mh^2) \end{bmatrix}$$

$$\overline{K_{a2}} = \begin{bmatrix} (k_x \ell^2 + mg\ell) & -k_x \ell (h + b) \\ -k_x \ell (h + b) & [k_\theta + mgh + k_x (h + b)^2] \end{bmatrix}$$

For convenience of analysis Eq. 18 is written in state-space form,

$$\dot{\overline{x}} = \overline{A}\overline{x} + \overline{B}_c \overline{f}_c \quad \overline{x} = \begin{bmatrix} \overline{q_b} \\ \overline{\dot{q}_b} \end{bmatrix} \quad (21)$$

in which \overline{x} is the state vector, and the system and control-feedback matrices are, respectively,

$$\bar{A} = \begin{bmatrix} -\bar{M}_b^{-1}\bar{C}_b & -\bar{M}_b^{-1}\bar{K}_b \\ \bar{I}_3 & \bar{O}_3 \end{bmatrix} \quad \bar{B}_c = \bar{M}_b^{-1} [1 \ 0 \ 0 \ 0 \ 0 \ 0]'$$

For the response calculations of this section, there is neither feedback control nor external excitation, so $f_c = 0$. In the state-space formulation, we have also an output equation,

$$\bar{y} = \bar{C}\bar{x} + \bar{D}f_c \quad (22)$$

In order to calculate and plot the quantities $x_c(t)$ and $x_o(t)$, we specify,

$$\bar{C} = \begin{bmatrix} 0 & 0 & 0 & 1 & 0 & 0 \\ 0 & 0 & 0 & 0 & 1 & 0 \end{bmatrix} \quad \bar{D} = \begin{bmatrix} 0 \\ 0 \end{bmatrix}$$

6.2 Undamped Vibration Modes

Calculation of the open-loop, undamped vibration modes for the three cases discussed in the previous section is done with the use of the PC-Matlab software. Appendix B contains the PC-Matlab files and tabulated results of all of the calculations presented herein.

6.2.1 Cart Fixed (2-DOF Model)

The calculated variation of natural frequencies of the lateral and torsional suspension as a function of h is shown in Figure 22. Also included in the figure are some experimentally determined frequencies. Several points are worth noting in this figure. The first and most important point is that the calculated torsion-mode frequency closely matches the suspended system the zero-g torsion mode frequency 0.967 Hz, (see Appendix B.2)

when $h = 0$. The rightward shift of the experimental points from the predicted curve is believed to be due to uncertainties in measurement of the effective cable attachment points in determining h . Because of cable stiffness effects, the cable end attachment points may not behave as perfect hinges as was assumed. Also note that the lateral mode frequency for this case with cart fixed is the simple pendulum frequency, 0.426 Hz, versus 0.265 Hz for zero-g (see Appendix B.2) and is insensitive to changes in h within the h range of practical interest.

6.2.2 Cart Free (3-DOF Model)

This is a useful theoretical case, even though it is not physically realizable due to the substantial friction in the linear bearing. The calculated results for this case are given in Appendix B.3, and the natural frequencies are plotted in Figure 23. Comparison of the results in Figure 23 with those in the previous figure shows that by freeing the cart the lowest two modes of the undamped 3-DOF model for $h = 0$ are nearly identical to the modes of the 0-g, 2-DOF test structure. Hence, if the linear bearing were frictionless, then the passive cable-suspension system described by the model with $h = 0$ would do an excellent job of simulating the 0-g case. It appears, then, that the primary function of the active horizontal-motion control system is to compensate for the friction in the linear bearing by forcing the wheel-cart to move as if the bearing were frictionless. In order to design such a control system, we must know at least the order of magnitude of the friction (as represented by the parameter c_v), and this issue is addressed in the next section.

6.3 Damped Vibration Modes

The experimental result suggests that the linear bearing's friction has a complex nature, probably much more like Coulomb friction than viscous damping. However, use of the linear analysis capabilities of PC-Matlab requires that the damping model be linear, so

the objective of the exercise described here was to infer a linear viscous damping constant c_v that influences the dynamic response in a fashion similar to the actual bearing friction.

The resonant driving and release is simulated by a simple initial-condition, with zero external excitation: the initial velocity has the shape of the undamped 3-DOF translation mode, and the initial displacement is zero. The subsequent time-history of response is calculated and plotted for a specified value of c_v .

In the time-history graphs to be discussed next, $x_c(t)$ is plotted with solid lines, and $x_o(t)$ is plotted with dot-dash lines. The first case is for $c_v = 0$ lb/ips, and it is a check on the functioning of the PC-Matlab solution (veloresp.m in Appendix B.4); the results are plotted on Figure 24a. The response is free, undamped vibration in the translation mode at 0.265 Hz of the 3-DOF model, in perfect agreement with the $h = 0$ modal results of Appendix B.2. This result tends to validate that veloresp.m is functioning correctly.

The other cases are for $c_v = 0.1, 1.0, 10$ and 100 lb/ips, and the results are plotted on Figures 24b, 24c, 24d, and 24e, respectively. For $c_v = 0.1$ lb/ips, the damping appears to be proportional and modal in the 0.265 Hz mode of the 3-DOF model. For $c_v = 1.0$ lb/ips, the damping appears to be nonproportional, which indeed it is, and the character of the response is quite different from that of the 0.265 Hz mode. For $c_v = 10$ lb/ips, motion x_c of the cart is very small, and motion x_o of the test structure is only lightly damped at a frequency almost indistinguishable from 0.426 Hz, the $h = 0$ translation mode frequency of the 2-DOF model with fixed cart. Finally, for $c_v = 100$ lb/ips, x_c is almost completely suppressed, and x_o is in free vibration at 0.426 Hz with almost imperceptible damping.

7.0 ACTIVE CONTROL OF LATERAL/TORSION SUSPENSION

7.1 General Design Considerations

Design of the control system is based on comparison of the two lower modes of the undamped, 1-g, $h = 0$, 3-DOF model (Figure 23) with the modes of the 0-g 2-DOF model, the ideal case (Appendix B.2), and with the modes of the fixed-cart, 1-g, $h = 0$, 2-DOF model (Figure 22). For convenience, those results are repeated below:

<u>2-DOF, 0-g</u>		<u>2-DOF, fixed-cart, 1-g</u>	
» modebase		» Dh=0.0;mode2dof	
<u>(mode 1)</u>	<u>(mode 2)</u>	<u>(mode 1)</u>	<u>(mode 2)</u>
modal =		modal =	
(x_o) 1.0000	0.0796	(ϕ) 0.8062	-0.0034
(x_e) 0.9634	1.0000	(θ) 1.0000	1.0000

freqs =		freqs =	
0.2677	0.9666	0.4263	0.9668

<u>3-DOF, 1-g</u>		
» Dh=0.0;mode3dof		
<u>(mode 3)</u>	<u>(mode 1)</u>	<u>(mode 2)</u>
modal =		
(x_o) 1.0000	1.0000	0.0937
(x_o) -0.0204	0.9872	0.0777
(x_e) -0.0205	0.9511	1.0000

freqs =	
2.3675	0.2650 0.9666

Mode 2 is essentially the same in all three cases, which shows that setting $h = 0$ in the 1-g cases is an effective passive method for preserving the 0-g rotation mode. Active control is required, therefore, only to preserve the 0-g translation mode, mode 1, in the environment of 1-g and the sticky linear bearing.

Observe in 3-DOF mode 1, the translation mode, that $x_c \approx x_o$, which means that the cart remains almost directly above the test structure's c.g. This suggests that the control system for the actual damped laboratory article should, for motion in the translation mode, maintain the cart directly above the test structure's c.g. Cart position x_c can be sensed with a potentiometer. Likewise, position of the test structure can be sensed with a noncontacting Kaman transducer, but x_o is not the test structure translation that should be sensed. The nodal point of 3-DOF mode 2, the rotation mode, is not right at the c.g., but rather a short distance above it. Therefore, sensing of x_o could cause the control system to modify the rotation mode, which would probably be counterproductive.

It is appropriate, therefore, to sense the translation of the test structure at the nodal point of the 3-DOF rotation mode, which is a distance d above the spring elastic center. The translation of the nodal point is denoted x_d and is given in terms of the defined DOFs by

$$x_d = x_e + d\theta = x_e + d \left(\frac{x_o - x_e}{b} \right) = x_o \left(\frac{d}{b} \right) + x_e \left(1 - \frac{d}{b} \right) \quad (23)$$

The ratio d/b is found from the shape of 3-DOF mode 2 to be

$$(1 - x_o/x_e)^{-1} = (1 - 0.0777)^{-1} = 1.0843.$$

It has been established that the control system should maintain $x_c \approx x_d$ in order to preserve the 0-g translation mode with minimal effect on the rotation mode. Accordingly, we define the error quantity

$$\epsilon = x_d - x_c = \overline{C}_\epsilon \overline{x} \quad (24)$$

where, from Eqs. 21 and 23, the output matrix is

$$\overline{C}_\epsilon = \left[0 \ 0 \ 0 \ -1 \ \frac{d}{b} \ \left(1 - \frac{d}{b} \right) \right] \quad (25)$$

We consider in subsequent sections methods for effecting control by making control force f_c a linear function of ϵ , and/or its time integral, and/or its time derivative. These types of control are commonly called proportional (P), integral (I), and derivative (D) control, and combinations thereof are referred to as PD, PID, etc. control.

7.2 Proportional Control

For proportional control, we define the feedback constant C_p and set

$$f_c(t) = C_p \epsilon(t) \quad (26)$$

Combining Eqs. 21, 24-26 then gives

$$\bar{\dot{x}} = (\bar{A} + C_p \bar{B}_c \bar{C}_\epsilon) \bar{x} = \bar{A}_c \bar{x} \quad (27)$$

The matrices \bar{A} , \bar{B}_c and \bar{C}_ϵ can be calculated by specifying h ($= 0$ in the following), c_v and d/b ($= 1.0843$ in Appendix B.5) and running the PC-Matlab m-file (see Appendix B.5). The effect of varying the proportional feedback constant C_p on the lateral mode eigenvalues is shown in Figure 25. For this case the damping constant $c_v = 1.0$ was assumed. Note the similarities between this figure and Figure 14, the open-loop case where the damping constant c_v was varied. The root loci are essentially the same in both figures, demonstrating that active control of the cart's lateral position relative to that of the suspended body effectively compensates for the adverse effects of cart damping with regard to simulating 0-g test conditions.

For all of the cases discussed to this point, the 0-g vibration modes of the test structure involve structural deformation and therefore have positive natural frequencies. There is interest also in the case for which the structure is not restrained by springs and therefore has at least one zero-frequency rigid-body mode in 0-g. For this case, then, we let stiffness constants k_x and k_θ be zero. To avoid the complication of repeated zero eigenvalues, we consider $h > 0$. In particular, we evaluate the case with numerical values $h = 1.75$, $mg = 100$ lb, $m_w g = 5.65$ lb, $\ell = 62.125$ ", with all other values the same as before. Changing these values in PC-Matlab and running the modified m-file (under the name k0mde3df.m) gives the following for the undamped, 1-g modes:

```

3-DOF, 1-g, Unrestrained
» Dh=1.75;k0mde3df
  (mode 3) (mode 1) (mode 2)
modal =
(x_c)  1.0000   1.0000  -0.7273
(x_o)  -0.0565   1.0000   0.0411
(x_e)  -0.0372   1.0000   1.0000

```

freqs =

```

1.7255   0.0000   0.8952

```

The translation mode now is a zero-frequency rigid-body mode, and the rotation mode has 0.8952 Hz natural frequency.

The modes above are for zero friction in the linear bearing. When c_v increases slightly above zero, then the rigid-body translation mode remains at zero frequency but has an exponential damping time constant. It is not appropriate, therefore, to plot the locus of

roots in the frequency vs. zeta form used for Figures 14 and 25. Accordingly, the appropriate m-files have been modified to calculate and plot loci of roots in the more traditional form of imaginary part vs. real part (see Appendix B.6).

The open-loop results for c_v varying 0-0.4 lb/ips are shown in Figure 26. There are three ranges of c_v in which the roots are qualitatively different: 0 to about 0.29, about 0.29 to about 0.36, and above about 0.36 lb/ips. In the middle range, the only oscillatory roots are those of the rotation mode.

The results of Figure 25 establish that proportional control tends to achieve the desired effect if the translation mode has positive natural frequency. The question now is whether or not proportional control performs as desired also for the zero-frequency mode; i.e., does proportional control move the roots of the rigid-body translation mode of Figure 26 toward the origin, decreasing the damping in that mode and making it appear more like the true undamped, 0-g mode? To answer this question, the closed-loop case is also modelled in Appendix B.6. The results are presented in Figures 27a thru 27c. In each figure, c_v is assigned a value and proportional feedback constant C_p is varied 0-2 lbs/in in increments of 0.1 lbs/in. In each case, proportional control forces the translation mode's roots toward the origin, which is the desired effect.

7.3 Proportional-Integral-Derivative Control

For general PID control, we define feedback constants C_p , C_i and C_d , and then express the control force as

$$f_c = C_p \epsilon(t) + C_i \int_0^t \epsilon(\sigma) d\sigma + C_d v(t) \quad (28)$$

The derivative term in Eq. 28 requires some explanation. It is not possible or even desirable in practice to implement an exact derivative operation, so a standard alternative procedure is to introduce a new variable $v(t)$ and to approximate the derivative with a single-pole high-pass filter,

$$\tau_d \dot{v} + v = \dot{\epsilon}(t) \quad (29)$$

For small values of time constant τ_d , we have $v \approx d\epsilon/dt$ for low-frequency $\epsilon(t)$ signals and $v \approx \epsilon/\tau_d$ for high-frequency signals. Hence, choosing τ_d appropriately results in a good approximate differentiation of low-frequency signals of interest without the undesirable differentiation of high-frequency noise. (A band-pass filter with appropriate parameters would be an equally accurate differentiator and a more effective noise attenuator, but it would increase the order of Eq. 29 and, hence, the number of states in the controller.) For example, setting $\tau_d = 0.025$ sec gives an approximate differentiator that is accurate to less than 9° of phase error and 1% of magnitude error for signals of 1 Hz or lower.

It is necessary now to write Eqs. 28 and 29 in a state-space form. To do so, we define the controller state variables,

$$\bar{z} = \begin{bmatrix} z_1 \\ z_2 \end{bmatrix} \quad z_1 = \int_0^t \epsilon(\sigma) d\sigma \quad z_2 = \int_0^t v(\sigma) d\sigma \quad (30)$$

Error signal $\epsilon(t)$ is the input to the controller. Then the definition of z_1 and the integral of Eq. 29, with the definition of z_2 , constitute the controller state equations,

$$\dot{\bar{z}} = \bar{A}_z \bar{z} + \bar{B}_z \epsilon \quad (31)$$

$$\bar{A}_z = \begin{bmatrix} 0 & 0 \\ 0 & -\frac{1}{\tau_d} \end{bmatrix} \quad \bar{B}_z = \begin{bmatrix} 1 \\ \frac{1}{\tau_d} \end{bmatrix}$$

Equation 29, the controller output equation, becomes

$$f_c = \bar{C}_z \bar{z} + D_z \epsilon \quad (32)$$

$$\bar{C}_z = \left[C_i \quad -\frac{C_d}{\tau_d} \right] \quad D_z = C_p + \frac{C_d}{\tau_d}$$

Finally, we combine Eqs. 21, 24, 31 and 32 to obtain the state equation of the entire closed-loop system, which consists of both the laboratory structure and the dynamic PID controller:

$$\begin{bmatrix} \dot{\bar{x}} \\ \dot{\bar{z}} \end{bmatrix} = \begin{bmatrix} (\bar{A} + D_z \bar{B}_c \bar{C}_c) & \bar{B}_c \bar{C}_z \\ \bar{B}_z \bar{C}_c & \bar{A}_z \end{bmatrix} \begin{bmatrix} \bar{x} \\ \bar{z} \end{bmatrix} \quad (33)$$

The roots of Eq. 33 are evaluated by three PC-Matlab m-files (see Appendix B.7). These files generated results which allow a quick assessment of the effects of derivative and integral feedback on the basic proportional-control system. The results are shown on Figure 28. The root loci on Figure 28 suggest that derivative and integral feedback are not very helpful and that simple proportional feedback is the most effective. This, however, is a cursory evaluation, and a more detailed analysis would be required to determine with certainty the relative merits of proportional, integral, and derivative feedbacks in this control problem.

7.4 Experimental Results

To evaluate the analytical results described in the previous sections, the lateral suspension system was supplemented with an active feedback control system. As pictured in Figure 6, the "moving cart" was attached to a drive belt and driven by a small DC motor. The absolute position of the cart was read by a potentiometer directly driven by the belt/motor.

In Section 7.1 the error signal, ϵ , was derived as the difference of the cart absolute position and the test structure's absolute position measured at the nodal point of its 3-DOF rotation mode. To implement this error as a feedback control signal, the test structure described in Section 2.0 was instrumented with a Kaman non-contact displacement probe at a point near the node of the rotation mode. The use of the non-contact probe allowed sensitive displacement measurements to be made without adding friction to the system. However, the non-contact probe provides linear output over a maximum range of two inches. This limit did not prohibit the evaluation of the active control technique, but, in order to achieve even the two inch range, the largest diameter (also two inches) non-contact probe was required. This large diameter did not allow displacement measurement at precisely the rotation mode nodal point. Instead, the displacement over a much larger area was sensed and averaged thus introducing effects of the rotation mode.

The active control system was implemented with a digital controller made by Spectrum Signal Processing. This IBM-PC compatible controller card utilizes a Texas Instruments (TI), TMS320C25 Digital Signal Processing (DSP) microprocessor to allow high throughput rates and extremely fast data processing rates. This card is supplemented by an additional input/output (I/O) card to provide four simultaneous sampling input

channels. Each channel provides 12 bit analog-to-digital (A/D) conversion at sample rates up to 58 kHz. The I/O card also provides two output channels. It is apparent that the high sample rates and indeed even the digital controller are not required to implement such a simple control algorithm, but the system can be expanded to provide multiple control loops for several suspension devices. As such, a high speed, high data throughput system was purchased for evaluation. Once setup, the digital controller also allows very easy implementation of new control laws or the inclusion of derivative or integral feedback as described earlier.

The proportional control scheme as described in Section 7.2 was implemented in the controller. The assembly language listing of the control algorithm is shown in Appendix C. The two previously calibrated, absolute position measurements were read by the A/D inputs of the I/O card. The difference of the two signals was taken to obtain the error, ϵ . The error was multiplied by a gain and output by the I/O card. The lateral suspension motor was driven by the output signal after being amplified and conditioned by a servo amplifier.

Results of this simple evaluation were disappointing. Rather than providing a smoothly operating suspension system which follows the motion of the test structure, the motor was driven into a relatively high frequency, limit-cycle oscillation. This result was clearly not predicted by the earlier analyses. The oscillations were not difficult to account for after a simple examination of the system. The oscillations were occurring at a frequency of approximately 2 Hz, clearly above the lateral frequency of the test structure, but closely matching the cart mode frequency. The cart mode response was greatly enhanced by the additional mass and dynamics of the vertical suspension system which also has structural system modes at approximately 2 Hz. This enhanced response and

the vertical suspension dynamics were being sensed by the potentiometer and fed back into the error signal, thus driving the system unstable.

A consideration was given to try to filter the feedback signals. However, to achieve the large rolloff in frequency desired to eliminate the spurious mode response, a sharp (80 dB/oct) filter is necessary. Such filters were available but were also found to have phase shifts at 0.3 Hz as large as 60 degrees. Such large phase shifts in the controller bandwidth are not acceptable and the technique had to be abandoned.

It was felt that simplifying the hardware of the complete test apparatus would provide a better evaluation of the method. Unfortunately, it was not possible to include this alternative approach within the current effort. Thus, the experimental results for the active system remain inconclusive.

8.0 CONCLUDING REMARKS

Exploratory studies have been conducted for very low frequency suspension systems for dynamic testing of large, flexible space structures. An experimental 3 DOF suspension apparatus supporting a simulated large space structure has been analytically modelled, fabricated and tested. The characteristics of the passive lateral suspension system augmented with active feedback control was also studied.

Conclusions drawn from the results of these analytical and experimental studies include:

1. The ZSRM provided minimum vertical mode suspension frequencies below 0.1 Hz and allowed a maximum travel of +/- 3 inches.

2. The torsion suspension concept introduced in this report is effective in simulating unconstrained conditions for the first torsion mode of beam-like structures.
3. For the lateral suspension system, damping and friction forces in the moving cart mechanism (a linear bearing) severely limited the ability of the system to simulate zero-gravity conditions.
4. Analytical studies indicated that active proportional feedback control of the moving cart would eliminate the adverse effects of damping identified during tests of the lateral suspension system. Attempts to experimentally demonstrate active augmentation of the 3 DOF suspension test apparatus were not successful, however, due to dynamic instabilities resulting from coupling of the higher frequency spurious modes of the overall system.
5. The digital control card used in the active control implementation was found to have extensive capability and would be suitable for control of several control loops for multiple suspension devices. However, the interface to the controller requires programming in TI assembly language thus entailing extensive time for familiarization. Furthermore the DSP chip on the controller card is limited to fixed-point arithmetic which further complicates the programming. For future applications, newer, floating-point arithmetic DSP chips are now available (at much higher cost) and offer alternative operating system environments to ease some of the interfacing difficulties.

9.0 REFERENCES

1. Kienholz, D.A., Crawley, E.F., and Harvey, T.J.: "Very Low Frequency Suspension Systems For Dynamic Testing". AIAA Paper 89-1194, Proc. 30th Structures, Structural Dynamics, and Materials Conference, Mobile, AL, April 1989.
2. Gold, Ronald R., Reed, Wilmer H., III: "Preliminary Evaluation of Suspension Systems for 60-Meter MAST Flight System". DEI Report. No. C2602-008, February 1987.

APPENDIX A
SUSPENSION SYSTEM ASSEMBLY PROCEDURE

By Edward Y. Brandt

Included in this Appendix are instructions for the assembly and installation of the experimental suspension system. The procedures should be followed carefully to avoid damage to the system and for safety reasons. Proper assembly of the system requires the presence of two persons. The necessary tools include open ended wrenches (3/8, 7/16, 1/2 inch) and a set of allen wrenches. A drawing of the complete assembly is shown in Figure 6. This drawing identifies the components which are discussed in the assembly procedures.

I. ASSEMBLY

- A. The lateral system, including the linear bearing assembly, motor, potentiometer, gears and drive belt should be installed first. The aluminum bar on which the linear bearing assembly rests must be supported at either end at a height of at least 13 feet from the floor. It is important that the bar is level.

- B. With the lateral system in place, the vertical system can be assembled and mounted to the lateral system by the following procedures:
 - 1. Attach the upper and side plates of the vertical system mounting box to the linear bearing block, then connect the lower mounting plate and the horizontal support member.

2. Insert the upper flexure assemblies into the ends of the horizontal support member and bolt in place.

NOTE: There are four holes in two of the flexure blocks for flexure length adjustment. For the current configuration the bolt must go through the third hole from the inboard end to make the vertical members parallel.

3. Slip the vertical members onto the flexure blocks and bolt into place.

4. Insert the threaded rod through the horizontal support member and lower mounting plate. Secure in place with two nuts, one above and one below.

5. Slide the main spring attachment plate onto the threaded rod and secure with a nut.

NOTE: The location of the plate along the threaded rod will vary greatly depending on the amount of weight being supported and the size of the main springs being used.

6. Attach the eyebolts to the plate and hang main springs.

NOTE: If more extension of the main springs is required, remove the threaded rod and attach the eyebolts directly to the lower mounting plate. By doing so the length of the main springs will increase with a loss of adjustment travel.

7. With the weight box supported, hang the lower subassembly on the main springs from the eye bolts. This lower subassembly includes the center linkage members, the center and side flexures, the torsion suspension assembly, the cables and the weight box.

8. Remove the support and add weights to the box until the desired weight is attained.
9. With the desired weight in the weight box, adjust the main spring position on the threaded rod so that the lower horizontal members can be attached to the bottom of the vertical members. If more adjustment is needed, adjust the eyebolts evenly.
10. Slide the side spring mounting brackets up the vertical member and secure them about three inches up the tube.
11. Connect the vertical members to the lower horizontal members with the lower flexure assemblies. The vertical motion stops are also installed at this time as they share a common bolt.
12. Adjust the main spring tension until the lower horizontal members are level.
13. Allow the side spring mounting brackets to rest on the backplates. Attach eyebolts to the bracket opposite the force gage with the eyebolts in their most extended position.
14. Attach the eyebolts to the side spring attachment bar in their most extended position and connect side springs.
15. Grasp the bar firmly while supporting the structure and stretch the springs until the center hole engages on the force gage stud. A second person should

secure the vertical members and secure the spring attachment bar on the stud with a nut.

16. Increase the extension/pretension of the side springs by adjusting the side eye bolts and the nut securing the spring attachment bar. The side spring pretension can be set to the proper level using the force gauge. Minor adjustments will be required on the main spring tension during this process in order to center the system.

II. PROCEDURES FOR CHANGING THE SYSTEM WEIGHT

- A. Never attempt to remove or add weight to the box without securing the box firmly in a fixed position. The vertical motion stops are not designed to withstand the force of the main springs. If the weight is removed without the proper precautions, the three lower flexures will be damaged and will need to be replaced.
- B. An alternative to securing the weight box in a fixed position is to disassemble the lower portion of the system using this procedure:
 1. Loosen side spring tension at all four eyebolts.
 2. Remove the side spring attachment bar from the force gage stud. Have a second person remove the nut and help support the structure.
 3. Remove one of the eyebolts from the bar to allow springs to hang.

4. Remove flexure blocks and vertical motion stops.
5. Reload box to desired weight.
6. Adjust the position of the main springs to set the correct vertical position of lower horizontal members.
7. Re-assemble in reverse order.

APPENDIX B.1

2-DOF Model of Full System in 1-g with Cart Fixed

A PC-Matlab m-file called hz2dof.m calculates and plots the natural frequencies of Eq. 20 versus the parameter h (denoted Dh in all m-files). The m-file is:

```
%hz2dof.m mod 1 2/2/90 To calc and plot nat freqs of 2-dof dei model.
%First calc mass & stiffness matrices (ref. Gold's derivation & my
%10/27/89 re-derivation), then calc the nat freqs in Hz.
%Required input is Low, Inc, Hii for Dh=Low:Inc:Hii.
%Output is a plot of the two nat freqs versus Dh, which is h1-h2.
Mg=99.48;g=386.4;M=Mg/g;Mw=2/g;lw=338/g;l=1777/g;
Kx=.756;Kt=194.5;b=3;L=88.625;
j=0;
for Dh=Low:Inc:Hii
    j=j+1;
    Dhb=Dh+b;mas2=[M*L^2 -M*L*Dh;-M*L*Dh lw+l+M*Dh^2];
    stf2=[Kx*L^2+Mg*L -Kx*L*Dhb;-Kx*L*Dhb Kt+Mg*Dh+Kx*Dhb^2];
    Hz=(eig(stf2,mas2).^ .5)/(2*pi);
    H(j)=Dh;Freqs(j,1:2)=[Hz(1) Hz(2)];
end
plot(H,Freqs(:,1),H,Freqs(:,2),'--'),grid,ylabel('FREQUENCY in Hz'),
xlabel('DELTA-H in inches'),
title('NATURAL FREQUENCIES OF DEI 2-DOF MODEL')
```

The user runs hz2dof.m in PC-Matlab by first defining Low, Inc, and Hii, which are the low value, increment, and high value, respectively, of h , and then typing the m-file name, hz2dof. M-file hz2dof.m generates a plot, Figure 22, of the two undamped natural frequencies (in Hz) versus h .

The mode shapes for this case are also of interest, so a separate m-file, mode2dof.m, was written to calculate them:

```
%mode2dof.m 2/2/90 Calc modes of 2-dof cable- and spring-supported
```

```

%dei model, given a Dh = h1 - h2.
%First calc mass & stiffness matrices (ref. Gold's derivation & my
%10/27/89 re-derivation), then calc the mode shapes & nat freqs in Hz.
%Required input is a value of Dh.
%Output is modal matrix and freqs in Hz.
Mg=99.48;g=386.4;M=Mg/g;Mw=2/g;lw=338/g;l=1777/g;
Kx=.756;Kt=194.5;b=3;L=88.625;
Dhb=Dh+b;mas2=[M*L^2 -M*L*Dh;-M*L*Dh lw+l+M*Dh^2];
stf2=[Kx*L^2+Mg*L -Kx*L*Dhb;-Kx*L*Dhb Kt+Mg*Dh+Kx*Dhb^2];
[modal,vals]=eig(stf2,mas2);modal
freqs=diag(sqrtm(vals)/(2*pi))'

```

This m-file calculates and prints the undamped mode shapes and natural frequencies of Eq. 20. The input is h , and the output consists of the modal matrix and the frequencies in Hz. The following is a listing of some results calculated by mode2dof.m:

```
» Dh=-1.6;mode2dof
```

```
modal =
```

```

-0.0635  0.0415
 1.0000  1.0000

```

```
freqs =
```

```

0.5330  0.3302

```

```
» Dh=-1.4;mode2dof
```

```
modal =
```

```

0.0830  -0.0432
 1.0000  1.0000

```

```
freqs =
```

```
0.3764  0.5834
```

```
» Dh=0.0;mode2dof
```

```
modal =
```

```
0.8062  -0.0034  
1.0000  1.0000
```

```
freqs =
```

```
0.4263  0.9668
```

```
» Dh=2.0;mode2dof
```

```
modal =
```

```
1.0000  0.0226  
0.0056  1.0000
```

```
freqs =
```

```
0.4299  1.3686
```

The first two cases above, $h = -1.6''$ and $-1.4''$, illustrate PC-Matlab's curious mode-order switching that produces the discontinuous jumps on Figure 22 at about $h = -1.5''$. The modal vectors are in the DOFs $[\phi \ \theta]'$. If the ϕ component is large relative to the θ component, this means that the mode shape is primarily pendulum translation of the test structure; if, on the other hand, the θ component is much larger than the ϕ component, this means that the mode shape is primarily pendulum rotation of the test structure. When $h = 2''$, the lower mode at 0.4299 Hz is almost purely translation, and the higher mode at 1.3686 Hz is almost purely rotation; moreover, translation and rotation are similarly decoupled in the two modes for all values of h greater than $2''$. However, as h decreases below $2''$, rotation becomes progressively more dominant in both modes.

At $h = 0''$, translation and rotation are strongly coupled in the lower mode; and at $h = -1.6''$ and $-1.4''$, both modes are primarily rotational.

APPENDIX B.2

2-DOF Model of Test Structure in 0-g

This is the ideal case. The objective of the horizontal-motion control system is to produce modes of the full 3-DOF system which are as close as possible to the corresponding modes of this 0-g 2-DOF model. The PC-Matlab m-file modebase.m, which follows, calculates the natural vibration modes of Eq. 19.

```
%modebase.m mod 2 3/5/90 Calc modes of basic 2-dof spring-supported
%dei model with gravity turned off completely.
%First calc mass & stiffness matrices (ref. my derivation in [xo xe]'
%coordinates), then calc the mode shapes & nat freqs in Hz.
%There is no input.
%Output is modal matrix and freqs in Hz.
Mg=99.48;g=386.4;M=Mg/g;l=1777/g;lw=338/g;Kx=.756;Kt=194.5;b=3;
lob2=(l+lw)/b ^ 2;mas=[M+lob2 -lob2;-lob2 lob2];
Kcm=Kt/b ^ 2;stf=[Kcm -Kcm;-Kcm Kx+Kcm];
[modal,vals]=eig(stf,mas);modal
freqs=diag(sqrtm(vals)/(2*pi))'
```

No input is required to modebase.m, and the output consists of the modal matrix and natural frequencies in Hz:

```
» modebase
```

```
modal =
```

```
1.0000 0.0796
0.9634 1.0000
```

```
freqs =
```

```
0.2677 0.9666
```

The modal vectors are in the DOFs $[x_o \ x_e]^T$, so the lower mode at 0.2677 Hz is almost pure translation, and the higher mode at 0.9666 Hz is primarily rotation, with its nodal point just above the c.g. of the test structure.

APPENDIX B.3

3-DOF Model of Undamped Full System in 1-g

This is a useful theoretical case, even though it is not physically realizable due to the substantial friction in the linear bearing. A PC-Matlab m-file called hz3dof.m calculates and plots the natural frequencies of Eq. 16 (with $c_v = 0$ and $f_c = 0$) versus h . The m-file is:

```
%hz3dof.m 2/2/90 To calc and plot nat freqs of 3-dof dei model.
%First calc mass & stiffness matrices (ref. Gold's derivation & my
%10/27/89 re-derivation), then calc the nat freqs in Hz.
%Required input is Low, Inc, Hii for Dh=Low:Inc:Hii.
%Output is a plot of the three nat freqs versus Dh, which is h1-h2.
Mg=99.48;g=386.4;M=Mg/g;Mw=2/g;lw=338/g;l=1777/g;
b=3;L=88.625;Kx=.756;Kt=194.5;j=0;
for Dh=Low:Inc:Hii
    Dhb=Dh+b;j=j+1;
    mass=[Mw+M M*L -M*Dh;M*L M*L^2 -M*L*Dh;-M*Dh -M*L*Dh lw+l+M*Dh^2];
    stif=[Kx Kx*L -Kx*Dhb;Kx*L Kx*L^2+Mg*L -Kx*L*Dhb;
    -Kx*Dhb -Kx*L*Dhb Kt+Mg*Dh+Kx*Dhb^2];
    Hz=(eig(stif,mass).^ .5)/(2*pi);
    H(j)=Dh;Freqs(j,1:3)=[Hz(1) Hz(2) Hz(3)];
end
plot(H,Freqs(:,1),H,Freqs(:,2),'--',H,Freqs(:,3),'-.'),grid,
ylabel('FREQUENCY in Hz'),xlabel('DELTA-H in inches'),
title('NATURAL FREQUENCIES OF DEI 3-DOF CABLE-SUPPORTED MODEL')
```

The user runs hz3dof.m in PC-Matlab by first defining Low, Inc, and Hii, which are the low value, increment, and high value, respectively, of h , and then typing the m-file name, hz3dof. M-file hz3dof.m generates a plot, Figure 23, of the three undamped natural frequencies (in Hz) versus h . The plot of second mode frequency on Figure 23 seems almost identical to the corresponding plot on Figure 22 for the 2-DOF system with wheel-cart translation x_c suppressed. Figure 23 shows also the frequency of the third mode at about 2.37 Hz, which is almost independent of h over the range plotted. The mode

shapes for this case are also of interest, so a separate m-file, mode3dof.m, was written to calculate them:

```
%mode3dof.m 2/19/90 Calc modes of 3-dof cable- and spring-supported
%dei model (in [xc xo xe]' dofs), given a Dh = h1 - h2.
%First calc mass & stiffness matrices (ref. Gold's derivation & my
%10/27/89 re-derivation) + transformation to [xc xo xe]' dofs.
%Then calc the mode shapes in [xc xo xe]' dofs & nat freqs in Hz.
%Required input is a value of Dh.
%Output is modal matrix and freqs in Hz.
%Mass matrix mass and stiffness matrix stif are generated but not printed.
Mg=99.48;g=386.4;M=Mg/g;Mw=2/g;lw=338/g;l=1777/g;
b=3;L=88.625;Kx=.756;Kt=194.5;Dhb=Dh+b;
mass=[Mw+M M*L -M*Dh;M*L M*L^2 -M*L*Dh;-M*Dh -M*L*Dh lw+l+M*Dh^2];
stif=[Kx Kx*L -Kx*Dhb;Kx*L Kx*L^2+Mg*L -Kx*L*Dhb;
-Kx*Dhb -Kx*L*Dhb Kt+Mg*Dh+Kx*Dhb^2];
T=[1 0 0;-1/L Dhb/(L*b) -Dh/(L*b);0 1/b -1/b];
mass=T'*mass*T;stif=T'*stif*T;
[modal,vals]=eig(stif,mass);modal
freqs=diag(sqrtm(vals)/(2*pi))'
```

This m-file calculates and prints the undamped mode shapes and natural frequencies of Eq. 16 (with $c_v = 0$ and $f_c = 0$). The input is h , and the output consists of the modal matrix and the frequencies in Hz. The following is a listing of some results calculated by mode3dof.m:

```
» Dh=-0.5;mode3dof
```

```
modal =
```

```
    1.0000    1.0000    0.2866
   -0.0204    0.9956    0.0998
   -0.0222    0.9462    1.0000
```

```
freqs =
```

2.3679 0.2632 0.8394

» Dh=0.0;mode3dof

modal =

1.0000	1.0000	0.0937
-0.0204	0.9872	0.0777
-0.0205	0.9511	1.0000

freqs =

2.3675 0.2650 0.9666

» Dh=0.5;mode3dof

modal =

1.0000	1.0000	-0.1135
-0.0204	0.9824	0.0662
-0.0187	0.9539	1.0000

freqs =

2.3678 0.2660 1.0788

The modal vectors are in the DOFs $[x_c \ x_o \ x_e]'$. It is clear from the results above, therefore, that the third mode at about 2.37 Hz is predominantly translation of the wheelcart, with very little motion of the test structure.

APPENDIX B.4

Damping Constant Representing Linear Bearing Friction

The calculation procedure in PC-Matlab follows. First, specify a h value (all results to follow are for $h = 0$ ") and run the m-file mode3dof.m presented in Appendix B.3; this generates the mass and stiffness matrices for the model and the mode shape to be used for the initial condition. Next, specify a value of c_v and run the m-file veloresp.m:

```
%veloresp.m 3/02/90 Calc time response to an initial velocity state
%of 3-dof cable- and spring-supported dei model (in [xc xo xe]' dofs),
%given a Dh = h1 - h2, and a cart viscous damping coefficient Cv.
%First, run mode3dof.m (requiring input Dh), which produces mass, stif,
%and modal. Then run this program, supplying input Cv.
stateic=[modal(:,2); zeros(3,1)];
minv=inv(mass);A=[-minv*diag([Cv 0 0]) -minv*stif;eye(3) zeros(3)];
Bc=[minv*[1 0 0]';zeros(3,1)];C=[0 0 0 1 0 0;0 0 0 0 1 0];D=[0;0];
t=0:.1:20;U=zeros(length(t),1);
resp=lsim(A,Bc,C,D,U,t,stateic);
plot(t,resp(:,1),t,resp(:,2),'-'),grid,xlabel('TIME sec')
ylabel('DISPLACEMENT inch'),
title('RESP. TO VELOCITY INITIAL CONDITION WITH PENDULUM MODE SHAPE')
```

APPENDIX B.5

Proportional Control

```
%statmats.m mod 1 3/04/90 Calc state matrices of 3-dof cable- and
%spring-supported dei model (in [xc xo xe]' dofs), given a Dh = h1 - h2,
%Cv = the viscous damping coefficient of the cart bearing,
%and dob = the ratio d/b. Required inputs are Dh, Cv and dob.
%The matrices calculated are the 3x3 mass, minv, and stif, and
%      A = the 6x6 plant state matrix,
%      Bc = the 6x1 control input matrix,
%      Bd = the 6x1 disturbance input matrix for excitation fe,
%      C = the 1x6 output matrix for measuring xe,
%      D = [0],
%      Ceps = the 1x6 output matrix for eps = xd - xc.
Mg=99.48;g=386.4;M=Mg/g;Mw=2/g;lw=338/g;l=1777/g;lt=l+lw;mi=1/M;
b=3;L=88.625;Kx=.756;Kt=194.5;Dhb=Dh+b;m3=lt/b ^ 2;Kg=M*g/L;RDh=Dh/b;
RDhb=RDh+1;k1=Kg*RDhb;k2=Kg*RDh;k3=Kt/b ^ 2;k4=-(k3+k2*(L/b+RDhb));
mass=[Mw 0 0;0 M+m3 -m3;0 -m3 m3];minv=[1/Mw 0 0;0 mi mi;0 mi mi+1/m3];
stif=[Kg -k1 k2;-k1 k3+Kg*(RDhb ^ 2+RDh*L/b) k4;k2 k4 Kx+k3+k2*(L/b+RDh)];
A=[-minv*diag([Cv 0 0]) -minv*stif;eye(3) zeros(3)];
Bc=[minv*[1 0 0]';zeros(3,1)];Bd=[minv*[0 0 1]';zeros(3,1)];
C=[0 0 0 0 0 1];D=[0];Ceps=[0 0 0 -1 dob 1-dob];
```

The eigenvalues and eigenvectors of \overline{A}_c reflect the character of the closed-loop system, Eq. 27. The procedure for calculating relevant parts of the eigensolution with PC-Matlab follows. First, specify values for h , c_v and d/b . The eigenvalues and eigenvectors of \overline{A}_c vary with feedback constant C_p . Hence, next specify an array of C_p values with the statement "Cp=1st value:increment:last value" (supply numerical values for 1st value, etc.), or with a "logspace" statement if an array equally spaced on the logarithmic scale is desired. Then run m-file proprloc.m:

```
%proprloc.m (04 Apr 90): Proportional control of horizontal motion;
%program plots locus of damped freqs vs. zetas of translation mode of
%3-DOF model as proportional feedback constant Cp varies;
%Action req'd to execute:
% First enter values for Dh, Cv and dob;
% next enter 'Cp=1st value:increment:last value;proprloc',
```

```

%where Cp is the array of equally spaced proportional feedback constants,
%which is printed out.
%Output: plot of frequency (Hz) vs. zeta for translation mode.
i=0;twopi=2*pi;j=sqrt(-1);statmats;Cp
for cp=Cp;
    i=i+1;
    a1=A+cp*Bc*Ceps;
    roots=eig(a1);sigmas=real(roots);omegas=imag(roots);
    zetas=-sigmas./sqrt(sigmas.^2 + omegas.^2);freqs=abs(omegas)/twopi;
    comfreqs(:,i)=zetas + j*freqs;
end
zpjf=comfreqs(3,:);frqvszta=zpjf.';plot(frqvszta,'x'),grid,
xlabel('ZETA'),ylabel('FREQ Hz'),title('FREQUENCY vs. DAMPING')

```

M-file proprloc.m uses statmats.m, and it calculates and plots the locus of complex eigenvalues of the translation mode of $\overline{A_c}$ as C_p varies.

APPENDIX B.6

Rigid-Body Modes

For the open-loop case, m-file olcvrl.m was modified to give k0olcvrl.m:

```
%k0olcvrl.m 4/23/90 Stiffnesses Kx and Kt
%set to zero, and with Mg=100, Mw=5.65/g, and L=62.125
%Action req'd to execute:
% First enter a value for Dh; next define an array of Cv values,
% as, for example with 'Cv=logspace(0,1)'; finally type 'k0olcvrl'
%Output: root locus plot
Mg=100.0;g=386.4;M=Mg/g;Mw=5.65/g;lw=338/g;l=1777/g;lt=l+lw;mi=1/M;
b=3;L=62.125;Kx=0;Kt=0;Dhb=Dh+b;m3=lt/b^2;Kg=M*g/L;RDh=Dh/b;
RDhb=RDh+1;k1=Kg*RDhb;k2=Kg*RDh;k3=Kt/b^2;k4=-(k3+k2*(L/b+RDhb));
mass=[Mw 0 0;0 M+m3 -m3;0 -m3 m3];minv=[1/Mw 0 0;0 mi mi;0 mi mi+1/m3];
stif=[Kg -k1 k2;-k1 k3+Kg*(RDhb^2+RDh*L/b) k4;k2 k4 Kx+k3+k2*(L/b+RDh)];
i=0;twopi=2*pi;j=sqrt(-1);
for cv=Cv;
    i=i+1;A=[-minv*diag([cv 0 0]) -minv*stif;eye(3) zeros(3)];
    roots(:,i)=eig(A);
end
plot(roots,'x'),grid,xlabel('REAL PART'),ylabel('IMAG PART')
title('LOCUS OF ROOTS OF UNSPRUNG 3-DOF MODEL AS Cv VARIES')
```

For the closed-loop case m-file proprloc.m was modified to give k0prrrloc.m:

```
%k0prrrloc.m 4/23/90 Similar to proprloc.m, but calling k0statmt.m so
%that stiffnesses are set to zero and some other parameters are updated
%proprloc.m (04 Apr 90): Proportional control of horizontal motion;
%root locus of 3-DOF model as proportional feedback constant Cp varies;
%Action req'd to execute:
% First enter values for Dh, Cv and dob;
% next enter an array for Cp;'k0prrrloc'
%Output: loci of all roots as Cp varies
i=0;twopi=2*pi;j=sqrt(-1);k0statmt
for cp=Cp;
    i=i+1;
    a1=A+cp*Bc*Ceps;roots(:,i)=eig(a1);
end
plot(roots,'x'),grid,xlabel('REAL PART'),ylabel('IMAG PART')
title('LOCUS OF ROOTS OF UNSPRUNG 3-DOF MODEL AS Cp VARIES')
```

M-file k0statmt.m referred to in k0prrlloc.m is the same as statmats.m, except that the values for k_x , k_θ , mg , $m_w g$ and ℓ were changed as stated above. Results of k0prrlloc.m are recorded on Figures 27 a-c.

APPENDIX B.7

PID CONTROL

Given a single value for each of the PID coefficients, pidroots.m listed below calculates all of the roots:

```
%pidroots.m 22 Apr 1990
%enter Dh, then run mode3dof.m, then run dobcalc.m to calc dob
%Enter Cv; then run statmats.m to calc A, Bc and Ceps
%Enter taud; prog. calcs Az and Bz
%Specify Cp and Ci and Cd;prog. calls freqzeta to calc roots
itaud=1/taud;Az=[0 0;0 -itaud];Bz=[1;itaud];A21=Bz*Ceps;
con=Cd/taud;Cz=[Ci -con];Dz=Cp+con;
a=[A+Dz*Bc*Ceps Bc*Cz;A21 Az];freqzeta
```

Two m-files calculate the loci of translation mode roots of Eq. 33 as controller coefficients vary. Program pidrlocd.m calculates the locus as C_d varies, with C_p and C_i fixed:

```
%pidrlocd.m 27 Apr 1990 Calculates the freq-zeta locus of the transl.
%mode of the 3-DOF model as derivative coefficient Cd varies.
%enter Dh, then run mode3dof.m, then run dobcalc.m to calc dob
%Enter Cv; then run statmats.m to calc A, Bc and Ceps
%Enter taud; prog. calcs Az and Bz
%Specify Cp and Ci and an array of values for Cd.
itaud=1/taud;Az=[0 0;0 -itaud];Bz=[1;itaud];A21=Bz*Ceps;
i=0;j=sqrt(-1);twopi=2*pi;Cd
for cd=Cd
    i=i+1;con=cd/taud;Cz=[Ci -con];Dz=Cp+con;
    a=[A+Dz*Bc*Ceps Bc*Cz;A21 Az];
    roots=eig(a);sigmas=real(roots);omegas=imag(roots);
    zetas=-sigmas./sqrt(sigmas.^2 + omegas.^2);freqs=abs(omegas)/twopi;
    comfreqs(:,i)=zetas + j*freqs;
end
zpjf=comfreqs(6,:);frqvszta=zpjf.';plot(frqvszta,'x'),grid,
xlabel('DAMPING FACTOR, ZETA'),ylabel('DAMPED FREQ Hz'),
title('LOCUS OF FREQ-ZETA OF 3-DOF CL-PID MODEL AS Cd VARIES')
```

Similarly, pidrloci.m calculates the locus as C_i varies, with C_p and C_d fixed:

```

%pidrloci.m 27 Apr 1990 Calculates the freq-zeta locus of the transl.
%mode of the 3-DOF model as integral coefficient Ci varies.
%enter Dh, then run mode3dof.m, then run dobcalc.m to calc dob
%Enter Cv; then run statmats.m to calc A, Bc and Ceps
%Enter taud; prog. calcs Az and Bz
%Specify Cp and Cd and an array of values for Ci.
itaud=1/taud;Az=[0 0;0 -itaud];Bz=[1;itaud];A21=Bz*Ceps;
i=0;j=sqrt(-1);twopi=2*pi;Ci
for ci=Ci
    i=i+1;con=Cd/taud;Cz=[ci -con];Dz=Cp+con;
    a=[A+Dz*Bc*Ceps Bc*Cz;A21 Az];
    roots=eig(a);sigmas=real(roots);omegas=imag(roots);
    zetas=-sigmas./sqrt(sigmas.^2 + omegas.^2);freqs=abs(omegas)/twopi;
    comfreqs(:,i)=zetas + j*freqs;
end
zpjf=comfreqs(6,:);frqvszta=zpjf.';plot(frqvszta,'x'),grid,
xlabel('DAMPING FACTOR, ZETA'),ylabel('DAMPED FREQ Hz'),
title('LOCUS OF FREQ-ZETA OF 3-DOF CL-PID MODEL AS Ci VARIES')

```

To generate the results shown on Figure 28, each of the three m-files was run separately, and its root locus was saved (with the "save" command in PC-Matlab). Then all three loci were loaded together (with the "load" command in PC-Matlab) and plotted on the same graph.

APPENDIX C

DIGITAL CONTROLLER PROGRAM

The control program implemented in the Spectrum Signal Processing TMS320C25 System Board is listed below. The program is written in TI (Texas Instruments) COFF assembly language. The program is compiled and linked with the TI COFF Assembler and Linker programs supplied with the system. To implement the executable program in the system board it must be downloaded using the Spectrum MON25 monitor program also supplied with the system.

```
*****
*                                     *
*                                     *
*       Two Channel Sample           *
*       With output proportional to error *
*               TMS320C25           *
*                                     *
*                                     *
*****
```

```
* Author   :   R. Gold
*           :   Dynamic Engineering, Inc.
* Tel      :   (804) 873-1344
* Date    :   4/23/90
```

```
* 320C25 LINKS
```

```
* DEFINE ADDRESS CONSTANTS
```

```
VAL0: .equ 01h
VAL1: .equ 02h
AY0: .equ 03h
AY1: .equ 04h
ERR: .equ 05h
TIMER: .equ 09h
STAT: .equ 08h
CTRL: .equ 08h
```

```

ADC:    .equ    0Ah
DAC0:   .equ    0Ah

CONB:   .equ    0500h
INB:    .equ    0510h

```

*** DATA CONSTANTS**

```

CH0:    .equ    090h
CH1:    .equ    0D1h

```

*** PROGRAM**

```

.sect "AORG0"
CNFD
LDPK    06h           ;Set address page

LARP    05h
LRLK    AR5,CONB
RPTK    06h           ;Move data into
BLKP    TAB0,*+      ;data memory

LACK    00h           ;Toggle calibration bit (5)
SACL    VAL0
OUT     VAL0,CTRL
LACK    020h
SACL    VAL0
OUT     VAL0,CTRL
LACK    00h
SACL    VAL0
OUT     VAL0,CTRL

CAL    IN    VAL1,STAT ;Read status reg
      LAC    VAL1     ;Mask calibration bit
      ANDK   020h     ;Loop till calibration complete
      BZ     CAL

```

LALK	0FCE1h	;Load 10 kHz sample rate to timer
SACL	VAL0	
OUT	VAL0,TIMER	
IN	VAL1,ADC	;Clear status flags eoc and timeout
LRLK	01h,INB	;Set table pointers to table ;base addresses
START	LRLK	02h,CONB+02h
LALK	CH0	;Select channel 0 for conversion
SACL	VAL0	;send out control word
OUT	VAL0,CTRL	
EOC0	IN	VAL1,STAT ;Read status reg
LAC	VAL1	;Mask eoc bit
ANDK	080h	;Loop till conversion complete
BZ	EOC0	
IN	AY0,ADC	;Read channel 0 data
LALK	CH1	;Select channel 1 for conversion
SACL	VAL0	;send out control word
OUT	VAL0,CTRL	
EOC1	IN	VAL1,STAT ;Read status reg
LAC	VAL1	;Mask eoc bit
ANDK	080h	;Loop till conversion complete
BZ	EOC1	
IN	AY1,ADC	;Read channel 1 data
LARP	02h	
LAC	AY1	
SUB	*+	
LARP	01h	
SACL	*	
LT	*	
LARP	02h	

MPY	*+
PAC	
ADD	*+
SUB	AY0
SACL	ERR
LT	ERR
MPY	*
PAC	
SACL	VAL0
OUT	VAL0,DAC0
B	START

TAB0: .word 090h,0D1h,0CB2h,09h,1C71h,02h

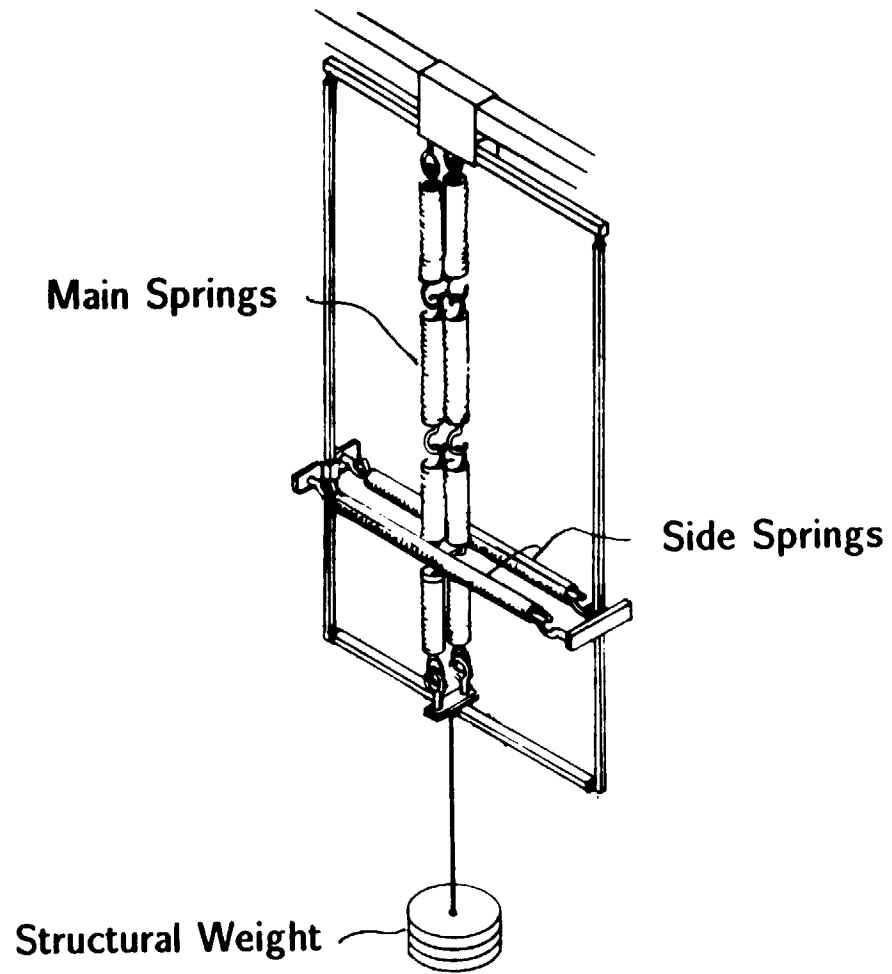


Figure 1. Vertical Suspension Test Apparatus

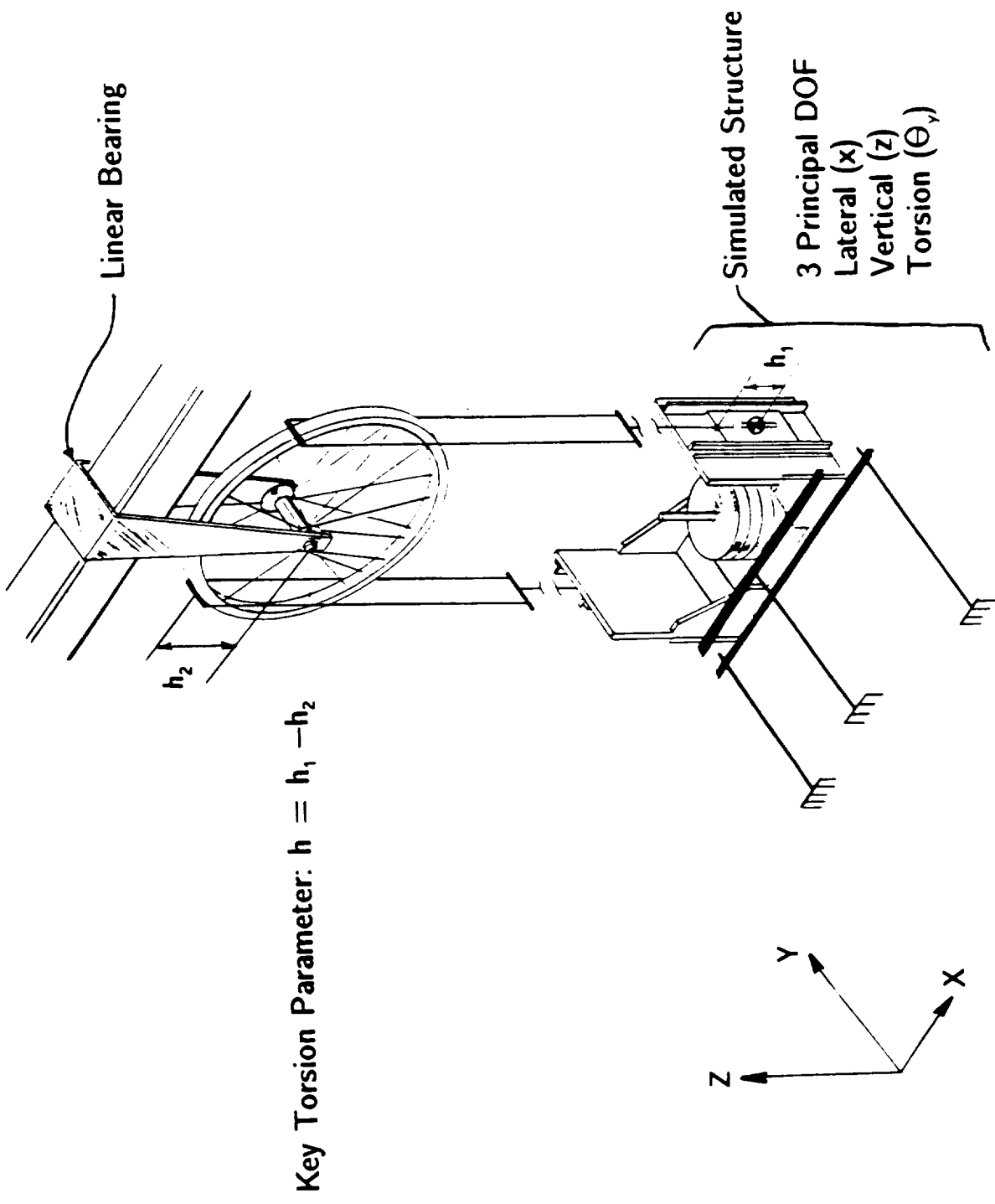
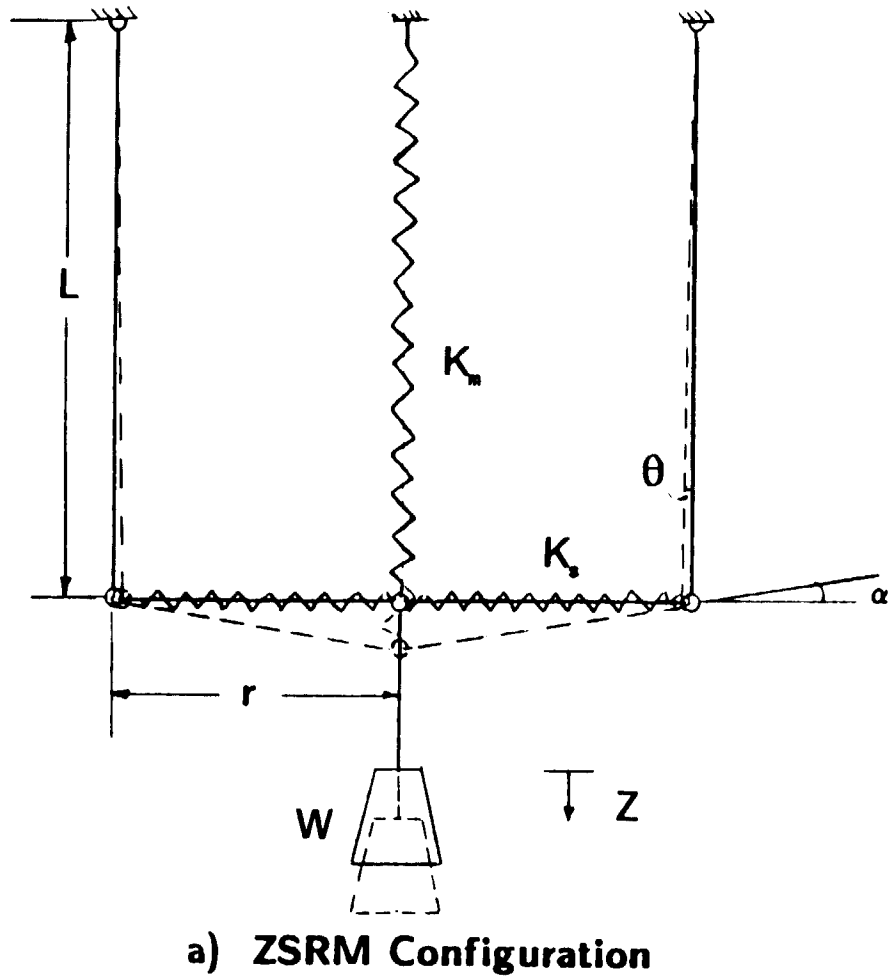


Figure 2. Lateral/Torsion Suspension Test Apparatus



b) Forces Acting at Center Point

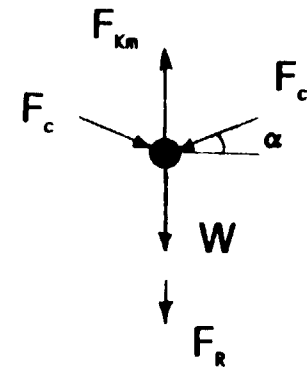


Figure 3. Zero Spring Rate Mechanism (ZSRM)

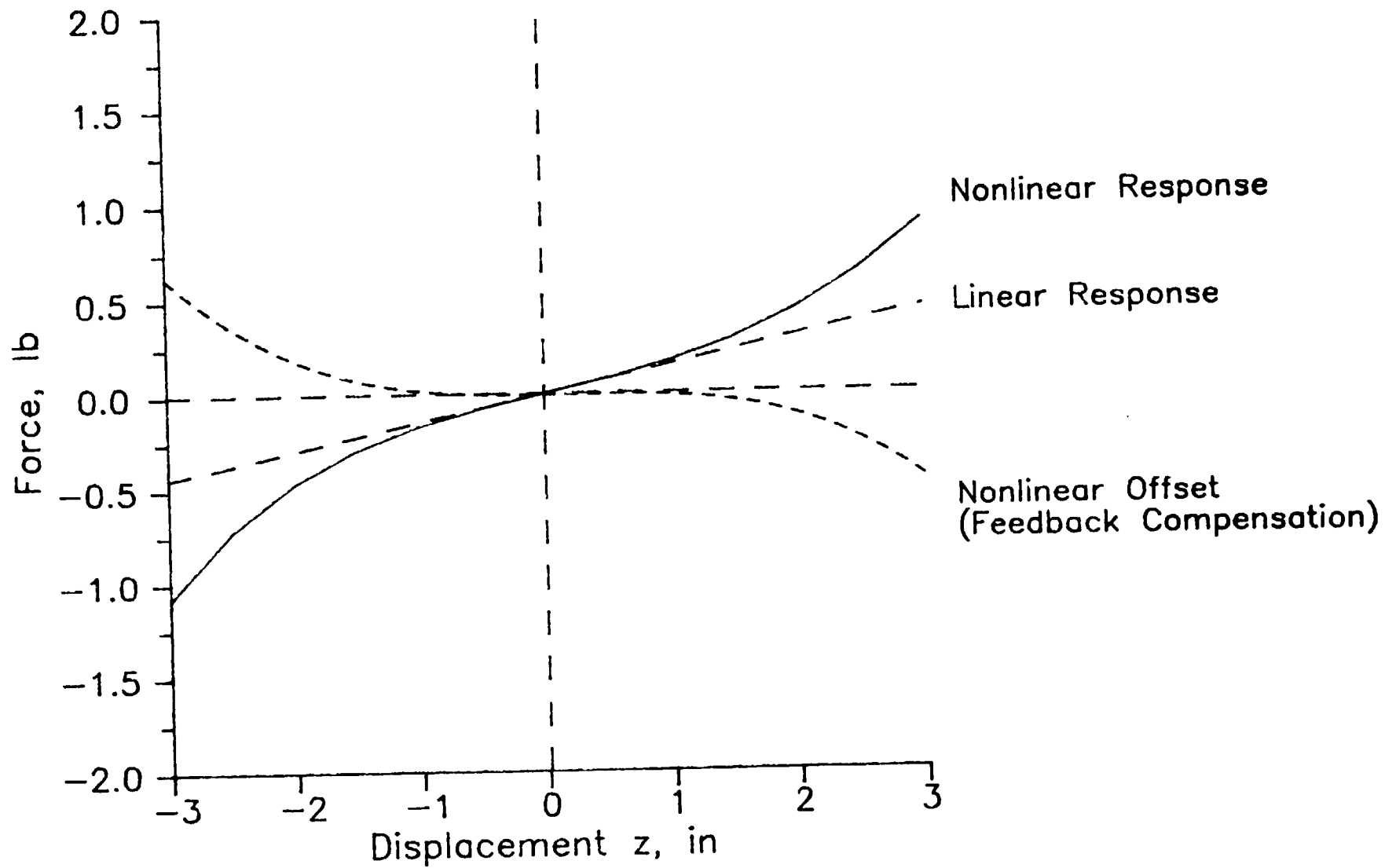
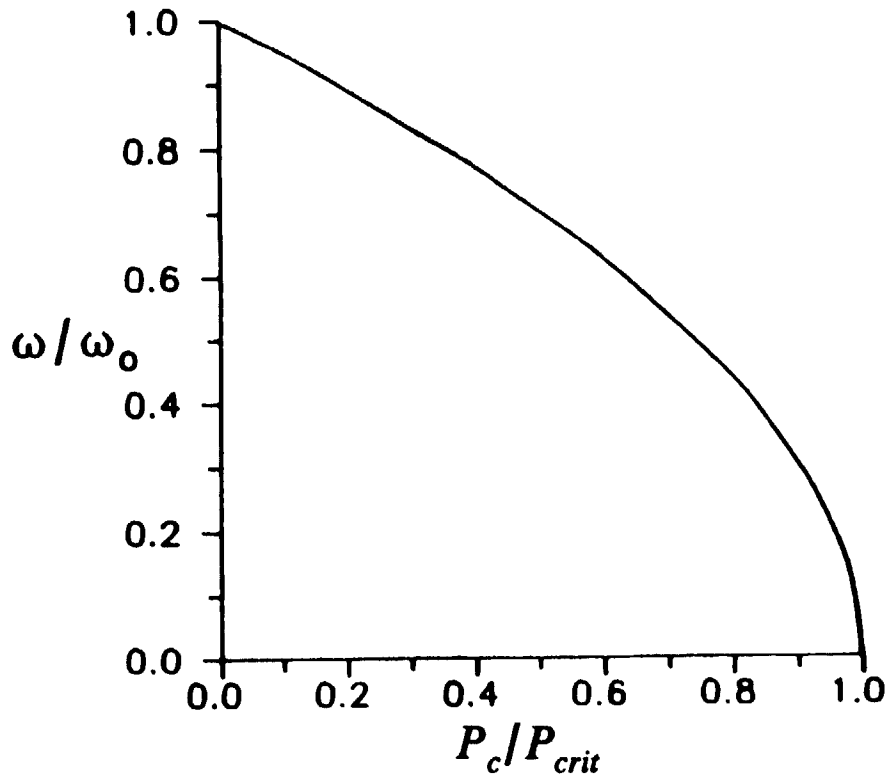


Figure 4. ZSRM Stiffness Characteristics



$$\omega_0 = \sqrt{\frac{K_m}{W/g}}$$

$$P_{crit} = \frac{K_m r}{2}$$

Figure 5. Effect of Side Spring Preload on System Frequency

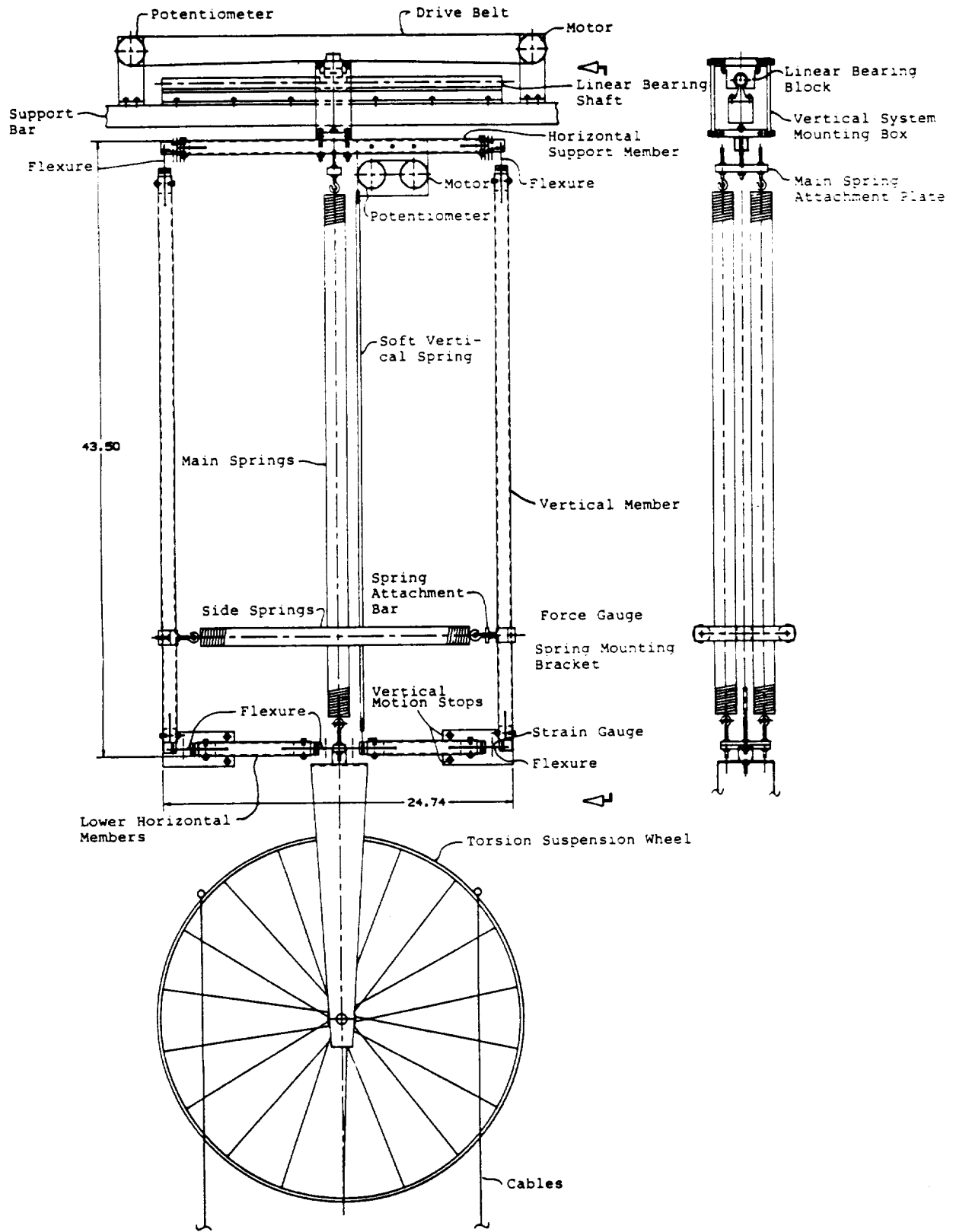


Figure 6. 3-DOF Suspension Test Apparatus

ORIGINAL PAGE IS
OF POOR QUALITY

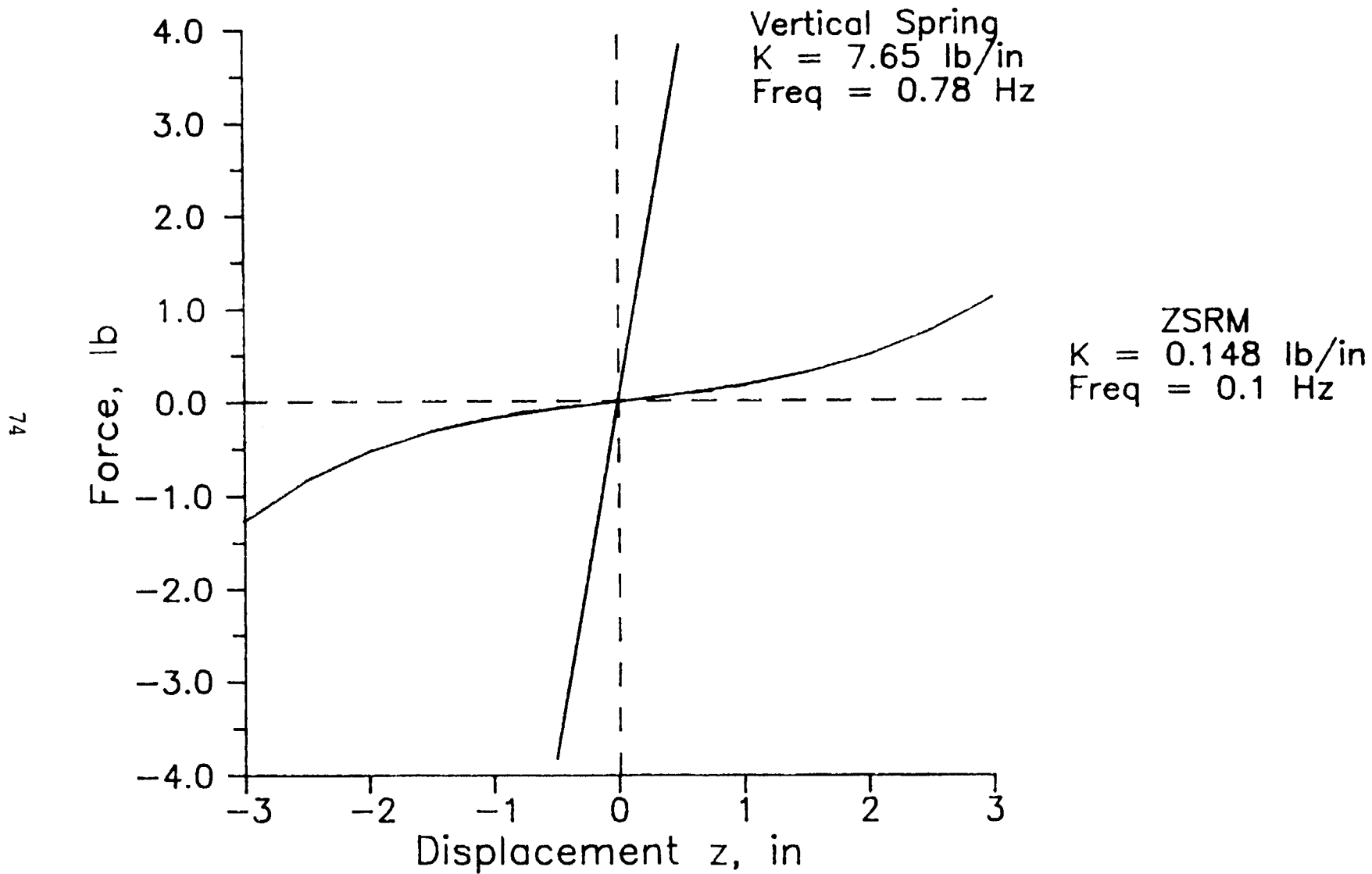


Figure 7. Stiffness and Frequency Comparisons, Main Spring vs. ZSRM

VERTICAL SUSPENSION 145 LB 1/19/90
1Hz A: AC/50mV B: AC/0.1V INST 0/16 DUAL 1k

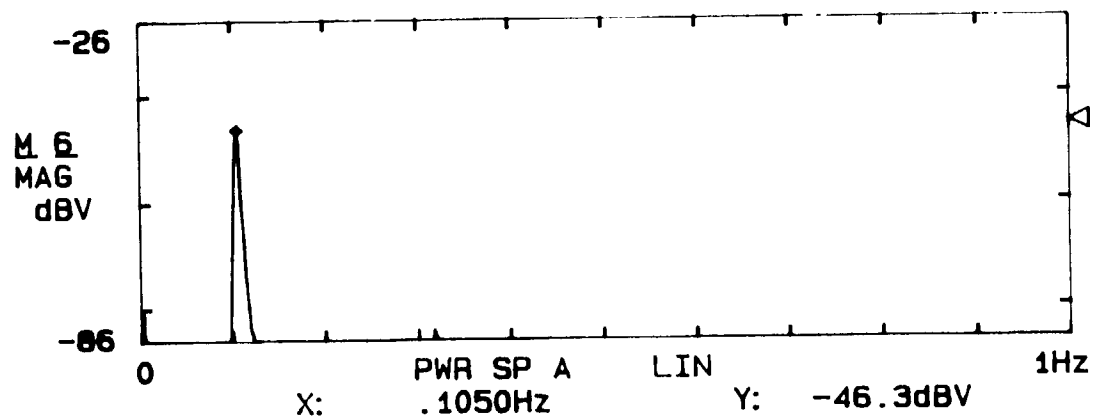
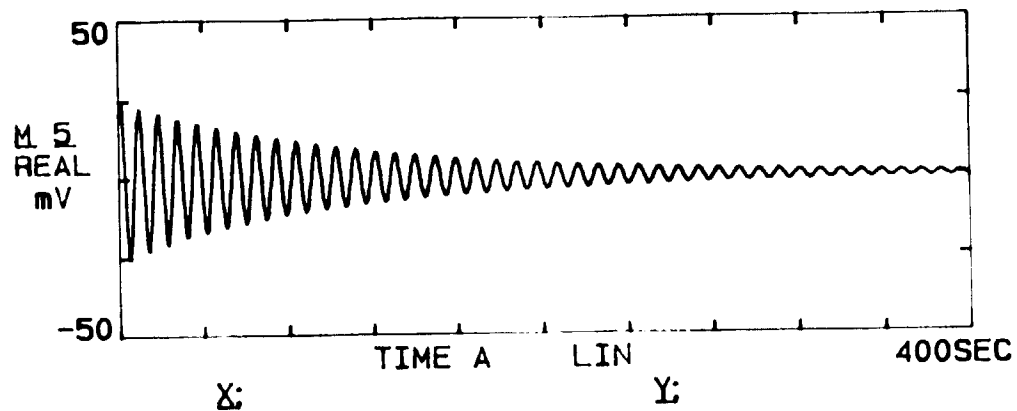
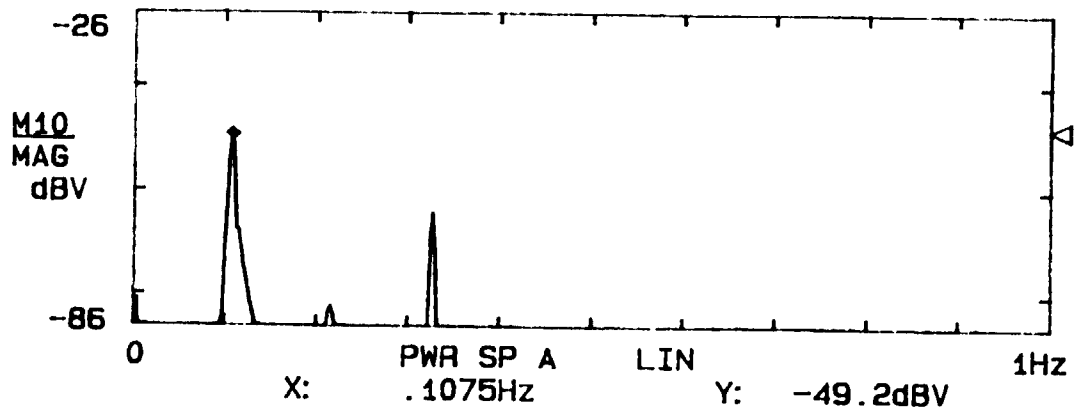
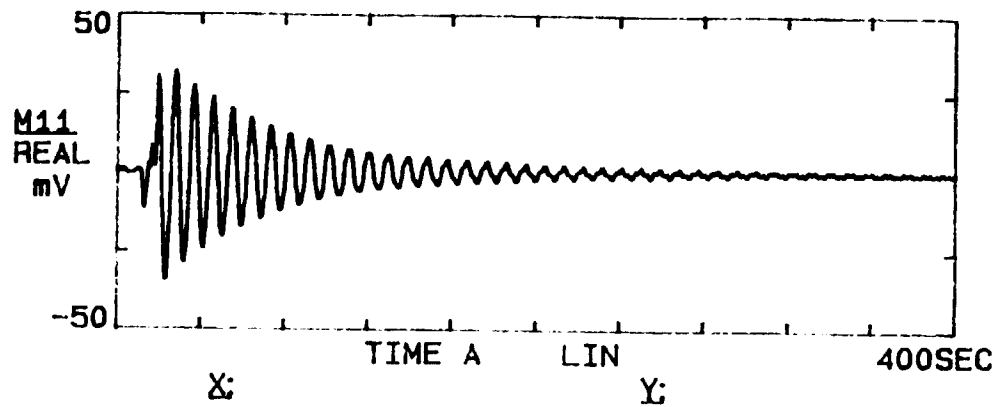


Figure 8a. Vertical Suspension Test Results, 145 lb Load

VERTICAL SUSPENSION 80. LB 4/19/90 06:56
100KHZ A: AC/ 50V B: AC/ 50V INST 0/16 DUAL 1K



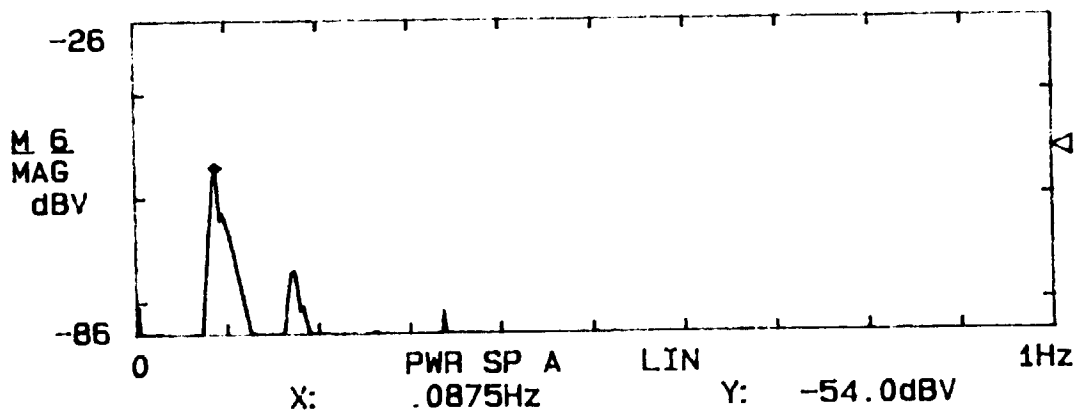
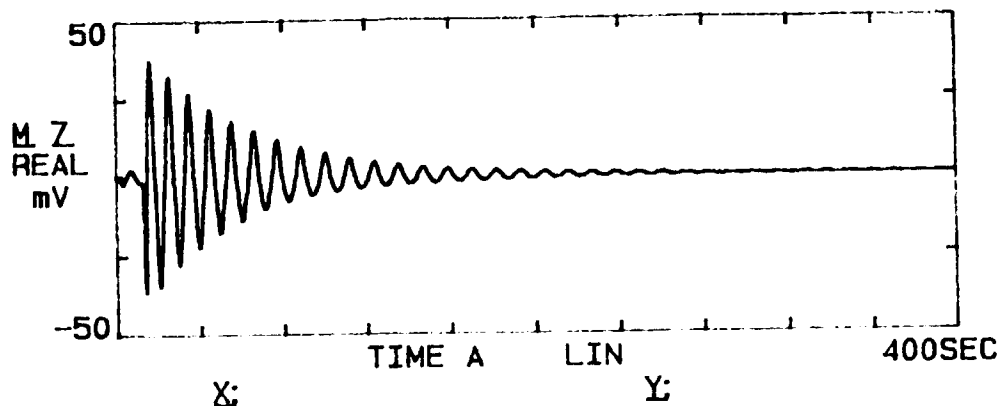
FILE No. 075

00:17

76

Figure 8b. Vertical Suspension Test Results, 80 lb Load

VERTICAL SUSPENSION 42.5 LB 4/19/90 05:38
 100kHz A: AC/ 50V B: AC/ 50V INST 0/16 DUAL 1k



00: 12

Figure 8c. Vertical Suspension Test Results, 42.5 lb Load

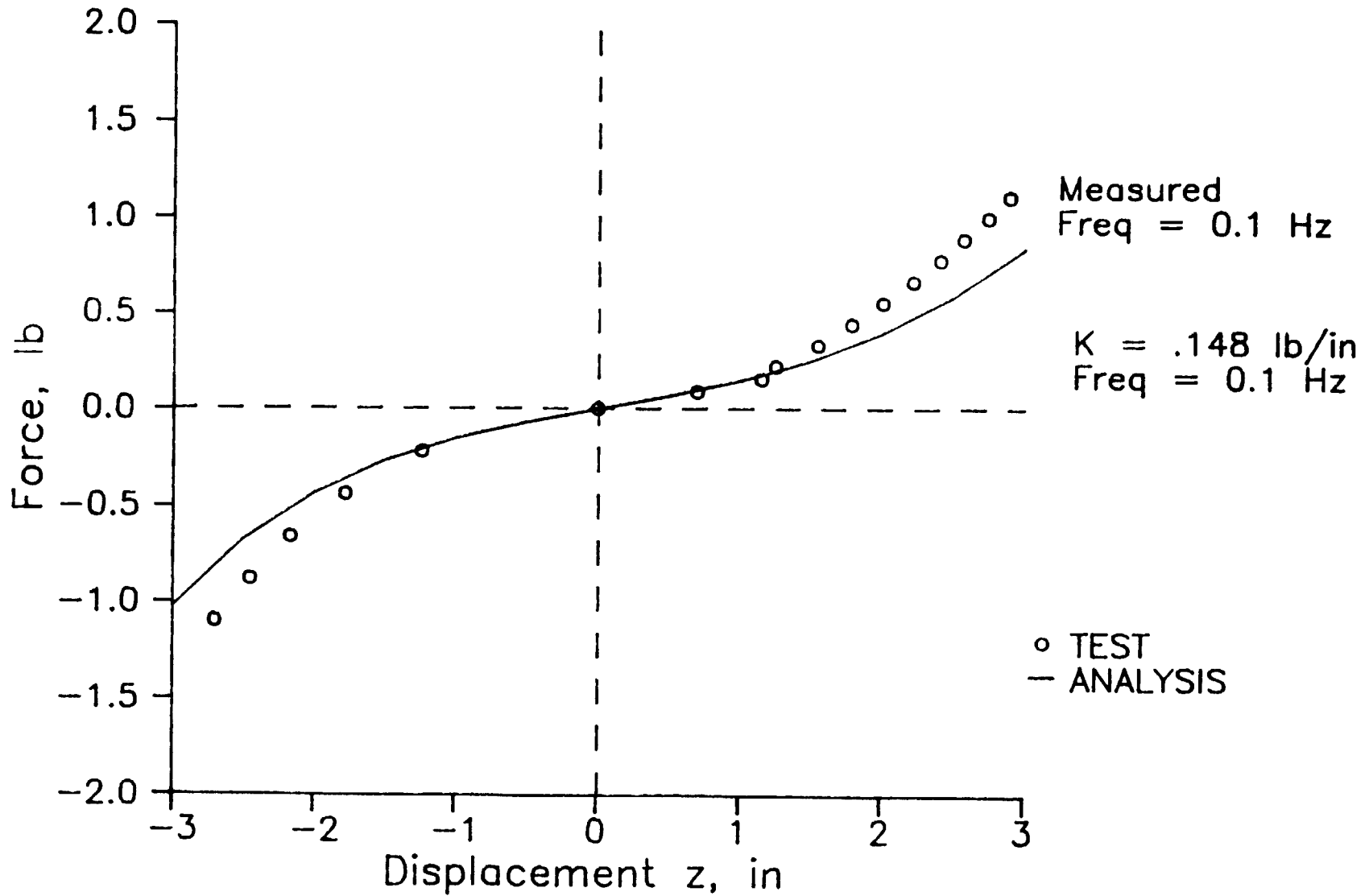


Figure 9a. Comparison of Analytical and Experimental Results, 145 lb Load

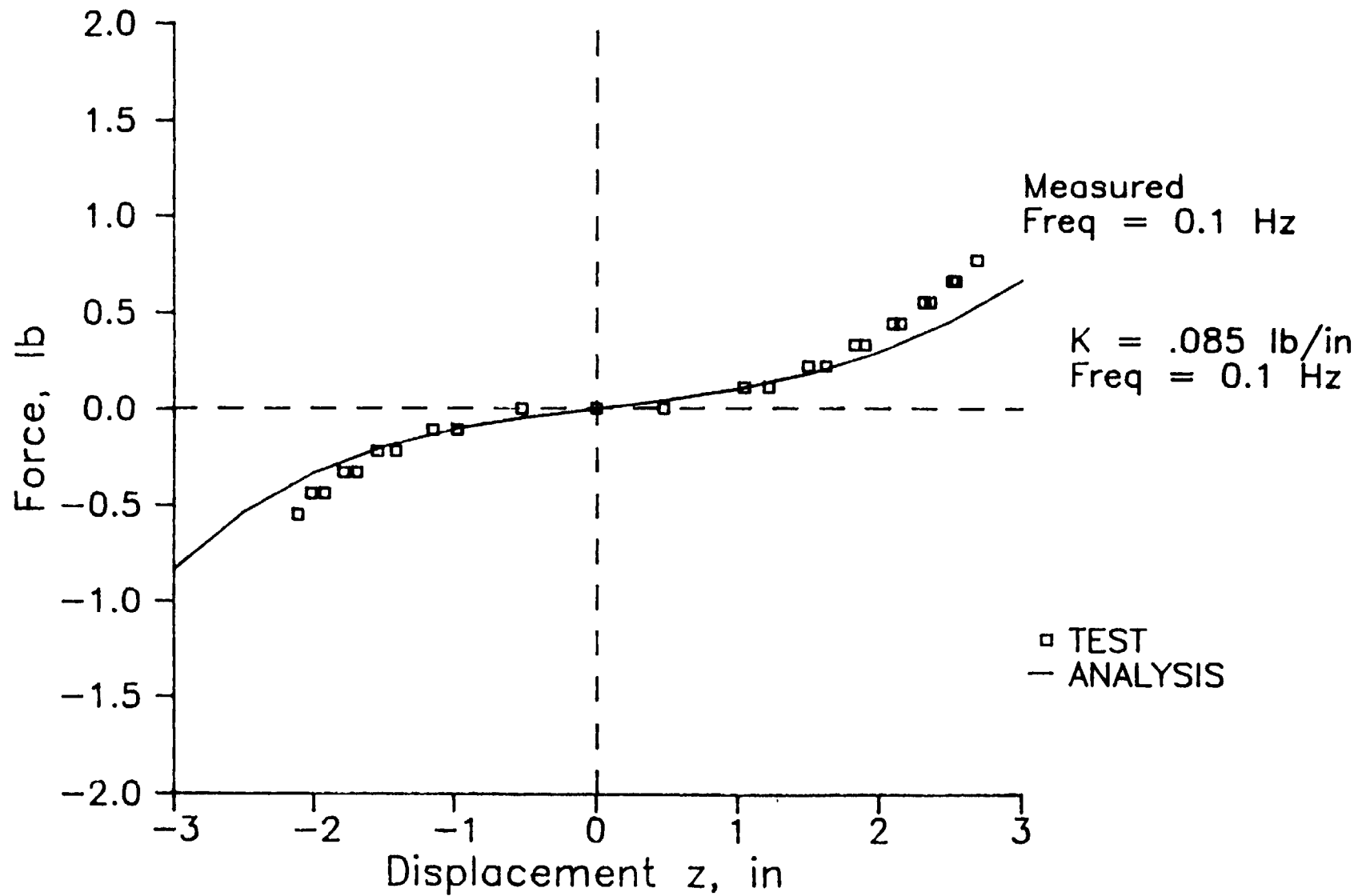


Figure 9b. Comparison of Analytical and Experimental Results, 80 lb Load

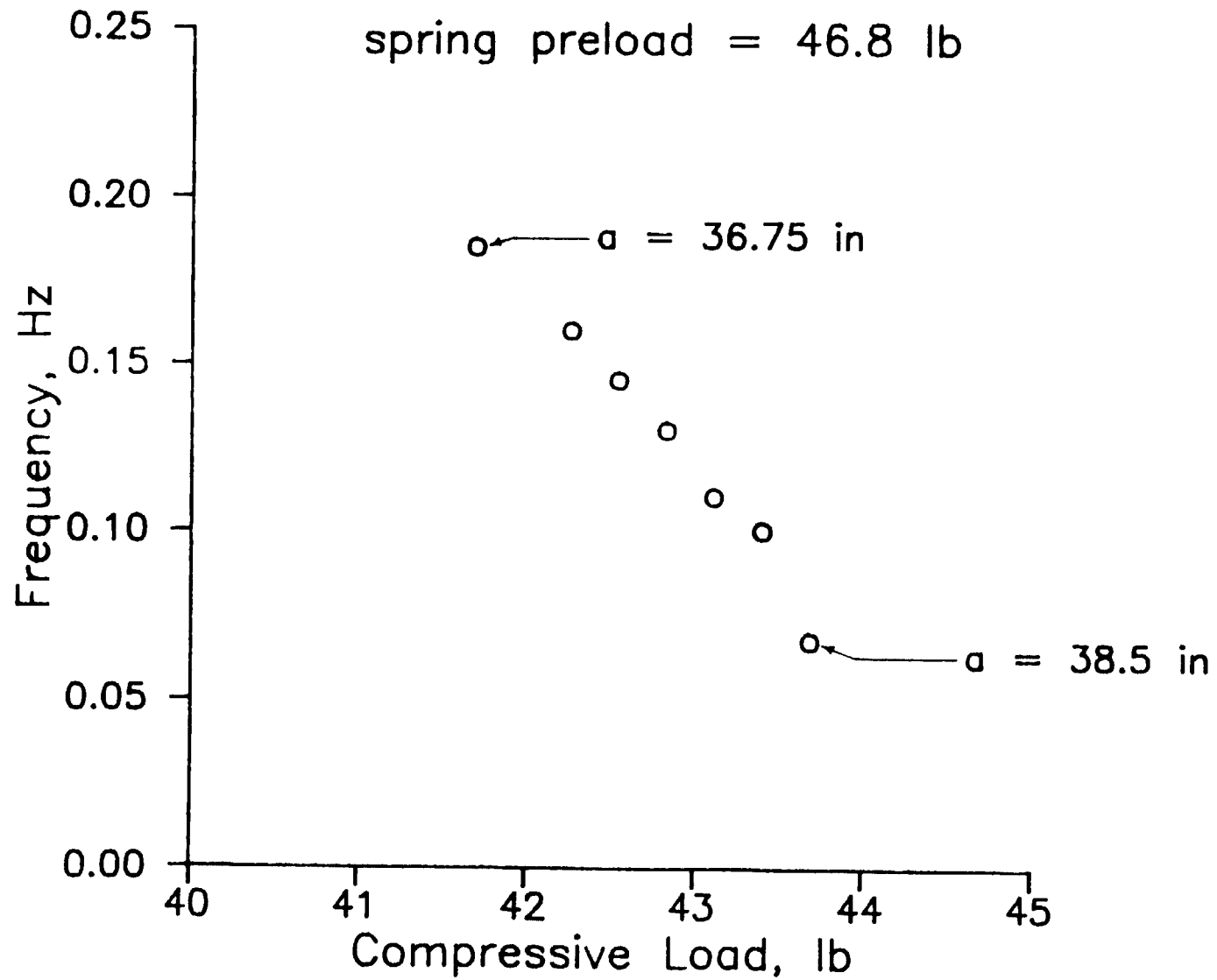


Figure 10. Change in Frequency with Side Spring Vertical Location

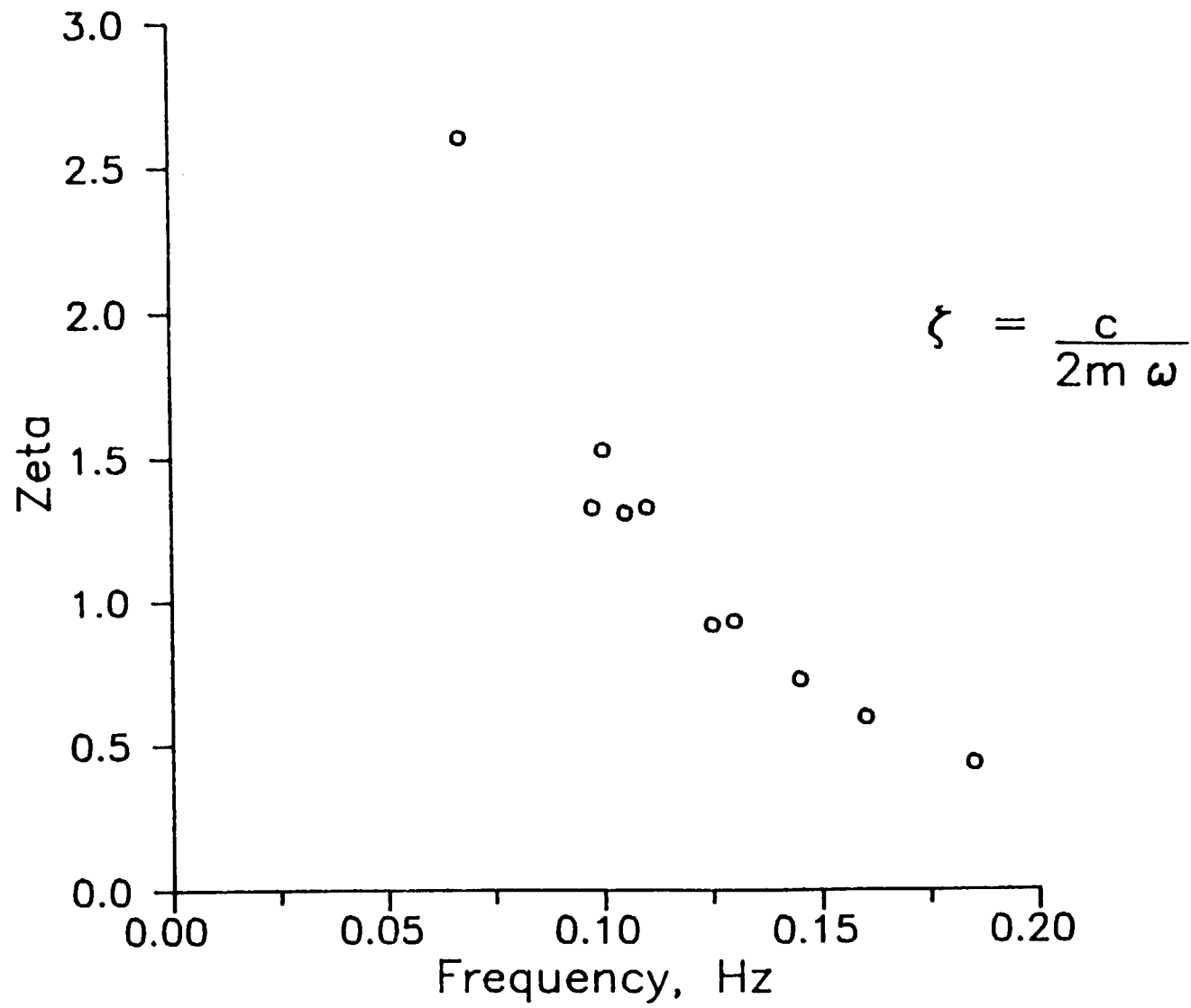


Figure 11. Change in ζ with Frequency

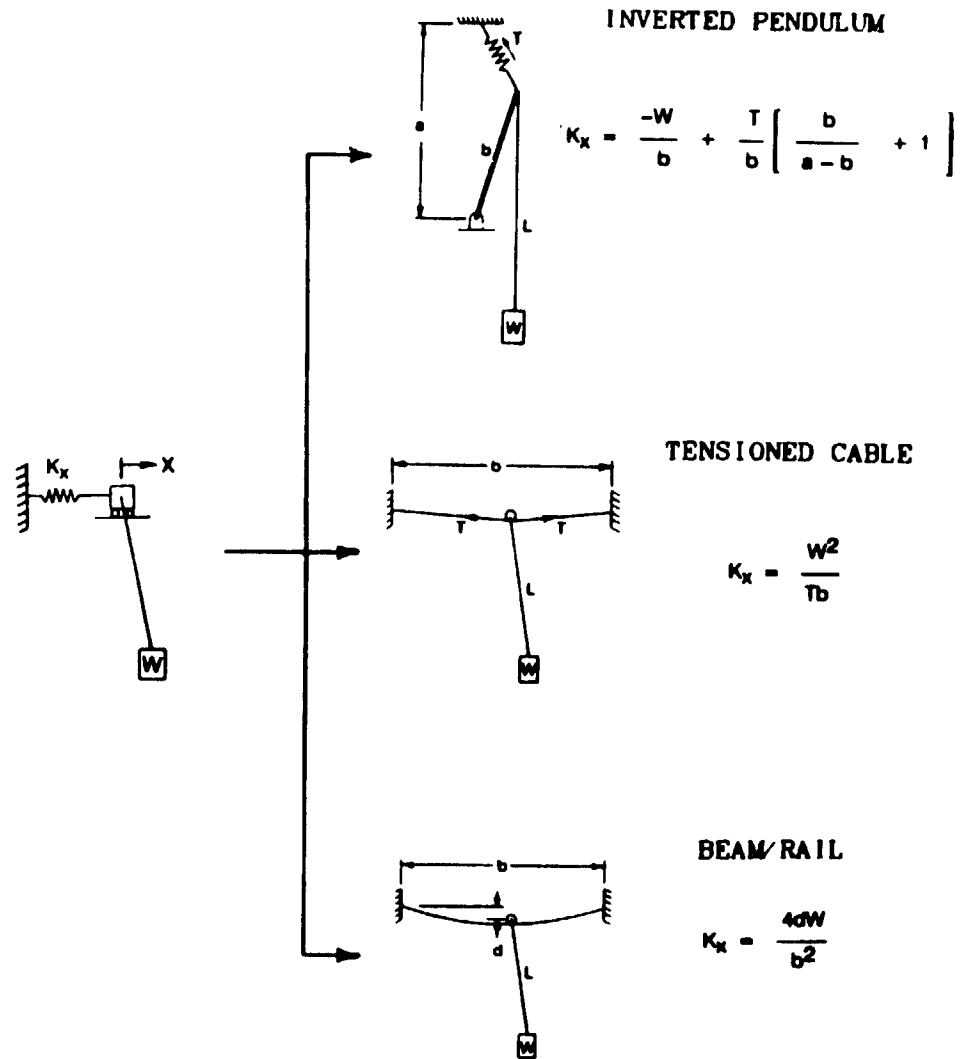
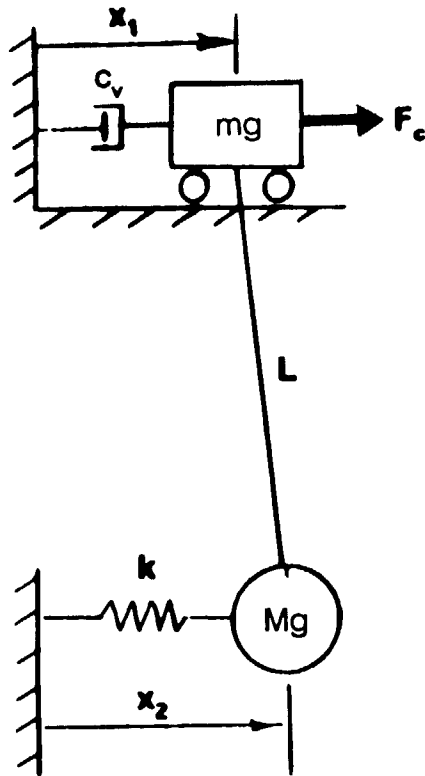


Figure 12. Moving Cart Analogy



EXAMPLE CASE

$Mg = 100$ lb, suspended weight

$mg = 2$ lb, cart weight

$g = 386$ in/sec², gravity constant

$L = 88.6$ in, pendulum length

$k = 0.756$ lbs/in, spring constant

$c_v = (\dots)$ lb-sec/in, viscous damping constant

$F_c = 0$ lb, feedback-control force

$x_1 =$ cart translation DOF

$x_2 =$ suspended weight translation DOF

Figure 13. Lateral Suspension Model

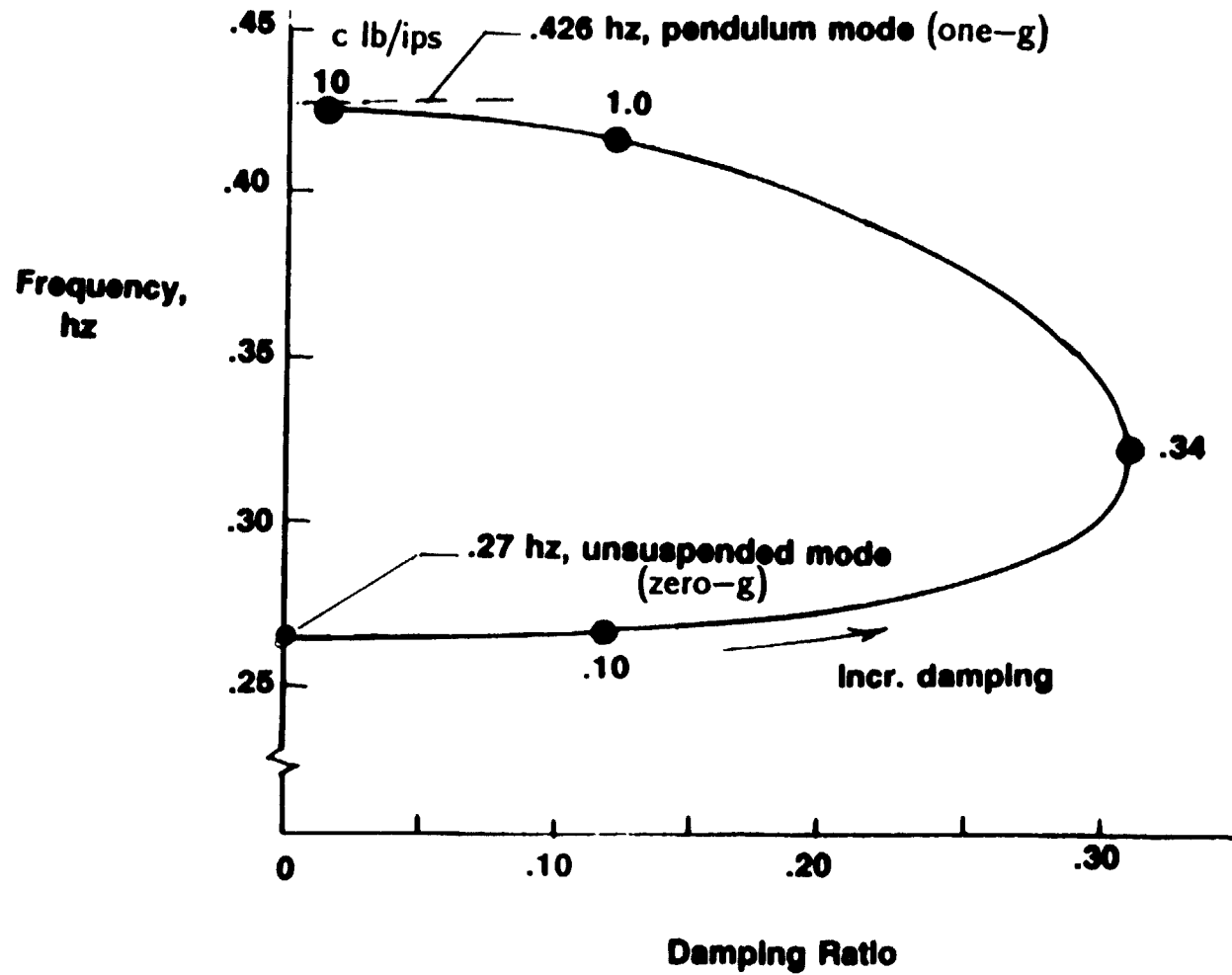


Figure 14. Effect of Cart Damping on Lateral-Mode Root

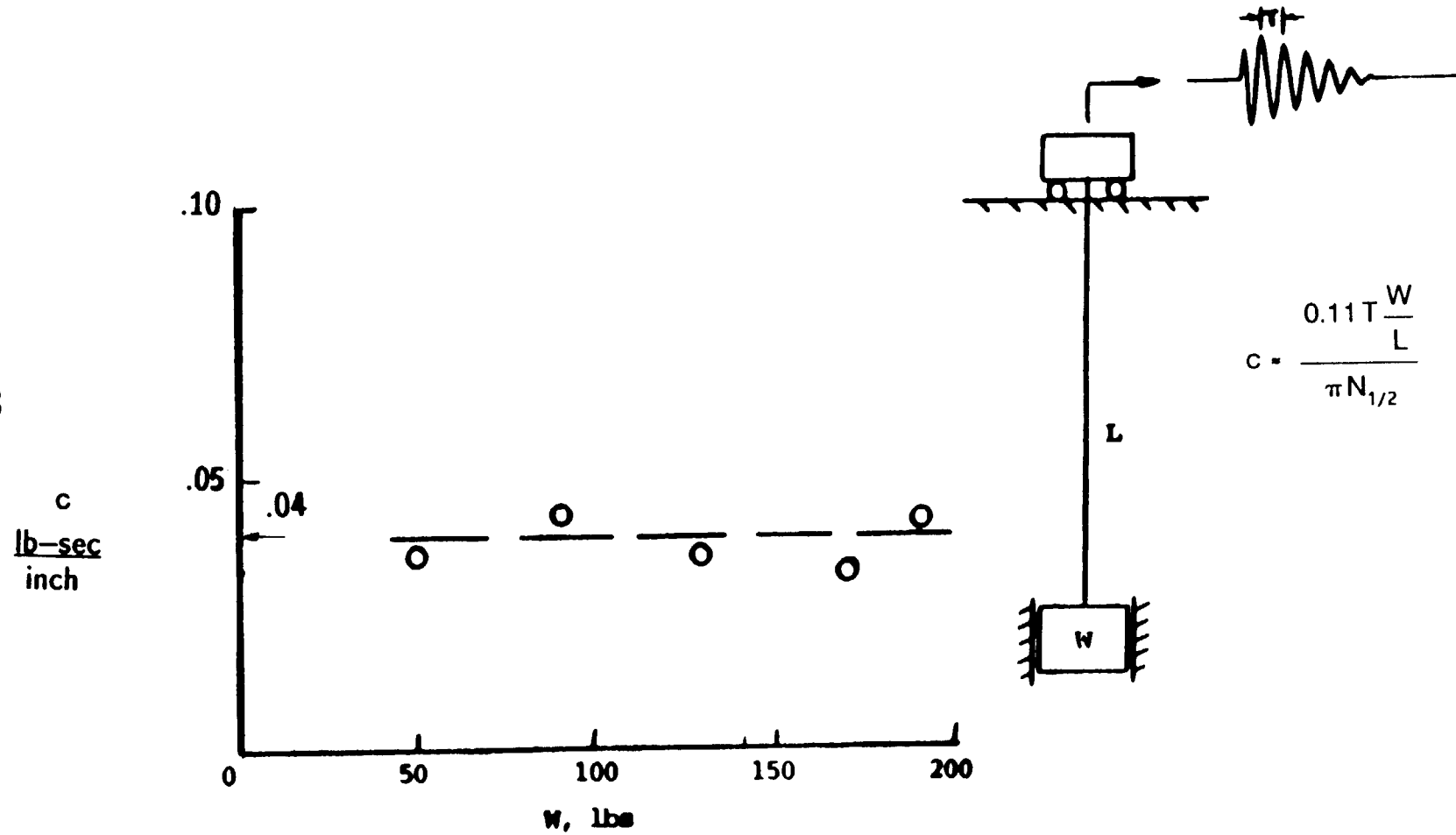


Figure 15. Equivalent Viscous Damping of Cart on Linear Bearing

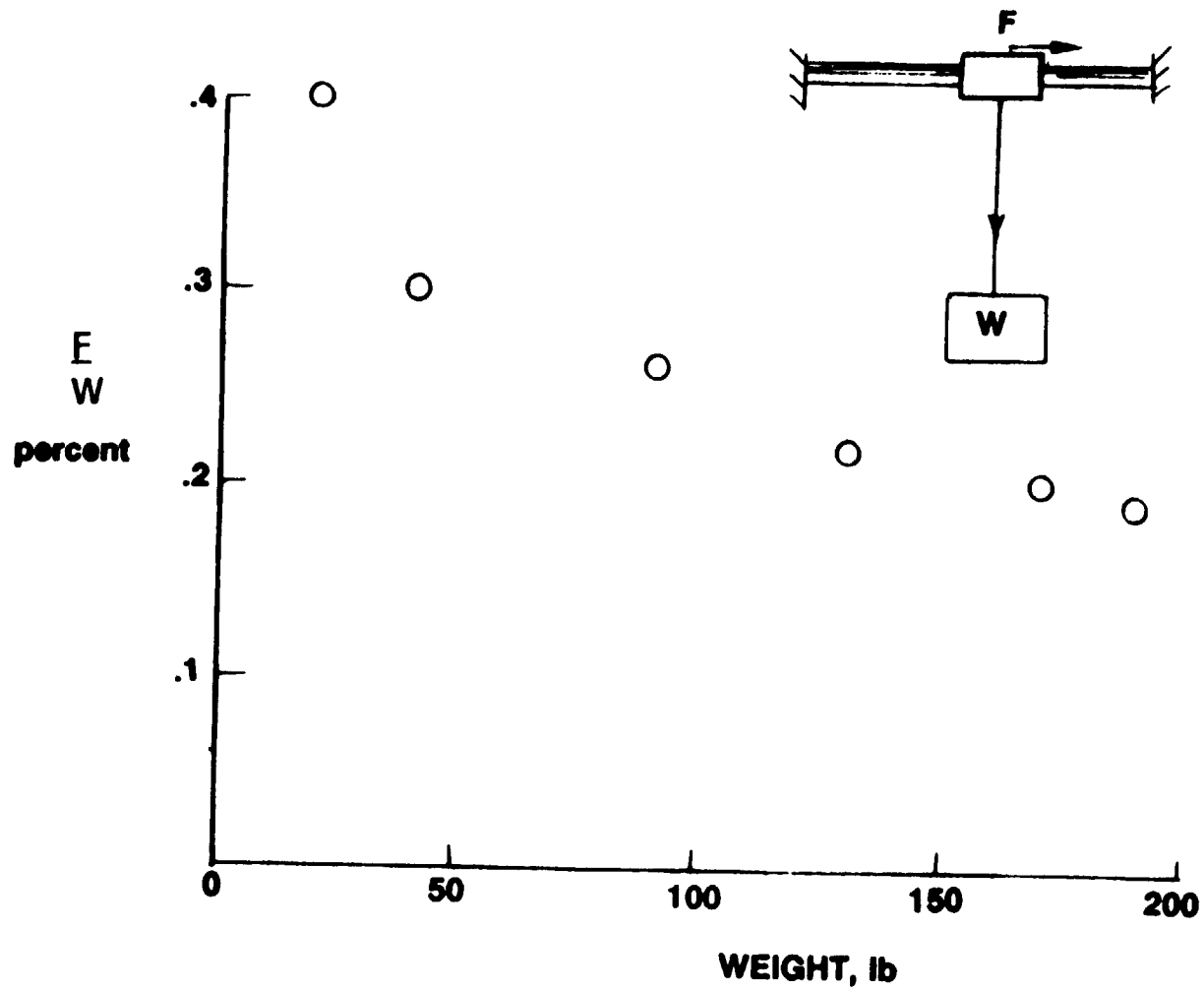


Figure 16. Linear-Bearing Breakout Force Coefficient

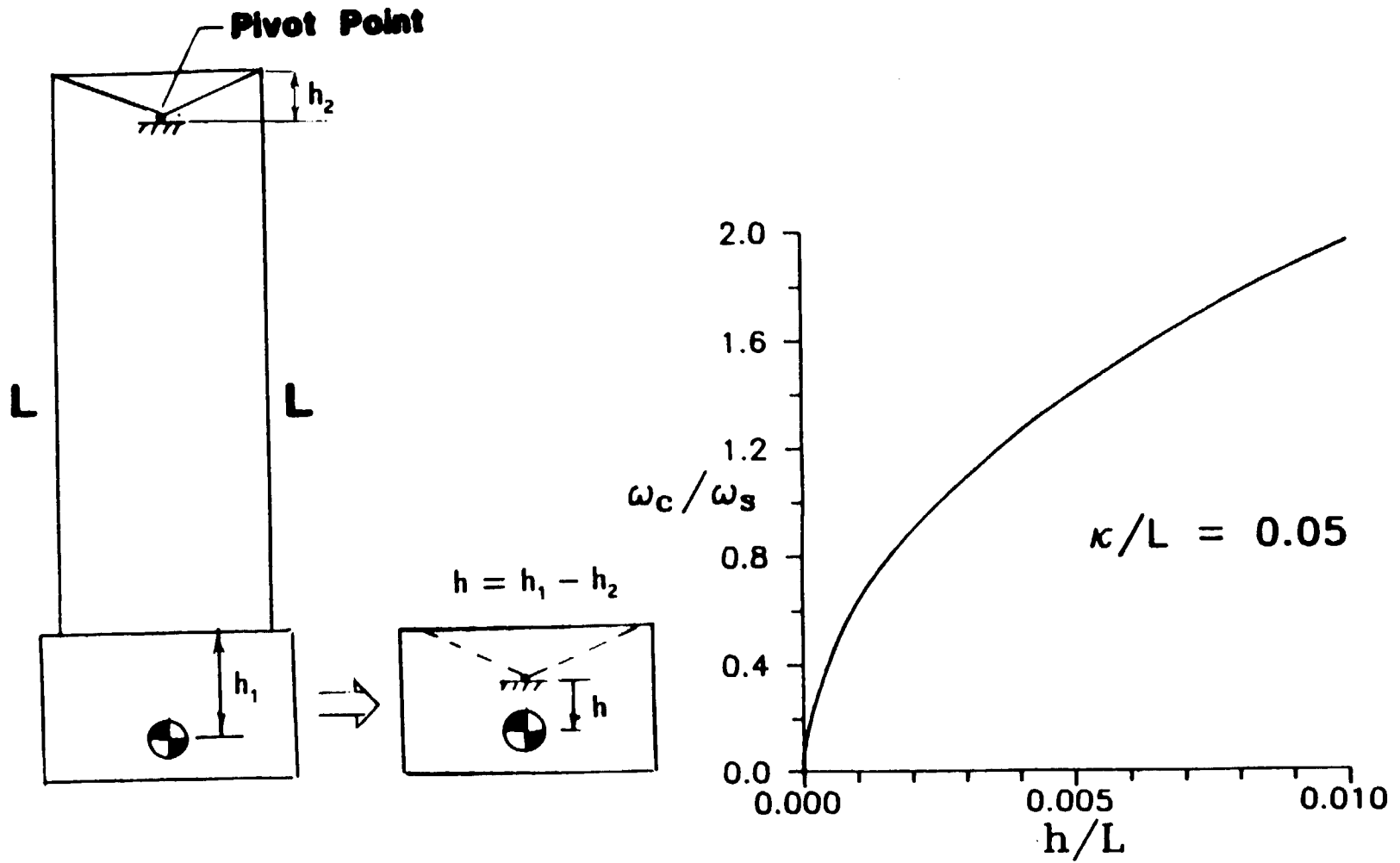


Figure 17. Low-Frequency Torsion Suspension System

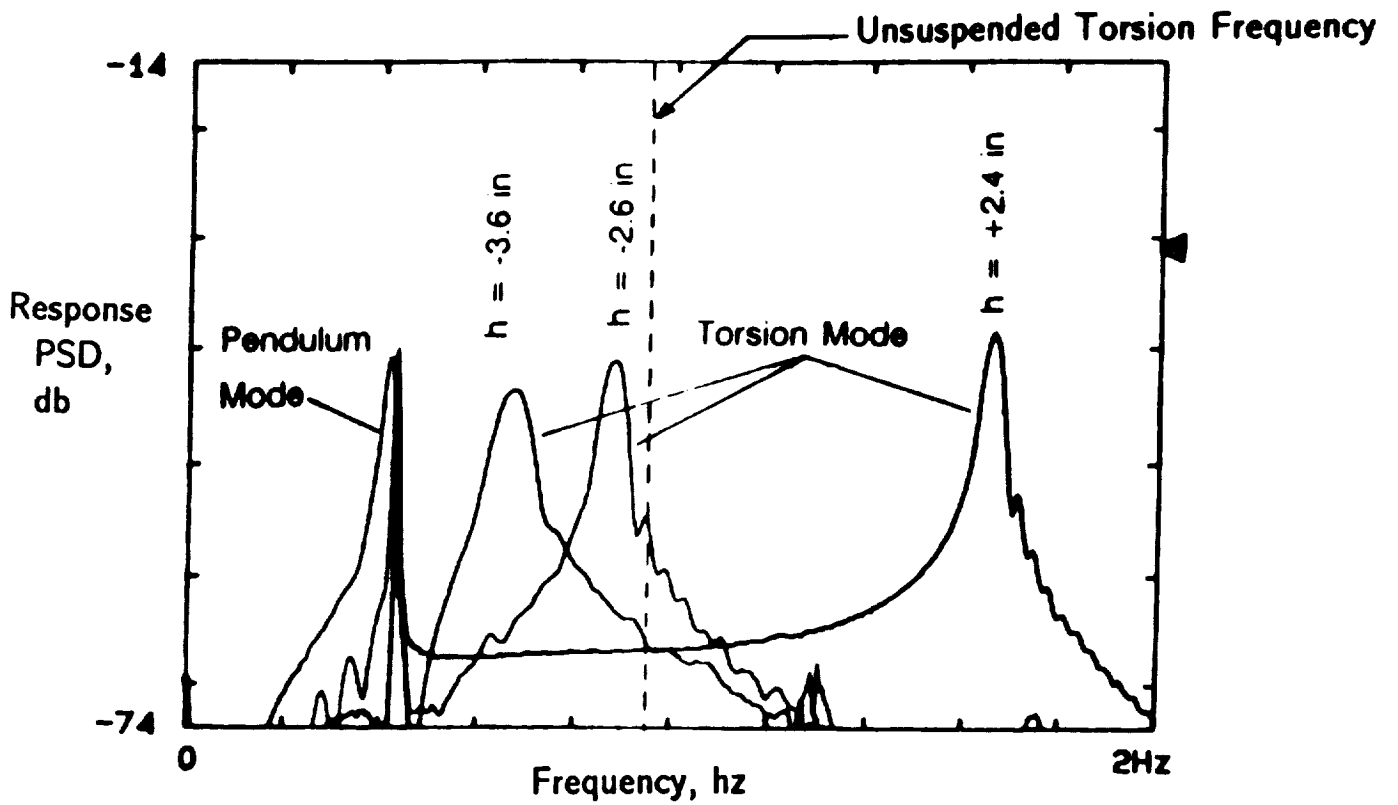
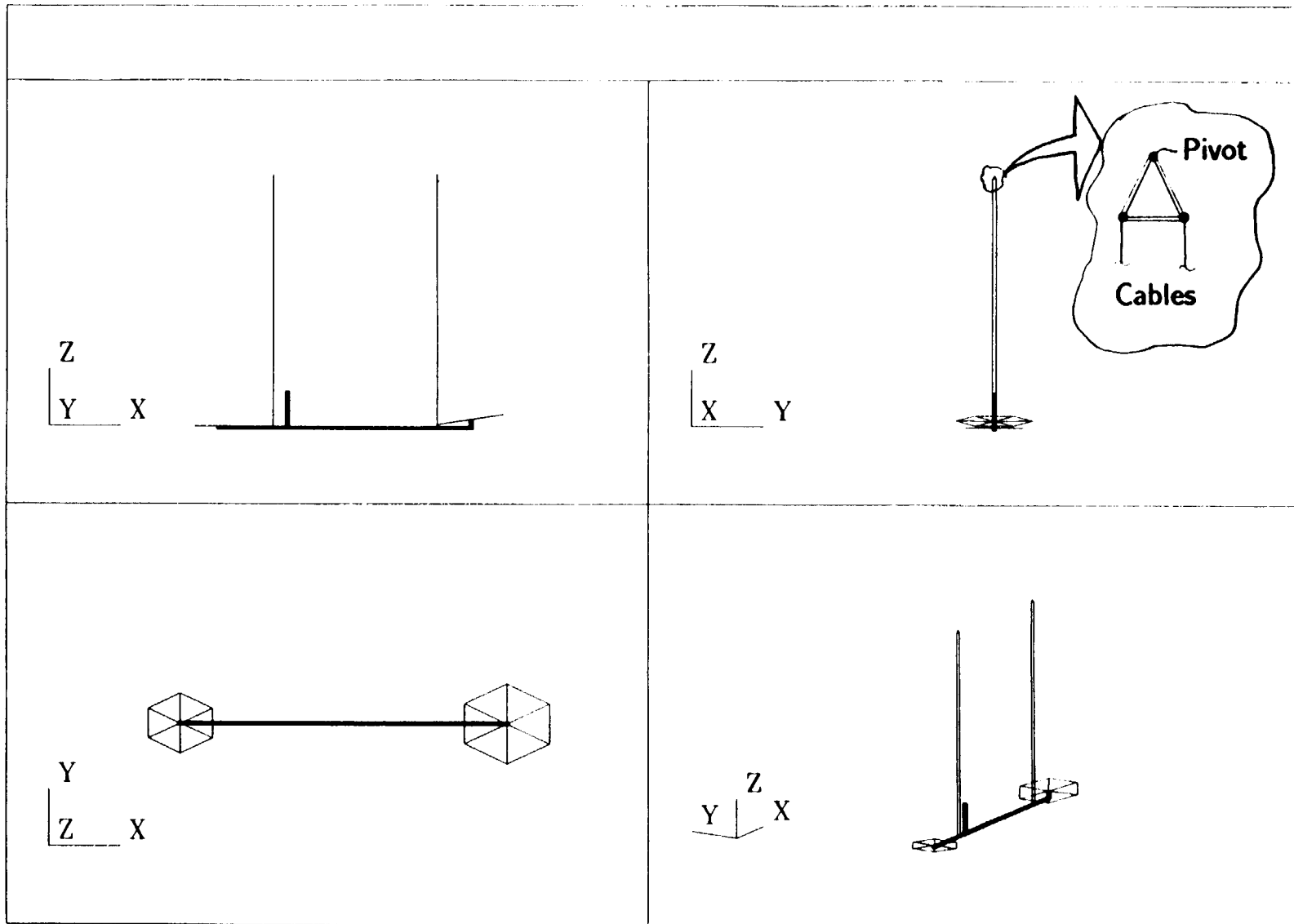
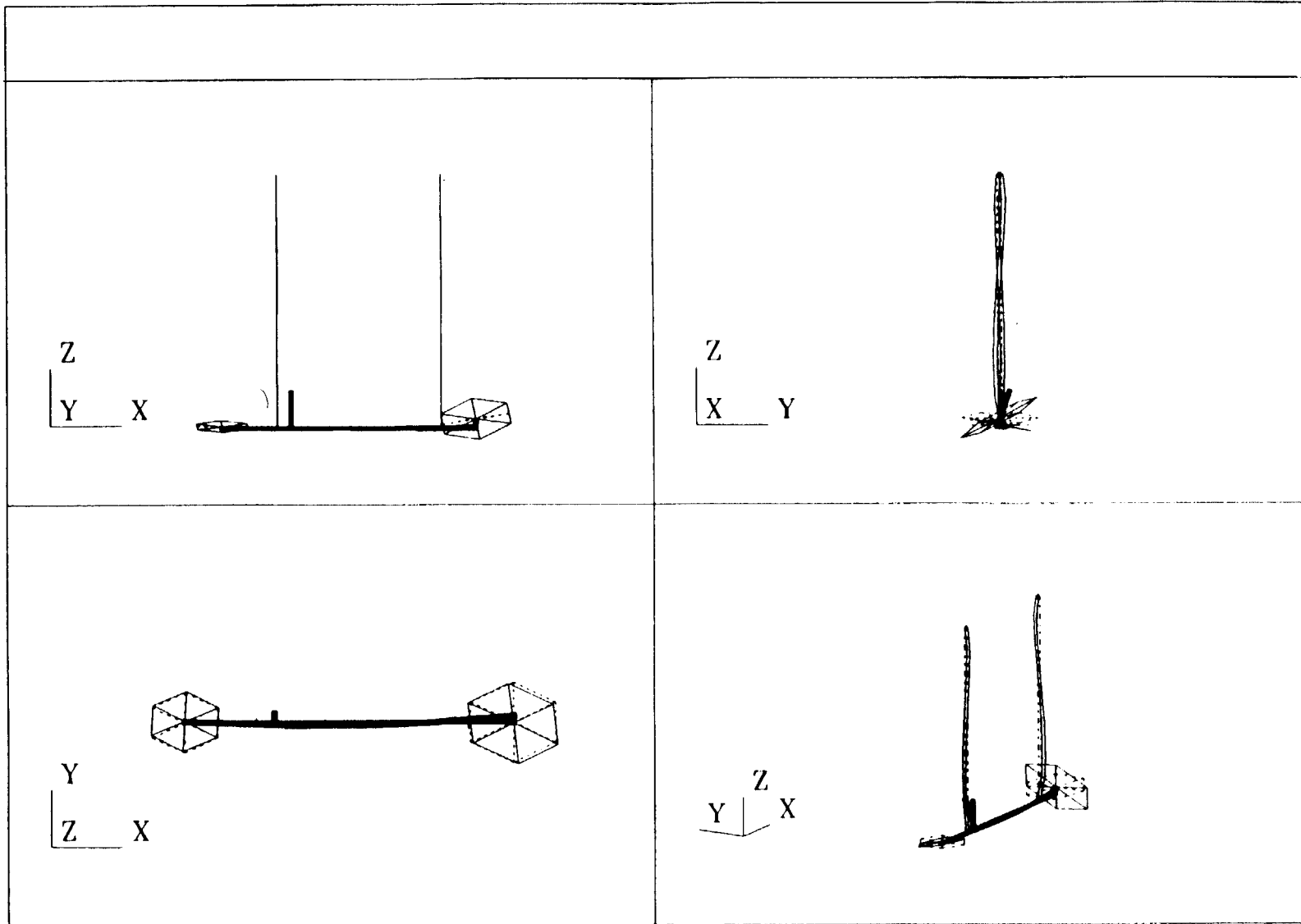


Figure 18. Effect of h on Frequency Spectra of Torsion Suspension System



UNDEFORMED SHAPE

Figure 19. Phase Zero Evolutionary Model with Torsion Suspension



1st TORSION
 FREQUENCY = 3.17 HZ.

Figure 20. Phase Zero Evolutionary Model with Torsion Suspension – 1st Torsion Mode

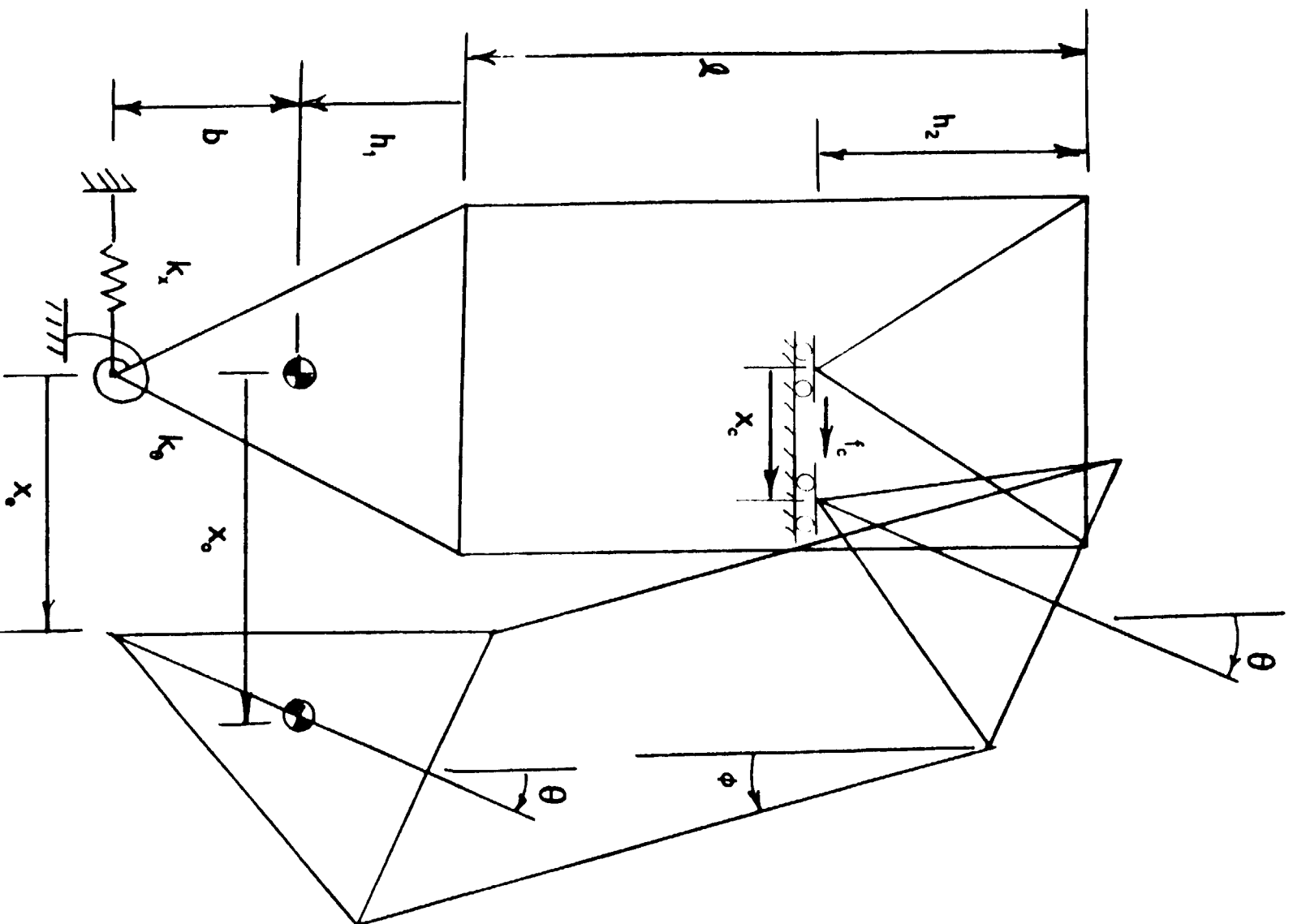


Figure 21. Test Article Geometry and DOFs

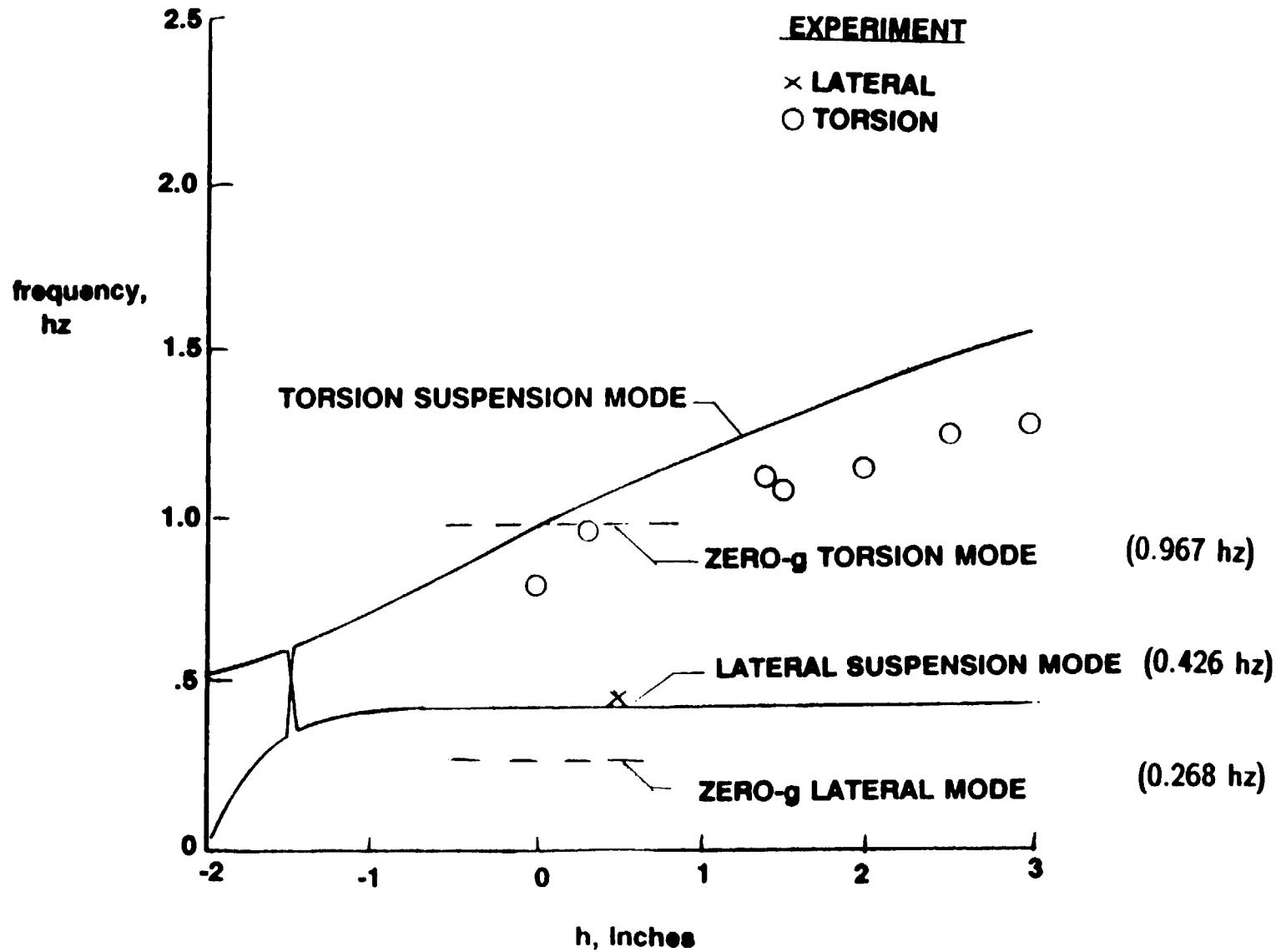


Figure 22. Natural Frequencies of the Lateral/Torsion System with Cart Fixed

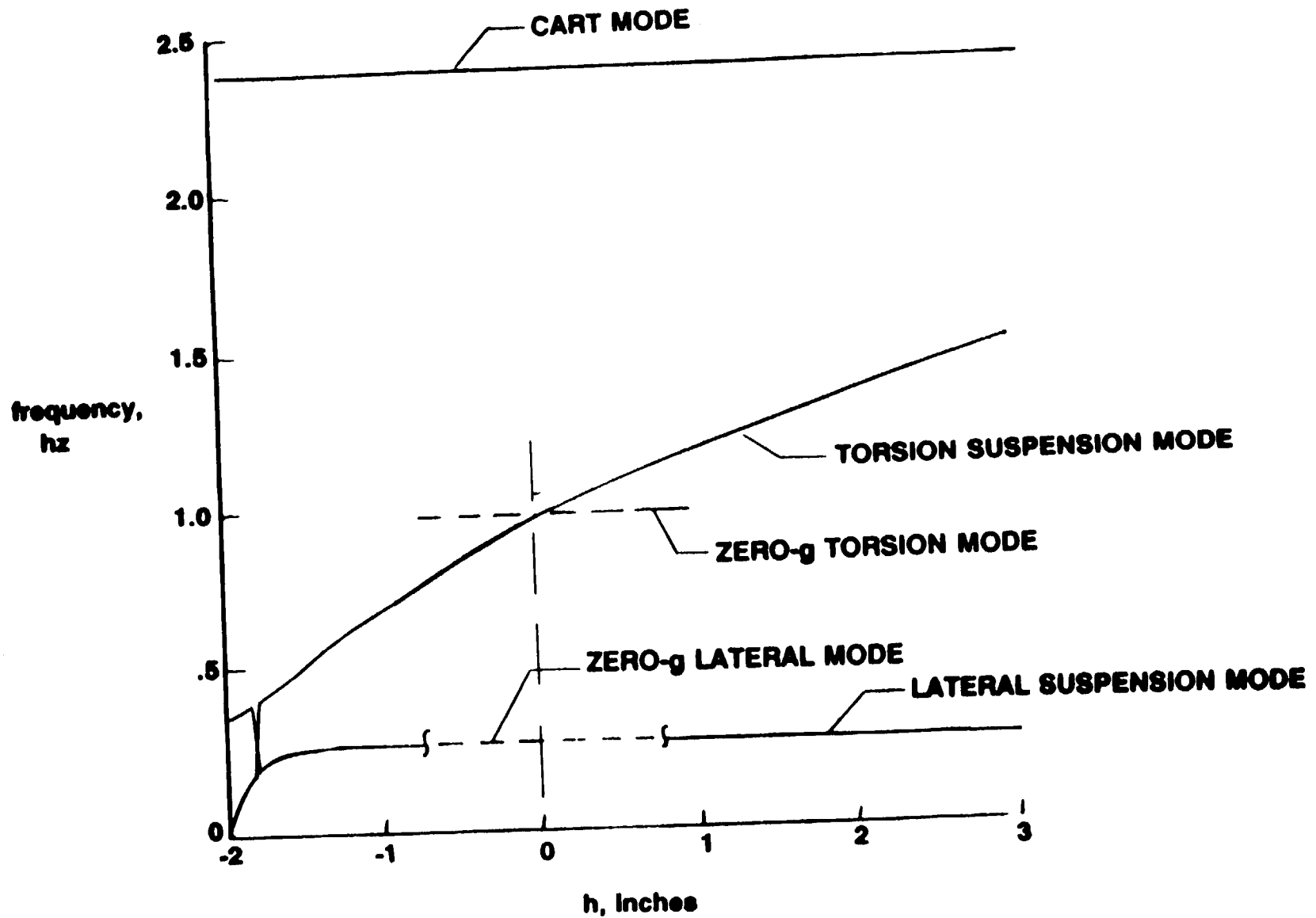
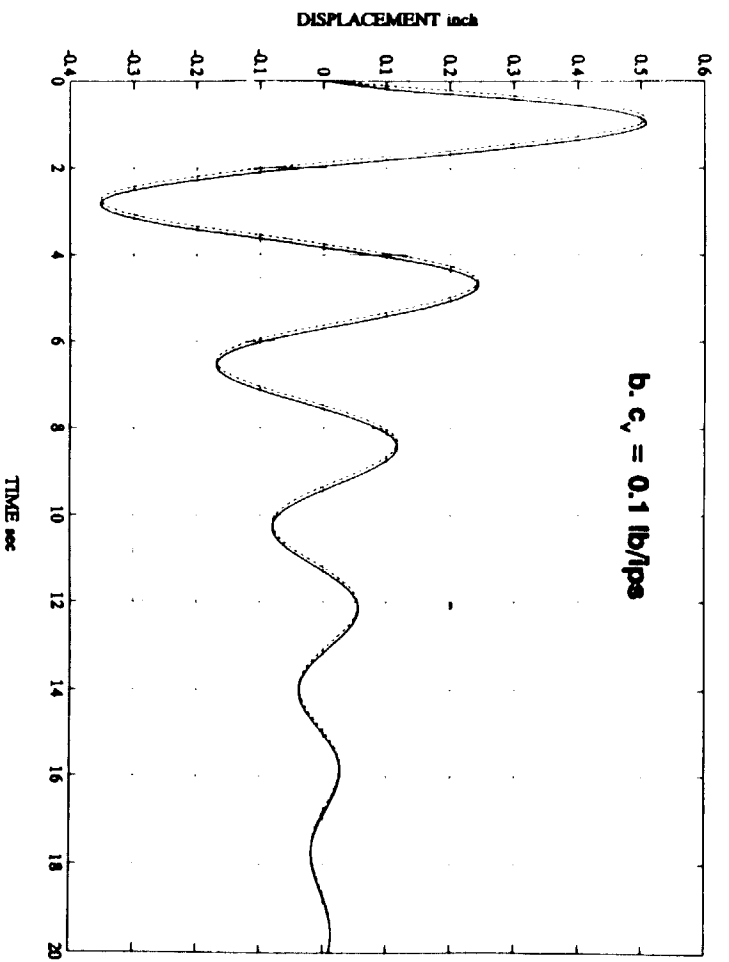
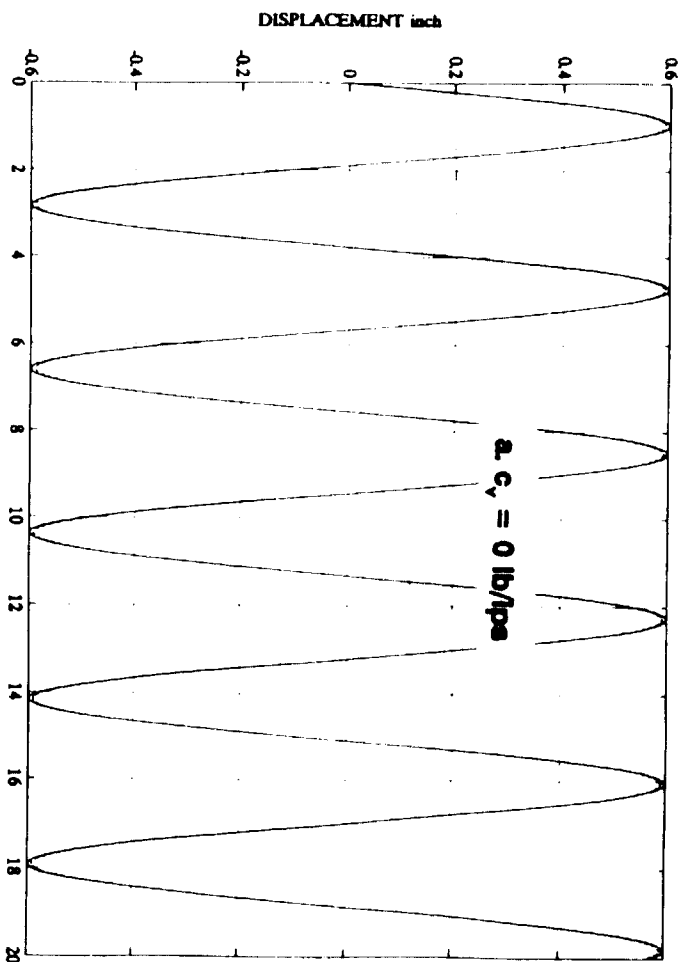


Figure 23. Natural Frequencies of the Lateral/Torsion System with Cart Free



**Figure 24a & 24b. Transient Response of Damped 1-g 3-DOF Model:
 $x_o(t)$ is solid, $x_o(t)$ is dot-dash**

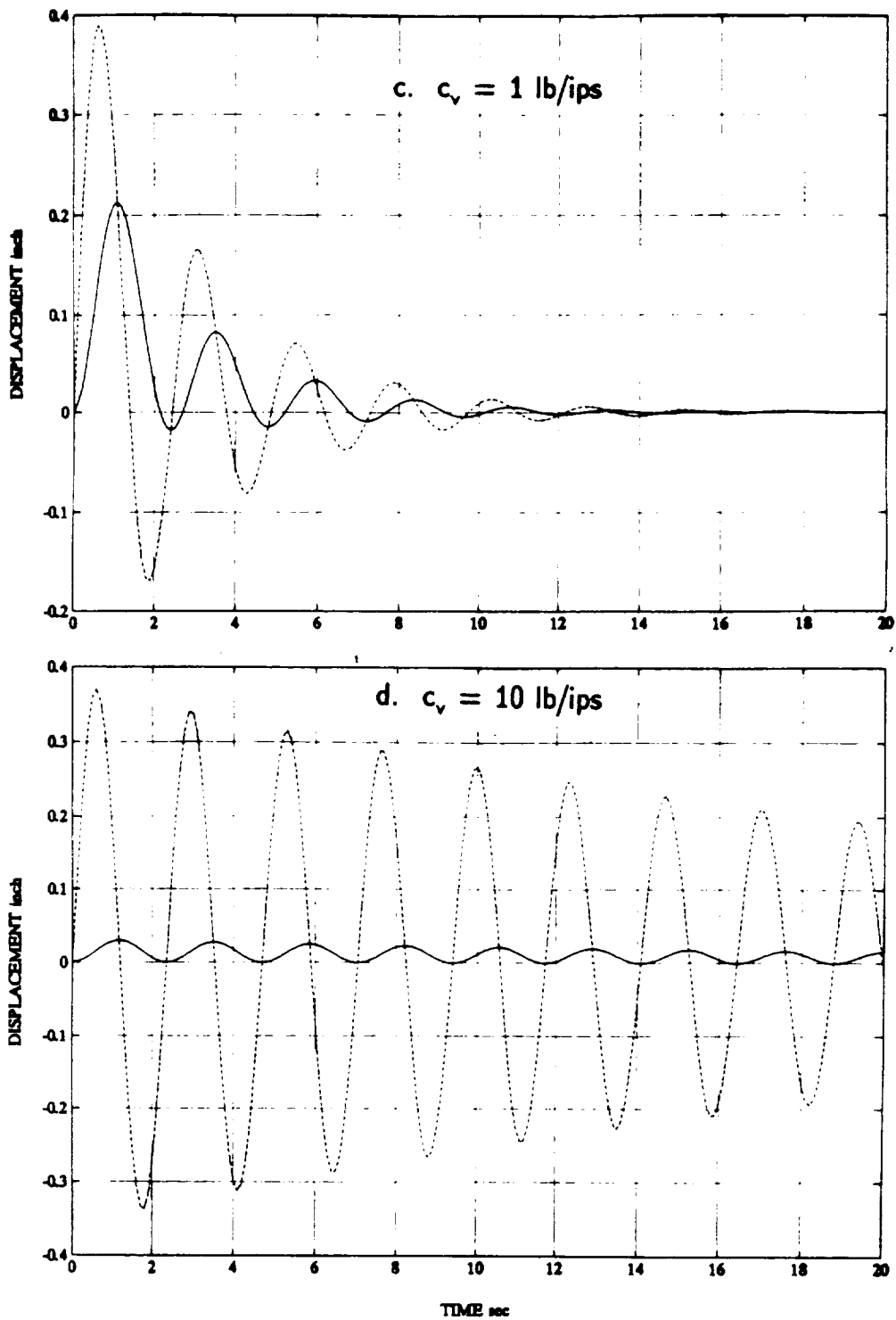
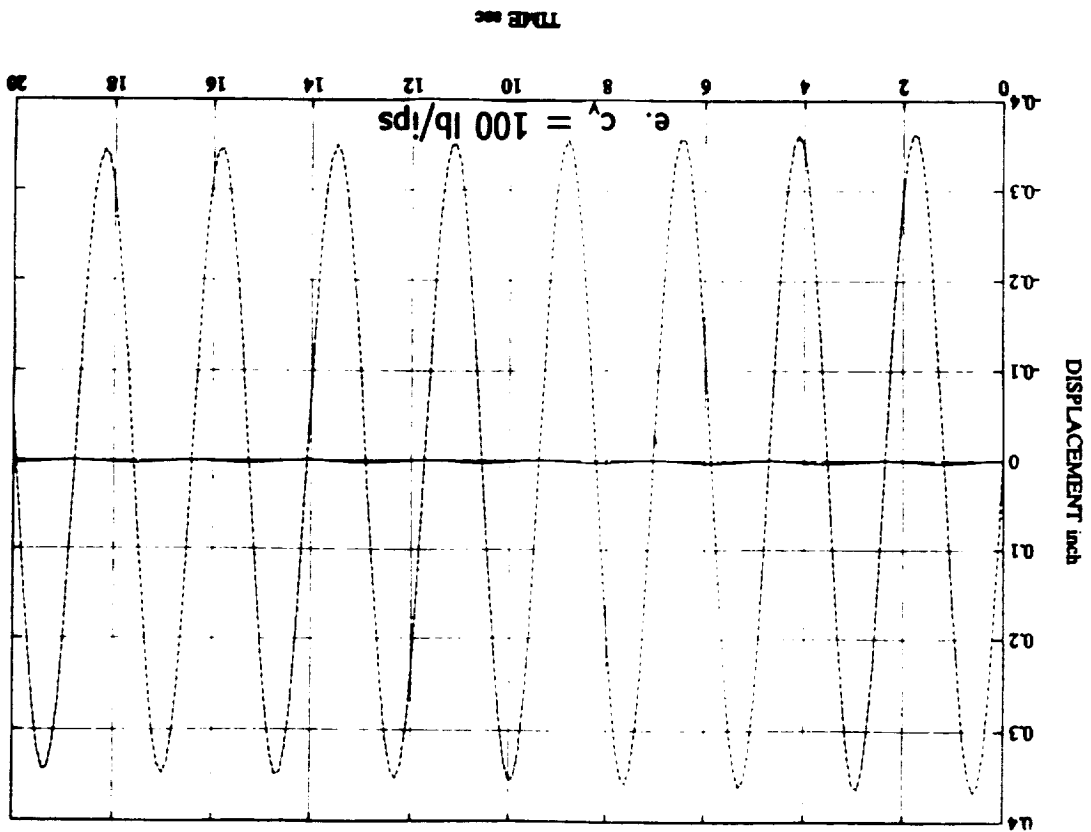


Figure 24. (Cont'd) Transient Response of Damped 1-g 3-DOF Model: $x_c(t)$ is solid, $x_o(t)$ is dot dash

Figure 24. (Cont'd) Transient Response of Damped 1-8
3-DOF Model: $x_c(t)$ is solid, $x_o(t)$ is dot dash



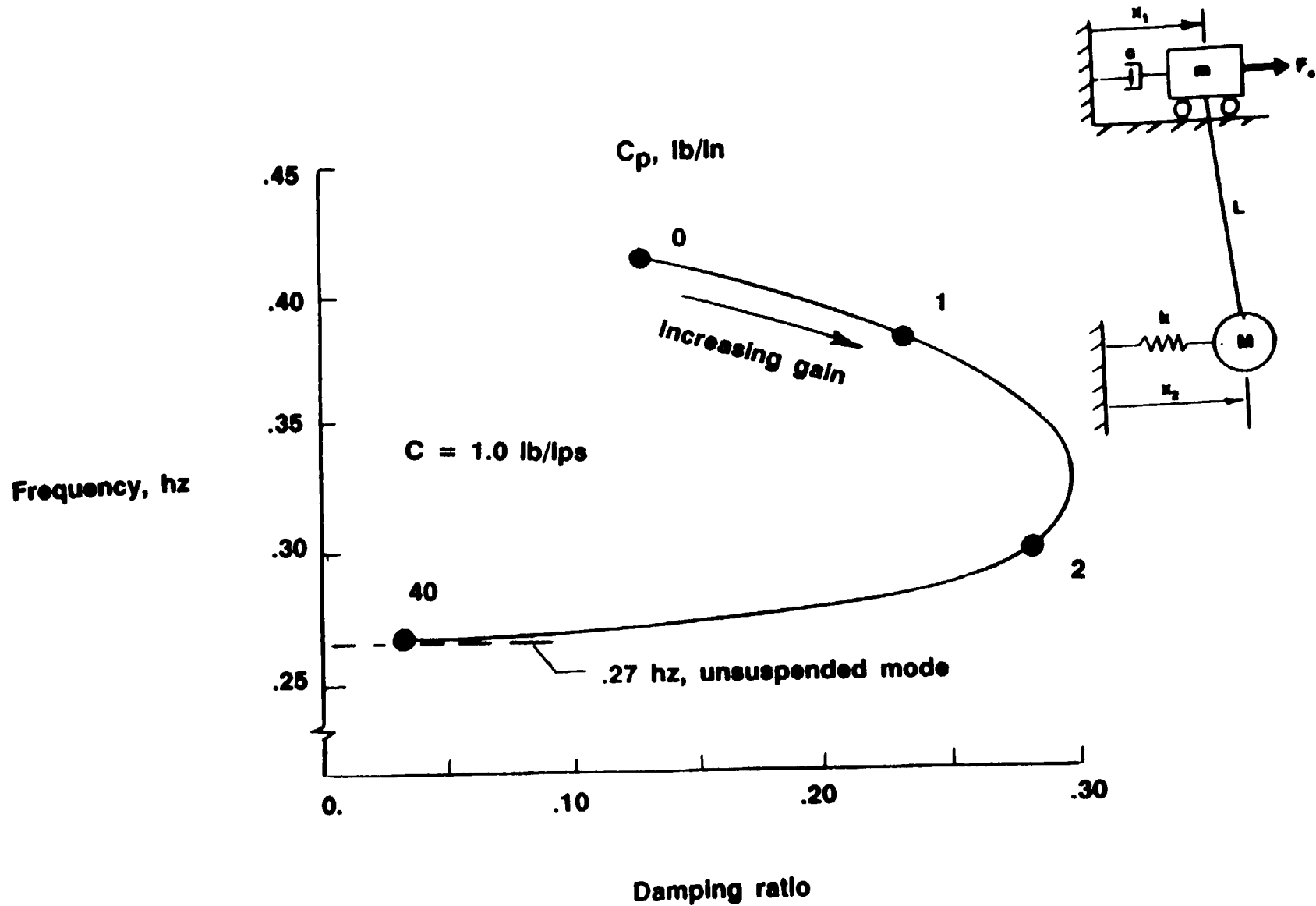


Figure 25. Effect of Active Control on Lateral-Mode Root
Control Force $F_c = C_p(x_2 - x_1)$

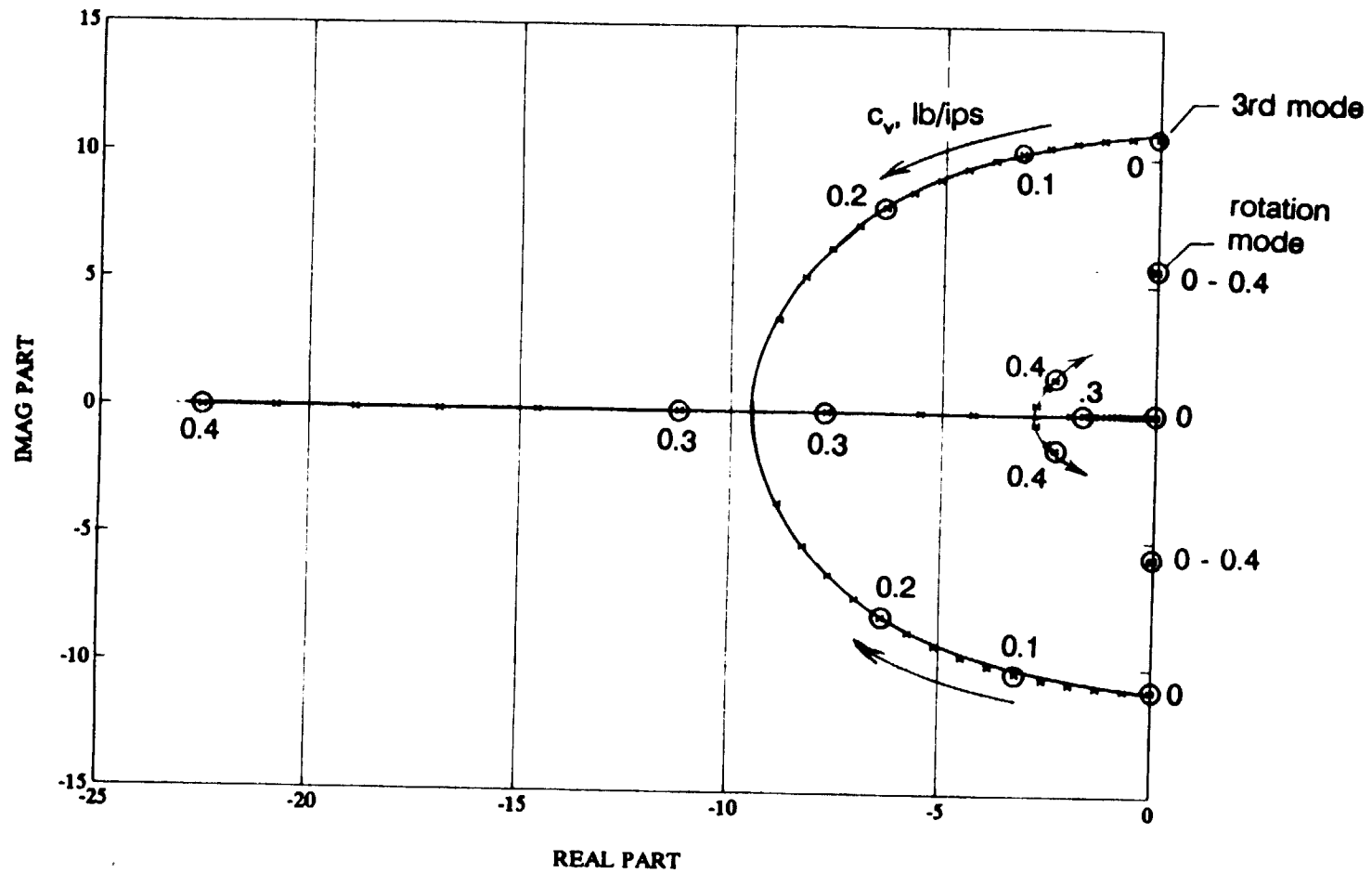


Figure 26. Zero stiffness Open-loop Loci of Roots as c_v Varies from 0 thru 0.4 ($m_g = 100$ lb, $m_{\text{lg}} = 5.65$ lb, $h = 17.5$ in, $L = 62.12$ in)

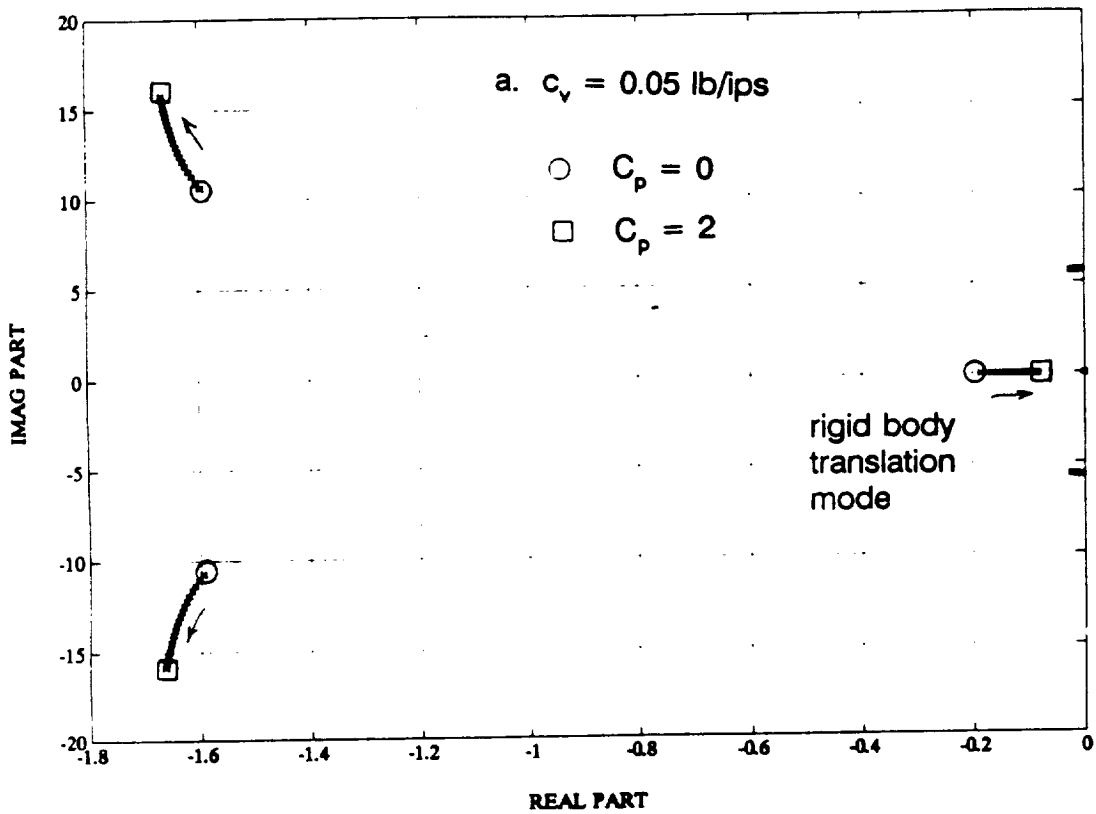
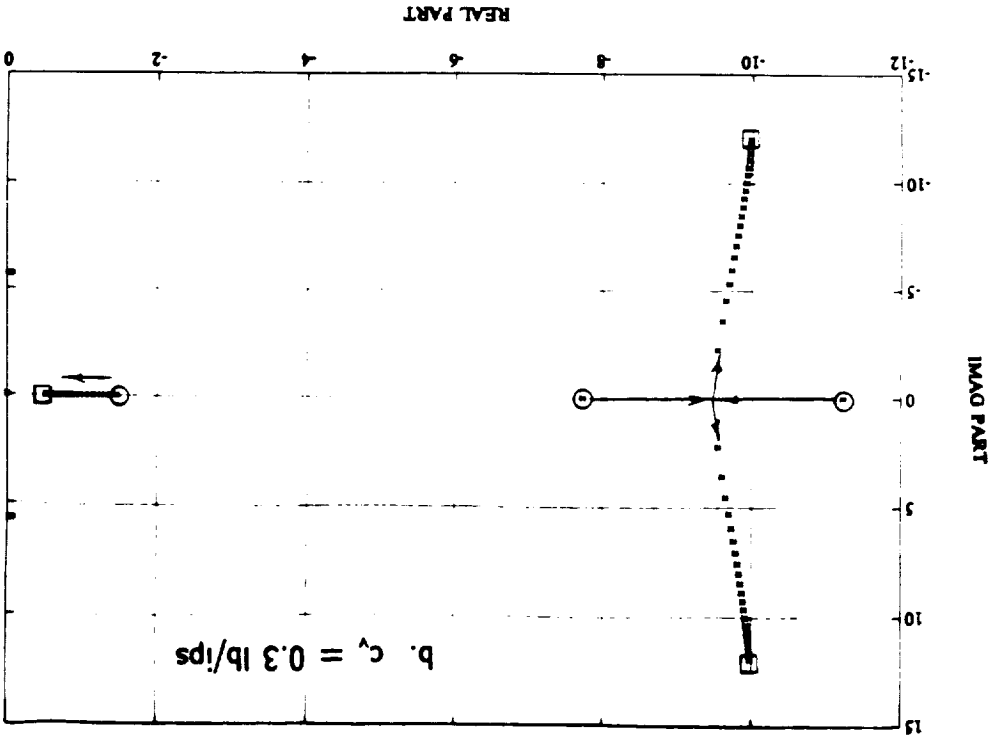
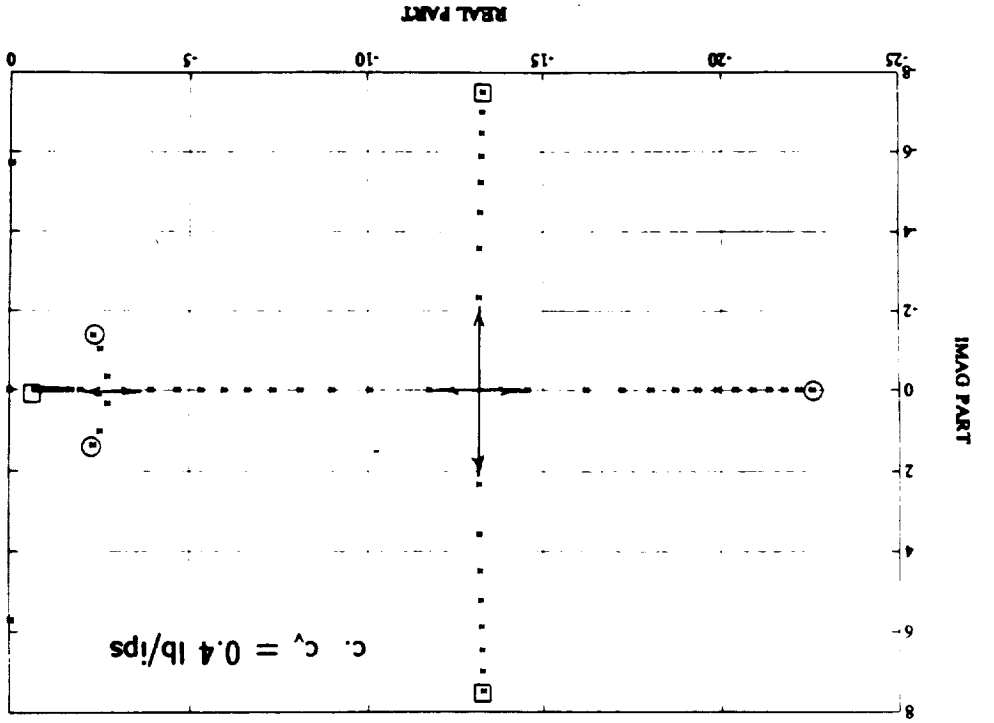


Figure 27. Zero-stiffness Proportional-control Loci of Roots $d/b = 1$

Figure 27. (Cont'd) Zero-stiffness Proportional-Control Loci of Roots



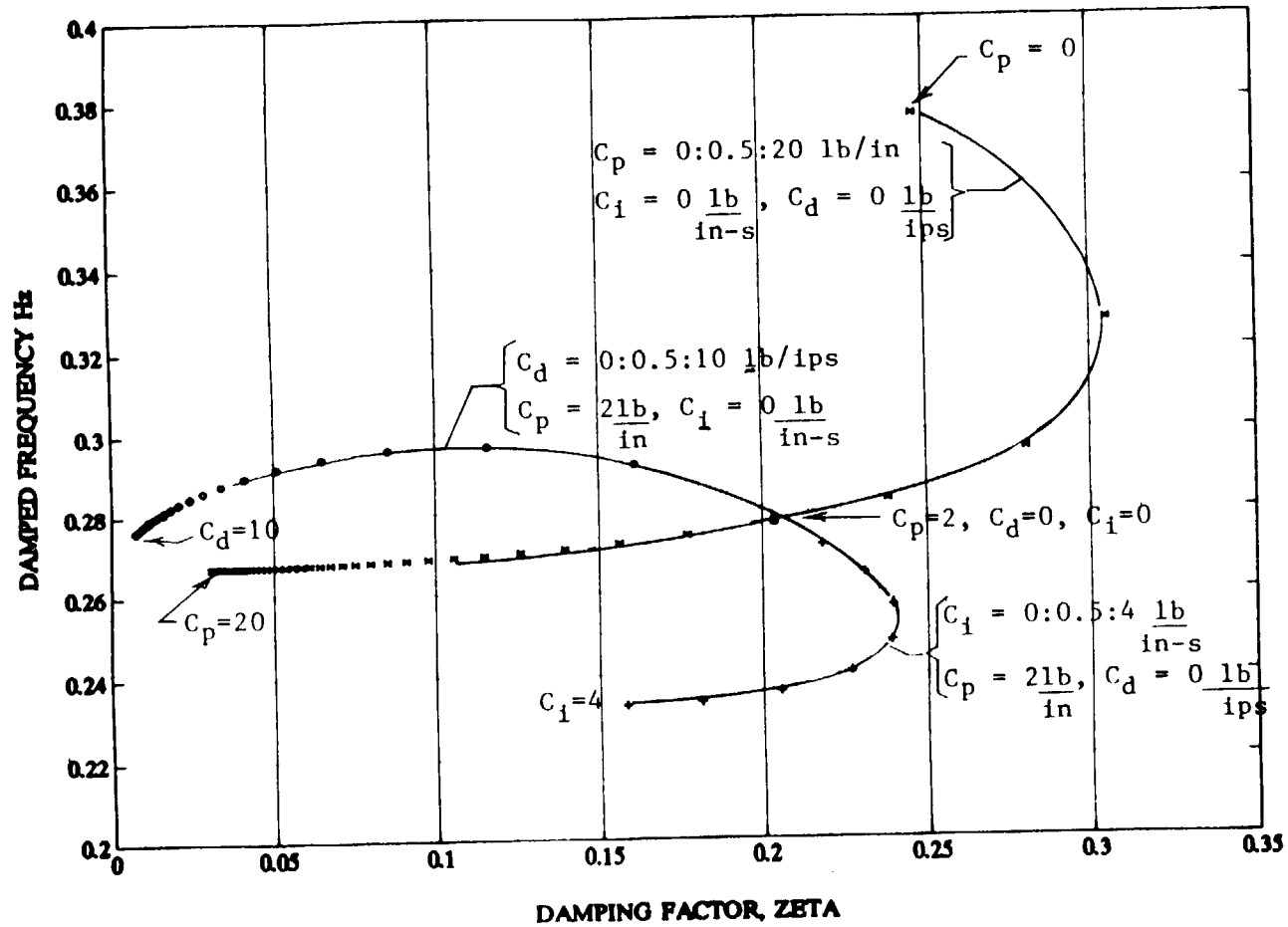
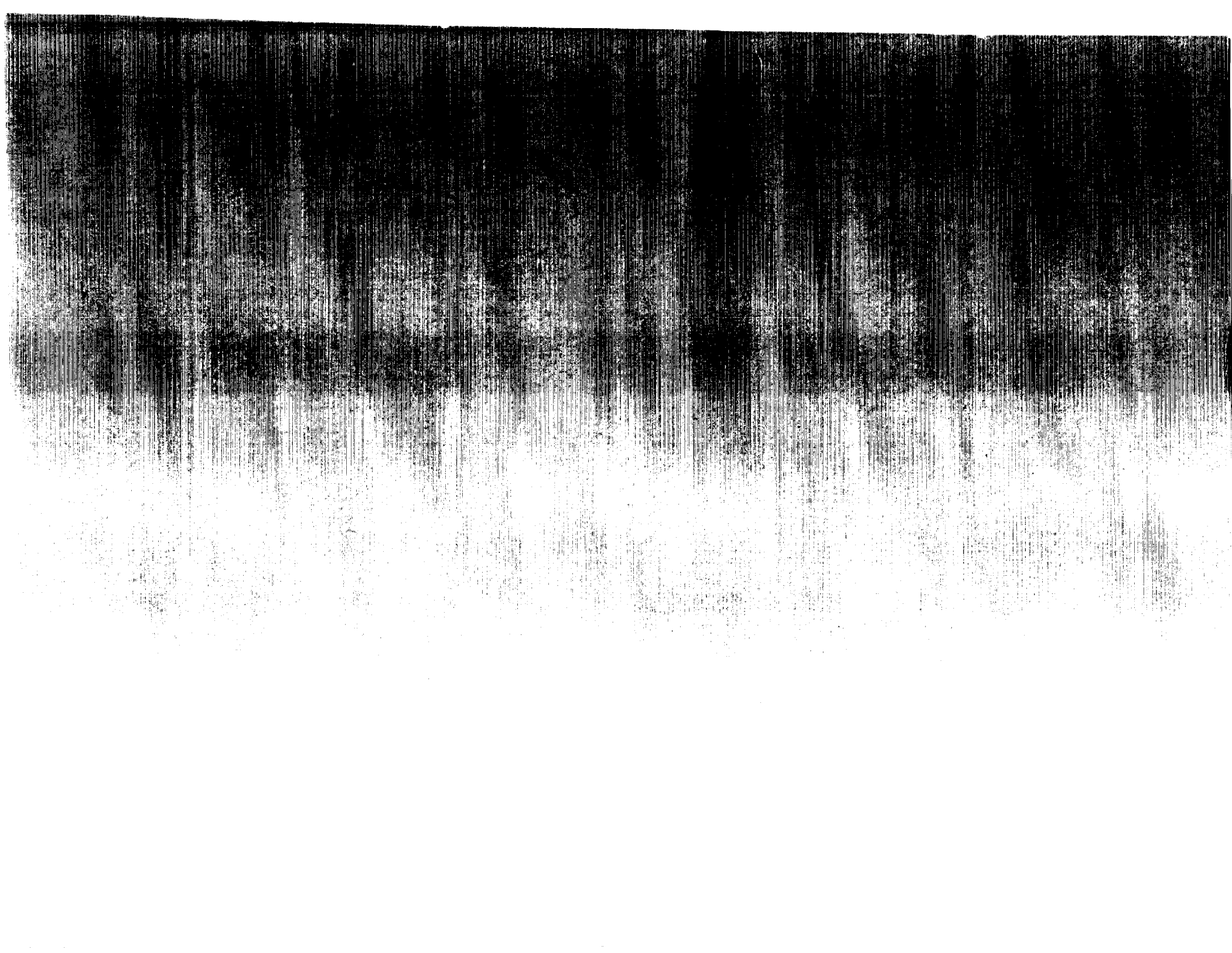


Figure 28. Loci of Roots for P, PD, and PI Types of Control for $h = 0''$, $d/b = 1.084$, $c_v = 0.5 \text{ lb/ips}$, $\tau = 0.025 \text{ sec}$



Report Documentation Page

1. Report No. NASA CR-4325		2. Government Accession No.		3. Recipient's Catalog No.	
4. Title and Subtitle Suspension Systems for Ground Testing Large Space Structures				5. Report Date October 1990	
				6. Performing Organization Code	
7. Author(s) Ronald R. Gold, Inger P. Friedman, Wilmer H. Reed III, and W. L. Hallauer				8. Performing Organization Report No. D-377	
9. Performing Organization Name and Address Dynamic Engineering, Inc. 703 Middle Ground Blvd. Newport News, VA 23606				10. Work Unit No. 585-01-91-01	
				11. Contract or Grant No. NAS1-18798	
12. Sponsoring Agency Name and Address National Aeronautics and Space Administration Langley Research Center Hampton, VA 23665-5225				13. Type of Report and Period Covered Contractor Report - Final	
				14. Sponsoring Agency Code	
15. Supplementary Notes Technical Monitor - Rudeen Smith-Taylor, Langley Research Center Ronald R. Gold, Inger P. Friedman, and Wilmer H. Reed III: Dynamic Engineering, Inc., Newport News, Virginia. W. L. Hallauer: Virginia Polytechnic Institute and State University, Blacksburg, Virginia					
16. Abstract <p>This report documents a research program for the development of improved suspension techniques for ground vibration testing of large, flexible space structures. The suspension system must support the weight of the structure and simultaneously allow simulation of unconstrained rigid-body movement as in the space environment. Exploratory analytical and experimental studies were conducted for suspension systems designed to provide minimum vertical, horizontal, and rotational degrees of freedom. The effects of active feedback control added to the passive system were also investigated. An experimental suspension apparatus was designed, fabricated, and tested. This test apparatus included a zero spring rate mechanism (ZSRM) designed to support a range of weights from 50 to 300 lbs and provide vertical suspension mode frequencies less than 0.1 Hz. The lateral suspension consisted of a pendulum suspended from a moving cart (linear bearing) which served to increase the effective length of the pendulum. The torsion suspension concept involved dual pendulum cables attached from above to a pivoting support (bicycle wheel). A simple test structure having variable weight and stiffness characteristics was used to simulate the vibration characteristics of a large space structure. The suspension hardware for the individual degrees of freedom was analyzed and tested separately and then combined to achieve a 3 DOF suspension system. Results from the exploratory studies should provide useful guidelines for the development of future suspension systems for ground vibration testing of large space structures.</p>					
17. Key Words (Suggested by Author(s)) Zero Spring Rate Mechanism (ZSRM), Lateral Suspension Torsion Suspension 3-DOF			18. Distribution Statement unclassified - unlimited subject category - 18		
19. Security Classif. (of this report) unclassified		20. Security Classif. (of this page) unclassified		21. No. of pages 116	22. Price A06



VSVN

Official Business
Penalty for Private Use, \$300

**National Aeronautics and
Space Administration
Code NTT-4
Washington, D.C.
20546-0001**

NOV 1977
NO 0-27